

Distribution agreement

In presenting this thesis or dissertation as a partial fulfillment of the requirements for an advanced degree from Emory University, I hereby grant to Emory University and its agents the non-exclusive license to archive, make accessible, and display my thesis or dissertation in whole or in part in all forms of media, now or hereafter known, including display on the world wide web. I understand that I may select some access restrictions as part of the online submission of this thesis or dissertation. I retain all ownership rights to the copyright of the thesis or dissertation. I also retain the right to use in future works (such as articles or books) all or part of this thesis or dissertation.

Signature:

Abigail Vanderheiden

Innate regulation of CD8+ T cells during West Nile virus
neuroinvasive disease

By

Abigail Vanderheiden
Doctor of Philosophy

Graduate Division of Biological and Biomedical Sciences
Immunology and Molecular Pathogenesis

Mehul Suthar
Advisor

Jeremy Boss
Committee Member

Arash Grakoui
Committee Member

Haydn Kissick
Committee Member

Jacob Kohlmeier
Committee Member

Accepted:

Lisa A. Tedesco, Ph.D.

Dean of the James T. Laney School of Graduate Studies

Date

Innate Regulation of CD8+ T cells in the Central Nervous System during West Nile Virus
Infection

By

Abigail Vanderheiden

B.S., University of Minnesota, 2016

Advisor: Dr. Mehul S. Suthar

Ph.D., University of North Carolina-Chapel Hill

An abstract submitted to the Faculty of the
James T. Laney School of Graduate Studies of Emory University
in partial fulfillment of the requirements for the degree of Doctor of Philosophy in Immunology
and Molecular Pathogenesis

2021

Abstract

Innate Regulation of CD8⁺ T cells during West Nile virus Neuroinvasive Disease

By Abigail Vanderheiden

Neuroinvasive West Nile virus (WNV) infection requires CD8⁺ T cell responses for virologic control in the central nervous system (CNS). Here, we investigate the regulation of CD8⁺ T cells in the CNS- draining lymph nodes (LNs), meninges, and brain parenchyma in a mouse model of WNV infection. First, we characterized WNV pathogenesis and the WNV-specific CD8⁺ T cell response in these various anatomic compartments. We found that the meninges and CNS-draining LNs have detectable WNV RNA early during pathogenesis. WNV-specific CD8⁺ T cells from the periphery and CNS-draining lymph nodes exhibited similar profiles, whereas WNV-specific CD8⁺ T cells from meninges and brain had distinct cytokine secretion, expression of activation markers, and functionality. Thus, CNS localized WNV-specific CD8⁺ T cells are subject to unique regulation during WNV infection. To explore how CNS-specific regulation occurs, we next investigated cell-intrinsic regulators of CD8⁺ T cell function in the CNS. Mitochondrial antiviral signaling (MAVS) protein, the central adaptor protein for RIG-I like receptor (RLR) signaling, is essential for promoting immunity against WNV infection in the CNS. MAVS is expressed in nearly every cell and is localized on the mitochondria. Here, we find that MAVS is found within CD8⁺ T cells and functions in a cell-intrinsic manner to promote mitochondrial respiration and cell proliferation. We demonstrate that ablation of MAVS in antigen-specific CD8⁺ T cells leads to dysregulated oxidative phosphorylation transcriptional profiles and decreased mitochondrial potential *in vivo* during virus infection. Through adoptive transfer experiments, we determine that MAVS is required for expansion of antigen-specific CD8⁺ T cells. Mechanistically, we found that MAVS functions in CD8⁺ T cells by positively regulating cell proliferation during virus infection. Our findings identify a non-canonical role for MAVS as a positive regulator of mitochondrial respiration and cell proliferation of antigen-specific CD8⁺ T cells during WNV neuroinvasive disease.

Innate Regulation of CD8+ T cells in the Central Nervous System during West Nile Virus
Infection

By

Abigail Vanderheiden

B.S., University of Minnesota, 2016

Advisor: Dr. Mehul S. Suthar

Ph.D., University of North Carolina-Chapel Hill

A dissertation submitted to the Faculty of the
James T. Laney School of Graduate Studies of Emory University
in partial fulfillment of the requirements for the degree of Doctor of Philosophy in Immunology
and Molecular Pathogenesis

2021

TABLE OF CONTENTS

Introduction (1-22)

- WNV pathogenesis and Immunity (1-9)
- CD8+ T cells during neuroinvasive WNV disease (9-14)
- Innate immune signaling during viral infection (14-19)
- Summary (20)
- Figure 1. CD8+ T cells use cytolytic and noncytolytic mechanisms to control virus in the CNS (21)
- Figure 2. MAVS is the central hub for the Rig-I like receptor signaling pathway (22)

Part 1: Entry of West Nile virus into the central nervous system draining lymphatics precedes differential programming of CD8+ T cells in the brain (23-59)

- 1.1: Introduction (25- 28)
- 1.2: Results (29- 38)
- 1.3: Discussion (39- 44)
- 1.4: Materials and methods (45- 49)
- 1.5: Figure legends (50-53)
- 1.6: Figure Set (55-59)
 - o Figure 1: WNV seeds the CNS-draining lymph nodes and meninges prior to parenchymal invasion (55)
 - o Figure 2: Activated dendritic cell kinetics differ between the CNS-draining lymph nodes, meninges, and parenchyma (56)
 - o Figure 3: Localization to the meninges, brain, and CNS-draining lymph nodes changes WNV-specific CD8+ T cell activation (57)
 - o Figure 4: CNS-localized W4B cells are transcriptionally distinct from splenic cells (58)
 - o Figure 5: W4B cells from the CNS have polyfunctional cytokine secretion and efficiently control WNV (59)

Part 2: Cell-intrinsic MAVS regulates mitochondrial metabolism to promote CD8+ T cell proliferation. (60- 104)

- 2.1: Introduction (62- 64)
- 2.2: Results (65- 74)
- 2.3: Discussion (74- 77)
- 2.4: Materials and methods (77-82)
- 2.5: Figures (85- 96)
 - o Figure 1: MAVS regulates mitochondrial number and elongation in activated CD8+ T cells (85-86)
 - o Figure 2: MAVS promotes oxidative phosphorylation in activated CD8+ T cells (87-88)

- Figure 3: MAVS-mediated metabolism promotes CD8+ T cell proliferation (89-90)
- Figure 4: *Mavs*^{-/-} W4B cells have dysregulated metabolic profiles during WNV infection (91-92)
- Figure 5: Cell-intrinsic MAVS promotes antigen-specific CD8+ T cell accumulation and cytotoxicity during WNV infection (93-93)
- Figure 6: MAVS promotes proliferation of antigen-specific CD8+ T cells during viral infection (95-96)
- 2.6: Supplemental Figures (97-104)

Discussion (105- 115)

- CD8+ T cell programming differs based on anatomic location (105- 109)
- MAVS and the mitochondrion (109-112)
- T cells and CNS function (112- 115)

References (116-135)

INTRODUCTION

West Nile Virus Pathogenesis and Immunity

West Nile Virus (WNV) is a neurotropic flavivirus that is endemic throughout the world. Originally identified in Uganda in 1937, WNV first came to the United States (U.S.) in 1999 where it caused an outbreak in New York and the surrounding region (1). WNV quickly disseminated across the U.S. and now causes annual outbreaks of encephalitis. Roughly 20% of infected individuals develop self-limiting febrile illness; however, in 1 out of 250 infected individuals WNV will spread to the central nervous system (CNS) (2, 3). WNV antigen has been detected in neurons and neuronal projections located in the spinal cord, brain stem, cerebellum, and cortices of infected individuals (4). WNV neuroinvasive disease can cause severe neurological symptoms including encephalitis, meningitis, and acute flaccid paralysis, along with milder symptoms such as disorientation or headaches (5-7). Patients that recover from WNV neuroinvasive disease often suffer from long term neurological impairment, including motor and memory dysfunction (8). Since 1999 there have been over 22,000 cases of WNV neuroinvasive disease in the U.S. and with no available vaccine or therapeutics approved for humans, WNV continues to represent a pressing public health problem (2).

WNV life cycle

WNV is an 11 kilobase positive sense single stranded RNA virus of the *Flaviviridae* family of arboviruses, other members of which includes Japanese Encephalitic Virus, Dengue Virus, and Zika Virus (9). WNV is an arthropod borne virus that circulates between birds and mosquitos with incidental infections in humans and other mammals including deer, rodents,

elephants and more (10, 11). WNV has been detected in up to 342 different species of birds across North America and Europe, with several different WNV lineages that circulate in avian populations. These lineages differ in pathogenicity with lineage 3 strains, such as Rabensburg Virus, causing subclinical infections in birds, while lineage 1 strains, such as NY99, caused widespread mortality in American crows (12). Interestingly, symptomatic Lineage 1 WNV infections in European avian populations are sporadic. Mutations in the NY99 strain could account for some of the differences in outcome between European and North American populations, as a single point mutation in the NS3 protein (T249P) identified in the NY99 strain caused higher viremia and mortality (13). Host genetics could also contribute to differential outcomes as certain species of birds are more susceptible to WNV with highest mortality rates found among American crows. Lastly, previous immunity could protect against mortality in European avian populations, as experimental inoculation of sparrows demonstrated the formation of neutralizing antibody responses to WNV (14). Challenge studies in house finches further showed cross-protection between St. Louis encephalitis virus and WNV, indicating that Flavivirus-experienced populations might be protected against novel strains (15). Regardless of symptom severity, experimental inoculation of sparrows and finches demonstrated high levels of viremia beginning within 24 hours and sustained until 6-7 days post infection (p.i.), thus enabling efficient infection of feeding mosquitos (14, 15).

WNV is circulated by *Culex* and *Aedes* mosquito species, which have a wide geographic range that contributes to the prevalence of WNV worldwide as well as the virus' ability to infect a large variety of mammals (16, 17). Once ingested during a blood-meal, WNV replicates first in the midgut of the mosquito and ultimately spreads to the salivary gland where it replicates to high levels, up to 10^7 plaque-forming unit equivalents (pfu) (18). Mosquitos protect against

pathology through Dicer2 dependent RNA-interference, which will bind to viral RNA and target it for degradation (19). Additionally, Dicer2 activation promotes the secretion of a Type I IFN analog (Vago) that activates the JAK-STAT pathway and further restricts viral burden in mosquitos (19-21). When a WNV infected mosquito encounters a mammal it will probe multiple times until reaching a blood vessel, depositing WNV into the skin with each probe. On average a mosquito will inoculate 10^6 pfu in a mammal host (22).

Entry of WNV to a target cell begins with binding to an unknown receptor, although several co-factors have been identified as supportive of WNV entry. The dendritic cell specific lectins, DC-SIGN and DC-SIGNR bind to glycosylated prM or E which enhances infection. However, neither DC-SIGN or DC-SIGNR were sufficient or necessary for WNV infection *in vitro* (23, 24). Additionally, DC-SIGN expression is restricted to a few immune cell subsets and WNV can infect a wide variety of cell types across various species, implying the existence of a highly conserved cellular receptor. Studies in a mosquito model of infection identified another lectin, mosquito C-type lectin, that enabled virus attachment and enhanced entry in a calcium dependent manner in mosquitos (25). Whether a similar pathway functions in mammalian cells is unknown. Non-lectin proteins have also been identified as entry co-factors, including transmembrane and immunoglobulin mucin (TIM) family phosphatidylserine binding proteins which facilitate infection by binding to phosphatidylserine on the surface of the WNV virion (26). Additionally $\alpha_v\beta_3$ integrin, which helps initiate the lipid raft pathway, has been reported as a WNV receptor through its ability to interact with WNV E protein (27, 28). However, later studies demonstrated that $\alpha_v\beta_3$ integrin was not necessary for WNV internalization, instead the virus utilizes the general lipid raft pathway to enter the cell (29). Upon attachment WNV virions are internalized by a clathrin-coated pit, and this process is dependent on Rab 5 (30, 31). After

internalization the endosome will acidify, inducing the E protein on the virion to extend into trimers to mediate fusion of the viral and endosomal membranes (32, 33). Thus, several proteins have been identified as supportive for WNV attachment and entry, but a definitive receptor is yet to be found.

Membrane fusion results in the release of infectious RNA directly into the cytosol, where the WNV genome is translated into a single polyprotein. WNV polyprotein is cleaved into 7 different proteins; three structural proteins (prM, E, C) that form the virion, and five non-structural proteins (NS1, NS2A, NS2B, NS3, NS4A, NS4B, and NS5) that have a variety of functions (33). Non-structural proteins NS3 and NS2B form a protease complex that is responsible for processing the viral polyprotein (34). Non-structural proteins also play a role in inhibiting the host immune response. For example, NS1 is a secreted glycoprotein that enables WNV infection by inhibiting the activation of complement protein C4 (35-37). Last, non-structural proteins have a key role in replicating the WNV genome. NS5 has both methyltransferase and RNA-dependent RNA polymerase activity, which enables copying into the antisense then back into the infectious form (38, 39). WNV genome replication occurs in specialized replication complexes formed by invaginations of the ER membrane which shield the dsRNA intermediate from host immune recognition (40, 41). The formation of ER replication complexes requires cholesterol redistribution and is dependent on NS4A-B and NS1 (42-44). After genome replication the ssRNA is secreted into the ER through a pore where it associates with structural proteins to form an immature virion (41). The immature virion travels through the ER-Golgi pathway and upon reaching the trans-Golgi a cellular furin protease will cleave immature prM into M (45). This results in a mature WNV enveloped virion with icosahedral

symmetry containing the replicated viral genome which is ultimately released from the cell through a secretory vesicle (46).

Pathogenesis of WNV infection in mice

WNV has an excellent mouse model that faithfully recapitulates natural infection by a mosquito via subcutaneous foot-pad injection (47). Once in the skin, the virus begins replication in keratinocytes, dermal dendritic cells (DCs), and Langerhans cells (48). Infected dendritic cells and other antigen presenting cells (APCs) home to the draining lymph node to initiate immunity, but this also results in the spread of the virus. Replication of WNV within the draining lymph nodes facilitates viremia by day 2 post-infection (p.i.) and subsequent spread to other target organs, which include the spleen (48). By day 4 p.i. viral burden reaches its peak in the spleen and serum, and is followed by neuroinvasion into the CNS beginning at day 6 p.i. (49). WNV replication peaks in the brain between day 8 and 10 p.i., and viral antigen has been noted in the cortex, brain stem, and spinal cord. WNV burden declines in the brain by day 15 p.i. However, WNV RNA is present in the brain and spinal cord for up to 3 months p.i. (50).

WNV can enter the brain through a variety of methods; first, the virus can enter the CNS via retrograde transport along nerves that are exposed in the periphery (51). WNV can move both retrograde and anterograde through axons and studies in hamsters found this contributes not only to entry to the CNS, but spread within the CNS as well (51). Second, excess inflammation caused by WNV infection can induce a breakdown of the blood-brain barrier (BBB) integrity, allowing the virus to directly cross the BBB (52). The BBB represents a vital barrier to infection, however cytokines released in response to infection, such as $\text{TNF}\alpha$ and $\text{IL-1}\beta$, weaken BBB integrity and promote the movement of WNV across the endothelial layer (53). Matrix-

metalloproteinase-9 is released by macrophages in response to WNV infection, and was found to increase BBB permeability thus facilitating WNV neuroinvasion *in vivo* (54). Conversely, Type I and III IFN production tightens the blood brain barrier (53, 55). Studies using a IFN λ -deficient mouse demonstrated that IFN λ had no effect on peripheral WNV infection or its replication in target cells. However, IFN λ was essential for promoting BBB integrity by regulating the localization of endothelial cell junction proteins, ZO-1 and claudin-5, to promote tight-junction formation and maintenance (55). Endothelial receptors can also regulate BBB breakdown, as ICAM-1 expression promotes BBB dysfunction and mortality *in vivo* (56). In contrast, AxL and MertK expressed on CNS radio-resistant cells tighten the BBB and restrict WNV entry to the parenchyma (57). Last, WNV can use the ‘Trojan Horse’ method of transit, in which an infected immune cell crosses into the CNS and disseminates the virus (58). Neutrophils are a target of WNV, and the entry of infected neutrophils into the CNS in a osteopontin-dependent manner promotes disease (58, 59). Once inside the CNS, WNV replicates directly in neurons and can spread transynaptically between neurons causing widespread infection (60). Ultimately, neuronal infection leads to pathology and neuronal death via upregulation of caspase-3 leading to apoptosis or targeting of infected neurons by infiltrating immune cells (61-63).

Immune cells circulating through the brain are primarily passing through blood vessels located in the meninges. The meninges is a protective tissue layer that envelops the brain and is comprised of the dura mater, arachnoid mater, and pia mater. The dura mater is the outermost layer and is highly vascularized. The arachnoid mater is the middle layer and is composed of a thin epithelial layer which serves as a barrier to limit the exchange of molecules from the dura mater into the subarachnoid space, a cerebrospinal fluid filled space. The final layer of the meninges, the pia mater, lines the outside of the parenchyma below the subarachnoid space and

is the final barrier to limit molecule movement into the brain (64). Recent work has highlighted the role of the meninges as an immunologically active space. The dura mater contains diverse subsets of immune cells even at steady state, including a substantial resident population of dendritic cells and border associated macrophages (65). Studies in models of multiple sclerosis have identified the meninges as an important checkpoint that licenses T cell entry into the parenchyma (66, 67). While the importance of meningeal immunity has been highlighted for autoimmune disorders, little is known about the contribution of the meninges to neuroinvasive viral infection.

The dura mater is also the location of the recently characterized CNS-draining lymphatic vessels. These vessels express Lyve-1 and CD31, classical markers of lymphatic vessels, and drain to the superficial and deep cervical lymph nodes (scLN and dcLN) (68) (Figure 1). The olfactory bulb and sinuses drain primarily to the scLN, while the cerebellum and cortices drain to the dcLN. CNS-draining lymphatics have been demonstrated to be functionally important for the drainage of CSF and macromolecules from the parenchymal space (69-71). Drainage through the CNS lymphatics is essential for CNS health, as studies in an Alzheimer's model demonstrated that disruption of meningeal lymphatic vessels exacerbated β -amyloid accumulation and disease severity (72). The CNS-draining lymphatics can also initiate immune responses to a CNS-specific antigen. In models of multiple sclerosis, drainage through the meningeal lymphatic system was necessary for the initiation of encephalitogenic T cell responses (68). Thus, the CNS-draining lymphatics are a key contributor to CNS immunity, however their role in the pathogenesis of viral infections is unclear.

Innate immunity to WNV infection in mice

Immunity to WNV begins with the production of cytokines by infected cells, especially Type I Interferons (IFN), which are protective against WNV as mice lacking the receptor for Type I IFNs (*Ifnar*^{-/-} mice) have greatly increased mortality compared to WT mice (73). Binding of Type I IFN to IFNAR results in the phosphorylation of receptor associated kinases, TYK2 and JAK1. These molecules relay the signal by phosphorylating a STAT-1 homodimer or a complex of STAT1/STAT2/IRF9, which then translocates to the nucleus to act as a transcription factor for antiviral gene expression (74). Several antiviral interferon-stimulated genes (ISGs) have been demonstrated to restrict WNV infection. RNaseL cleaves viral RNA products to amplify detection by pattern recognition receptors, and inhibits WNV replication in macrophages and murine embryonic fibroblasts (75). Subsequently, mice lacking RNaseL have increased viral load in peripheral tissues early during the course of WNV infection (76). The ISG protein kinase R (PKR) is a serine/threonine protein kinase that inhibits the translation of viral RNA, and was also found to contribute to early protection against WNV infection in mice (76). Characterization of ISGs is still ongoing, but IFITM3, IFIT2, Viperin, and *Ifi2712a* have all been identified as having roles in restricting WNV infection of the CNS (77-80). Thus, Type I IFN signaling restricts WNV infection through the induction of ISGs.

Type I IFN also serves to activate a variety of innate immune cells, including natural killer (NK) cells, neutrophils, and dendritic cells (DCs). NK cells can bind WNV E protein via NKp44, to trigger degranulation which may help clear infected cells (81). While depletion of NK cells does not alter WNV pathogenesis in mice, studies of mice lacking IFN signaling identified IFN-promoted NK cell expansion as critical for the restriction of WNV in the liver (82, 83). Type I IFN production will also recruit neutrophils, and accordingly increased numbers of neutrophils are detectable in the CNS and periphery after WNV infection (84). Antibody

depletion of neutrophils before infection resulted in lower viral burden, whereas depletion after infection increased viral burden. Suggesting that neutrophils may be pathogenic early, but protective later in the course of WNV infection to protection (58). Further studies are needed to more precisely delineate the role of NK cells and neutrophils during WNV infection.

Dendritic cells are not only a key target of WNV infection, but also play a crucial role in restricting viral infection, secreting Type I IFN and inflammatory cytokines, and initiating adaptive immunity (84-88). There are many subsets of dendritic cells, including conventional dendritic cells (cDCs), which are descended from the DC precursor and excel at antigen presentation. Specific deletion of IFNAR on cDCs led to higher viral burden and increased mortality in mice, supporting a protective role for cDCs during WNV infection (86). cDCs can be divided into two subsets, cDC Type I (cDC1) and Type II (cDC2). cDC1s are defined as IRF8+XCR1+ and are characterized by their ability to cross-present antigen on MHC-I to efficiently prime CD8+ T cells (89, 90). In contrast, cDC2s are defined as IRF4+CD172a+ and primarily present antigen on MHC-II to prime CD4+ T cells (90). Selective deletion of cDC1s but not cDC2s through the ablation of *Batf3*, demonstrated that antigen presentation by cDC1s is essential for the generation of protective CD8+ T cell responses against WNV infection in mice (91). Thus, cDCs play an important role not only in restricting WNV infection, but also initiating WNV-specific adaptive immunity.

CD8+ T cells during neuroinvasive West Nile Virus Infection

Adaptive immune responses are essential for protection against WNV with both B and T cells playing critical roles in limiting viral replication. WNV-specific antibodies are detectable in

recovered patients against a variety of WNV proteins and have been demonstrated to neutralize the virus post-attachment (92, 93). Mice lacking B cells display increased pathology in the brain and higher viral loads (52). Murine studies also found that WNV-specific IgM and IgG provide protection as demonstrated by passive transfer studies (94, 95). Analysis of serum from WNV convalescent patients have identified CD4⁺ T cell responses directed against the E protein of WNV (96). In mice, CD4⁺ T cells are important for protection against WNV with *Cd4*^{-/-} mice demonstrating increased morbidity, higher viral loads, and increased pathology between 10-15 days p.i. (97). CD8⁺ T cells also play an essential role in protection against neuroinvasive West Nile Virus infection. Analysis of symptomatic WNV patients identified WNV-specific CD8⁺ T cell responses, which were primarily restricted to a few epitopes (98). WNV-specific CD8⁺ T cells were found to produce IFN γ and TNF α in response to stimulation with WNV peptide. Additionally, the de-granulation marker CD107a was upregulated on WNV-specific CD8⁺ T cells and correlated with neuroinvasive disease in humans (99). Early studies in mice demonstrated that *MhcI*^{-/-} or *CD8 α* ^{-/-} mice had increased morbidity and viral burden as compared to WT mice. Histopathology analysis also showed greater neuronal death in the mice lacking CD8 α , thus demonstrating the necessity of CD8⁺ T cells in protection against neuronal injury (100).

Dynamics of CD8⁺ T cells during WNV infection

The CD8⁺ T cell response to viral infection begins when a naïve CD8⁺ T cell circulating through secondary lymphoid organs encounters an antigen-presenting cell (APC). Naïve T cells are activated by T cell receptor (TCR) interactions with cognate antigen presented on MHC-I, co-stimulation through CD28, and cytokine polarization directed by cDCs (reviewed in (101)). In

WNV infection, cDC1 presentation of WNV-peptide complexed to MHC-I was demonstrated to be essential for the proper priming of CD8⁺ T cells (91, 102, 103). Secretion of Type I IFN by cDCs or other APCs provides an additional signal to bolster cytotoxic T cell responses against WNV (103). After TCR stimulation, CD8⁺ T cells will undergo rapid proliferation and differentiation into short-lived terminal effector cells (SLECs) or memory precursor effector cells (MPECs). Effector CD8⁺ T cells will downregulate CD62L and upregulate CD44 and other adhesion markers to allow migration into tissue where CD8⁺ T cells will identify infected cells for killing (101, 104). During WNV infection of wild-type mice, CD8⁺ T cells increase in number in the spleen until their expansion peaks around day 7 post infection. In the brain, CD8⁺ T cells begin infiltrating the parenchyma at 7 days p.i. and peak in numbers between 9-11 days p.i. (100). After peak infection, SLECs will undergo apoptosis, and overall numbers of CD8⁺ T cells will contract by day 10 p.i. in the spleen and day 15 p.i. in the brain of WNV infected mice (100). After contraction, MPECs will differentiate into memory CD8⁺ T cells, which can reside in the brains of mice recovered from WNV as tissue resident memory CD8⁺ T Cells (Trm) (105).

Several different TCR specificities can be found throughout the course of the CD8⁺ T cell response to WNV, however the repertoire is primarily comprised of one immunodominant TCR clonality specific for the peptide sequence SSVWNATTAI, found within the NS4B protein of WNV (106). Our lab has previously generated and characterized a transgenic mouse model with CD8⁺ T cells specific to this NS4B immunodominant epitope, referred to as W4B CD8⁺ T cells (104). In our W4B mouse model, more than 95% of the CD8⁺ T cells stain positive for the NS4b tetramer. Comparison of W4B cells to wild-type (WT) CD8⁺ T cells found similar rates of expansion, cytokine profiles, and tissue residency. Additionally, transfer of W4B cells to naïve

mice provided protection against WNV in the brain. Thus, W4B mice represent a powerful tool through which we can track and assess WNV specific CD8⁺ T cell responses (104).

Regulation of CD8⁺ T cells in the CNS

WNV neuroinvasion induces an influx of CD8⁺ T cells into the brains of infected mice, however the entry of WNV-specific CD8⁺ T cells into the brain parenchyma is tightly regulated. Release of CCL5 and CCL3 in the cortex or cerebellum of WNV-infected mice promotes CCR5 dependent entry of CD4⁺ and CD8⁺ T cells into the brain (107). CXCL10 produced by infected neurons also promotes recruitment of CD8⁺ T cells to the brain via interactions with CXCR3 (108, 109). Other cytokines restrict the ability of CD8⁺ T cells to enter the parenchyma, such as CCR7, which promotes return of CD8⁺ T cells to the lymph node thus restricting neuroinflammation during WNV infection (110). IL-17 α may also play a role in regulating the migration of CD8⁺ T cells, as mice lacking IL-17 α showed an increase in the number of both CD4⁺ and CD8⁺ T cells in the brain (111). WNV infection of neurons prompts the secretion of high levels of IL-1 β , which restricts the influx of CD8⁺ T cells into the brain (112). Mechanistically, IL-1 β binds to IL-1R on the endothelial cells of the blood-brain barrier prompting the secretion of CXCL12 into the blood vessel. CXCL12 binds to CXCR4 expressed on circulating CD8⁺ T cells, which keeps the T cells in the blood vessel, and prevents unnecessary CD8⁺ T cell infiltration into the parenchyma (113). Beyond chemokine interactions, activation receptors can also regulate CD8⁺ T cell entry to the CNS. CD40 expression on endothelial cells of the brain was essential for promoting the movement of CD8⁺ T cells out of blood vessels and into the brain parenchyma during WNV infection (114). When taken together,

these studies demonstrate that the migration of CD8⁺ T cells into brain parenchyma is a controlled process that is fine-tuned by the integration of signals from multiple cytokines.

Differential localization to the parenchyma, meninges, CNS-draining lymph nodes and periphery may impact T cell programming. In the lymphocytic choriomeningitis virus (LCMV) model, splenic antigen-specific CD8⁺ T cells from white pulp and red pulp of the spleen exhibited phenotypic and functional differences, supporting that anatomic localization can influence antiviral T cell responses via environmental cues (115). During coronavirus infection, CD8⁺ T cells were shown to require a re-activation signal for effective viral clearance after recruitment by CCL19 and CCL21-producing stroma cells in the meninges (116). In the experimental autoimmune encephalitis (EAE) model, CNS-infiltrating auto-reactive CD4⁺ T cells have been shown to contribute to CNS damage following reactivation within the meninges upon stimulation from local APCs presumably presenting myelin antigen (66, 117). Last, during WNV infection, there is evidence that upon CNS entry, CD8⁺ T cells are ‘re-licensed’ via interactions with brain-resident CD11c⁺ DCs (118). Altogether, these findings suggest that localization to the CNS space re-programs antigen specific CD8⁺ T cells; however, the impact of re-programming on T cell function is not well understood.

Mechanisms of viral clearance by CD8⁺ T cells

Once CD8⁺ T cells enter the brain parenchyma, they utilize a variety of cytolytic and non-cytolytic mechanisms to control WNV infection. Early studies found that production of IFN γ and TNF α by CD8⁺ T cells is associated with a better prognosis (100, 112). Mechanistic work in mice has determined that IFN γ and TNF α protect against mortality, and restrict viral

infection of neurons non-cytolytically through JAK/STAT signaling (49, 119, 120). Perforin is a cytotoxic molecule released by effector CD8⁺ T cells that activates the intrinsic apoptotic pathway, and was found to be essential for limiting viral burden and mortality during WNV neuroinvasive disease in mice (82). FasL and TRAIL are both expressed on the surface of effector CD8⁺ T cells and bind to receptors on the target cell to induce the extrinsic apoptotic pathway. FasL and TRAIL were demonstrated to promote CD8⁺ T cell mediated control of WNV in the brain by inducing apoptosis of infected neurons (121, 122) (Figure 1). Thus, CD8⁺ T cells use a variety of mechanisms to control WNV infection in neurons.

Innate Immune Signaling during viral infections

Toll-like Receptor Pathway

Toll-like receptors (TLRs) are a family of 12 membrane embedded pattern recognition receptors (PRRs) that detect pathogen associated molecular patterns (PAMPs). TLRs can be localized to the cell surface, endosome, or lysosome. TLRs detect a variety of bacterial, fungal, and viral PAMPs depending on the location and TLR identity. Cell surface localized TLRs primarily recognize bacterial and fungal motifs, such as TLR4 which recognizes LPS. However, TLR3, 7, and 9 are endosomal TLRs that recognize viral RNA (dsRNA, ssRNA, and CpG motifs respectively) (123, 124). TLRs are composed of a leucine-rich repeat ectodomain that recognizes the PAMP, a transmembrane domain, and a Toll-IL-1R (TIR) domain that initiates downstream signaling. Upon recognition of a PAMP, the TLR will recruit adaptor proteins MyD88 or TRIF to the TIR domain which will relay the signal and result in the eventual translocation of NF κ B or IRF-3, -7 to the nucleus. Together these transcription factors induce production of Type I IFN

and the initiation of anti-viral gene expression (125). During WNV infection, the TLR pathway helps protect against disease as TLR3 and TLR7, but not TLR9, promote survival and restrict viral burden in the CNS (126, 127). Accordingly, MyD88 signaling also restricted CNS viral burden to promote survival and reduce pathology during WNV infection of mice (128). Thus, the TLR pathway is critical for restricting WNV infection.

Nod-like Receptor Pathway

Nod-like receptors (NLRs) are a family of pattern recognition receptors that are comprised of three general domains, a protein-protein interaction domain (CARD or PYD), a nucleotide binding domain responsible for oligomerization of the NLRs, and a leucine rich region which senses the pathogen. NLRs are encoded by a family of 22 genes and can recognize a wide variety of PAMPs and danger-associated molecular patterns (DAMPs) ranging from LPS to viral RNA/ DNA to intracellular ATP. Two of the best studied NLRs are NLRP3, which can recognize a broad range of fungi, bacteria, and virus, and NLRC4, which primarily recognizes bacteria (129, 130). Once a NLR encounters a PAMP, it will oligomerize with other NLR proteins and recruit apoptosis associated speck like protein (ASC). ASC is composed of a PYD and CARD domain. The PYD domain interacts with the NLR while the CARD domain can bind to pro-caspase-1. Assembly of NLR, ASC, and pro-caspase 1 forms a complex called the inflammasome, which induces the auto-proteolytic cleavage of pro-caspase-1 into active, enzymatic caspase-1 (131). Cleaved caspase-1 will subsequently cleave pro-IL-1 β or pro-IL-18 into the mature form resulting in cytokine release from the cell to begin a pro-inflammatory response (131). Activated caspase-1 can also cleave Gasdermin D, which subsequently inserts into the plasma membrane to form pores and ultimately results in pyroptosis, a form of pro-

inflammatory cell death (132). Thus, recognition of a virus by NLRs results in inflammasome formation and pro-inflammatory cytokine release or cell death.

During WNV infection of mice, NLRP3 but not NLRC4 was found to promote survival (112). NLRP3 restricted viral burden in the CNS and promoted IL-1 β secretion (112). Accordingly, ASC also protected against mortality and CNS viral burden during WNV infection (133). Production of IL-1 β and expression of IL-1R are essential for protection against WNV and limiting CNS viral burden (112). IL-1R signaling on dendritic cells or macrophages was key to inducing expression of antiviral genes and Type I IFN during WNV infection *in vitro* (134). Analysis of IL-1 β *in vivo* has demonstrated that IL-1R signaling is also essential for the dendritic cell mediated priming of T cells and regulating recruitment of T cells across the BBB (113, 118). Together these data demonstrate the importance of inflammasomes and IL-1 β signaling in controlling WNV infection.

Rig-I-like Receptor Pathway

The Rig-I-like receptor (RLR) family is a group of DExD/H box RNA helicases which includes RIG-I, MDA5, and LGP2 that function as pattern recognition receptors (PRRs) to recognize viral RNA. RIG-I and MDA5 detect non-self, viral RNA by binding to pathogen associated molecular patterns (PAMPs). WNV contains multiple PAMPs that allow RIG-I to bind both positive and negative sense WNV RNA (135). Upon binding of viral RNA by RIG-I and MDA5, the PRRs undergo K63-linked ubiquitination which induces a conformational change allowing their CARD domains to become accessible (136, 137). LGP2 lacks CARD domains and does not bind viral RNA (138). Instead, LGP2 appears to act as a negative regulator

of RIG-I activation by preventing its ubiquitination, thus providing a mechanism for fine tuning of the RLR pathway response during viral infections (139, 140). Upon adoption of an 'open' conformation the CARD domains of RIG-I and MDA5, will bind to mitochondrial antiviral signaling protein (MAVS), which is the central adaptor protein for the RLR pathway. MAVS consists of a CARD domain, a proline rich region, and a transmembrane domain that tethers MAVS to the mitochondrial membrane. Binding of RIG-I/MDA5 to the MAVS' CARD domain will induce oligomerization of MAVS on the mitochondria (141). The MAVS aggregate is then able to recruit a wide variety of proteins and serve as a scaffolding complex for the phosphorylation or ubiquitination of downstream signaling molecules (138) (Figure 2).

The MAVS signalosome serves as the central hub for the RLR pathway and during canonical RLR signaling, MAVS aggregates recruit TBK1 and IKK ϵ to undergo phosphorylation. Activated TBK1 and IKK ϵ in turn phosphorylate IRF3 and IRF7, allowing their translocation to the nucleus where the IRFs promote transcription of Type I IFN (85) (Figure 2). During WNV infection of dendritic cells *in vitro*, MAVS was shown to be essential for the induction of Type I IFN. Interestingly, Type I IFN could be produced independently of IRF3 and IRF7, and instead the RLR pathway could signal through IRF5 to induce Type I IFN. Thus, IRF-3, -5, and -7 play semi-redundant roles in initiating the Type I IFN response during WNV infection (85). ELF4 was also found to be critical in protection against WNV, as activation of ELF4 by the MAVS signalosome results in cooperative binding of ELF4 and IRF-3,-7 to enhance Type I IFN production (142). Thus canonical RLR signaling results in a highly coordinated and regulated production of Type I IFN.

However, MAVS has been linked to a multitude of pathways beyond Type I IFN production. MAVS aggregates promote the phosphorylation of IKK α and IKK β , which in turn

activate NF- κ B (138). NF κ B is an positive regulator of the immune response that will promote the activation of DCs, antiviral effector genes, and the production of pro-inflammatory cytokines (reviewed in (143)) (Figure 2). MAVS signaling can also induce cell death through the activation of caspases-3/7, caspase-8, p53 signaling, or NLRP3 inflammasome formation (144-146) (Figure 2). Additionally, RLR signaling is linked to the regulation of mitophagy and mitochondrial dynamics. RIG-I mediated induction of the RLR pathway promotes mitochondrial elongation and autophagy *in vitro* (147, 148). RLR mediated autophagy is dependent on LC3 and induced by ectopic expression of MAVS, which results in a disruption of the mitochondrial membrane potential. This initiates a feedback-loop mechanism, in which mitophagy prevents excess Type I IFN production during viral infections (148) (Figure 2). MAVS interacts with several key regulators of mitochondrial dynamics. MAVS signaling is inhibited by NLRX1, a NOD-like receptor, and mitofusin-2 (MFN2), a key regulator of mitochondrial fusion (149, 150). Whereas, mitofusin-1 (MFN1) and Tom70, a mitochondrial protein translocase, potentiate MAVS signaling (149-152). Thus, MAVS signaling serves as central hub for controlling cytokine production, cell death, and even metabolism.

RLRs during WNV infection

The RLR pathway is critical for protection against *flaviviruses*, including WNV. *Ex vivo* studies in mouse embryonic fibroblasts found that both RIG-I and MDA5 are activated by WNV infection, with RIG-I playing a role early in infection, and MDA5 predominating later during infection (153). *In vivo*, mice lacking RIG-I or MDA5 have increased mortality during WNV infection. MDA5 knockout mice have higher viral loads in the serum and CNS (154). MAVS also has an important role in protection against WNV infection, as *Mavs*^{-/-} mice have increased mortality, viral load in both the periphery and CNS, and pathology as compared to WT mice.

MAVS not only promotes Type I IFN production, but also restricts inflammatory cytokine production, regulates dendritic cell subset composition, and contributes to the formation of balanced T and B cell responses (84).

Studies of T and B cell responses have demonstrated significant impacts of the RLR pathway on adaptive immunity. Antibody levels are altered in mice lacking MAVS and follow-up studies with a non-pathogenic strain of WNV (WNV-Madagascar) found that MAVS signaling in cDCs drove memory B cell responses (84, 87). Mice lacking MAVS also have altered CD4 T cell responses as investigations with WNV-Madagascar found that primary CD4 T cell responses require MAVS signaling, but recall responses are unaffected (155). Additionally, MAVS promotes the expansion and function of T regulatory cells (Treg) in the CNS in an extrinsic manner (84, 156). CD8⁺ T cell responses are also impacted by RLR signaling. Cell-intrinsic LGP2 was found to promote CD8⁺ T cell fitness and survival by regulating CD95 dependent apoptosis in the CNS (157). Adoptive transfer studies identified MDA5 as necessary for CD8⁺ T cell control of virus in the CNS but not the periphery (154). Finally, global loss of MAVS signaling results in an exaggerated influx of CD8⁺ T cells into the parenchyma (84). However, the cell-specific impact of MAVS signaling on CD8⁺ T cell function in the CNS has not been addressed.

Summary

In the following work, we explore the regulation of CD8⁺ T cells in the CNS during WNV infection. In part 1, we investigate the contribution of anatomic localization to the regulation of CD8⁺ T cell phenotype and function. We demonstrate that substantial differences exist in the expression of activation markers, inhibitory receptors, and cytokine secretion between WNV-

specific CD8⁺ T cells localized to the periphery, CNS-draining lymph nodes, meninges, and brain parenchyma. Peripheral and brain parenchymal localized CD8⁺ T cells had the most disparate phenotypes, with substantial transcriptomic differences in cytokine responses, effector molecules, and metabolic pathways. A co-culture system determined that brain resident CD8⁺ T cells were more efficient at controlling WNV than peripheral CD8⁺ T cells. We next investigated cell-intrinsic factors that might contribute to the unique profile of brain localized CD8⁺ T cells. As RLR signaling pathway components have been previously implicated in the regulation of CD8⁺ T cell responses in the CNS, in part 2 we determined the cell-intrinsic role of MAVS in CNS-localized CD8⁺ T cells. First, we found that MAVS promotes mitochondrial elongation and oxidative phosphorylation in response to TCR stimulation. *In vivo* this led to a dysregulated metabolic profile and decreased mitochondrial potential in the absence of MAVS. Furthermore, MAVS-mediated metabolism promoted CD8⁺ T cell expansion in response to TCR stimulation and was essential for promoting the expansion of WNV-specific CD8⁺ T cells in the CNS in a mouse model. Together, these data find that cell-intrinsic MAVS regulates mitochondrial metabolism to promote WNV-specific CD8⁺ T cell expansion in the CNS.

Figure 1.

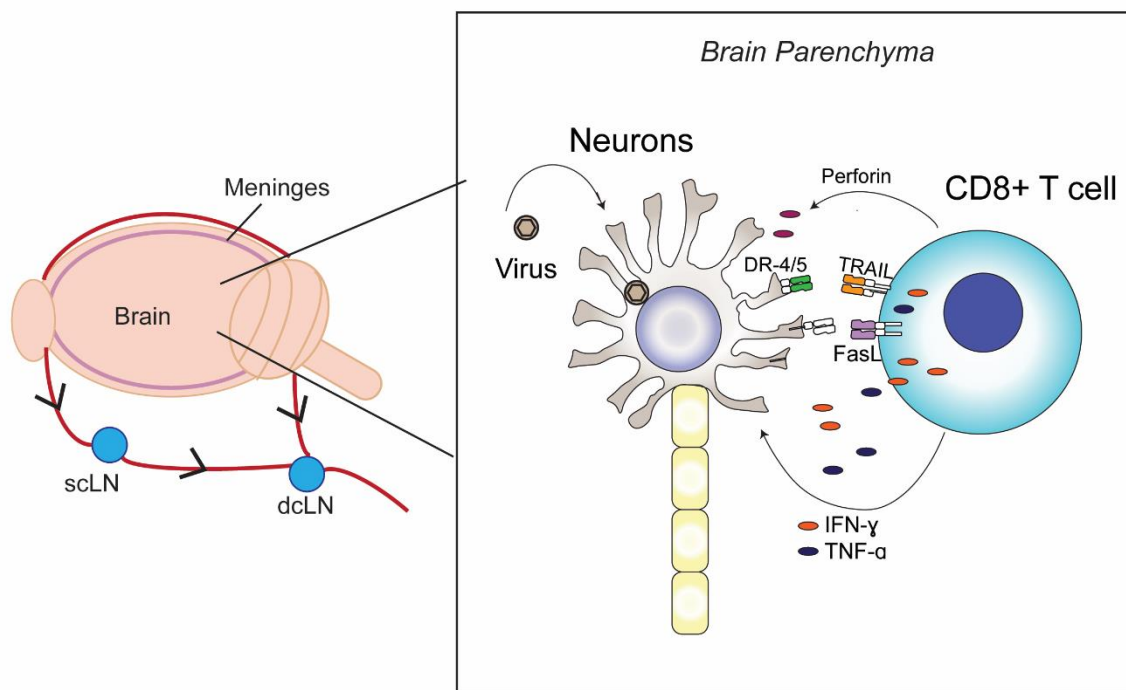


Figure 1. CD8+ T cells use cytolytic and non-cytolytic mechanisms to control virus in the CNS. The brain parenchyma is enclosed by a meningeal layer through which lymphatic vessels run. These lymphatic vessels take up cerebrospinal fluid, macromolecules, and immune cells which are drained to either the superficial cervical or deep cervical lymph node (scLN and dcLN). WNV replicates directly in neurons upon reaching the brain parenchyma. WNV-specific CD8+ T cells home to the infected parenchyma where they identify infected neurons and use cytotoxic molecule secretion (perforin), cytotoxic receptor expression (FasL, TRAIL), and non-cytotoxic cytokine secretion (TNF α , IFN γ) to control viral replication in neurons.

Figure 2.

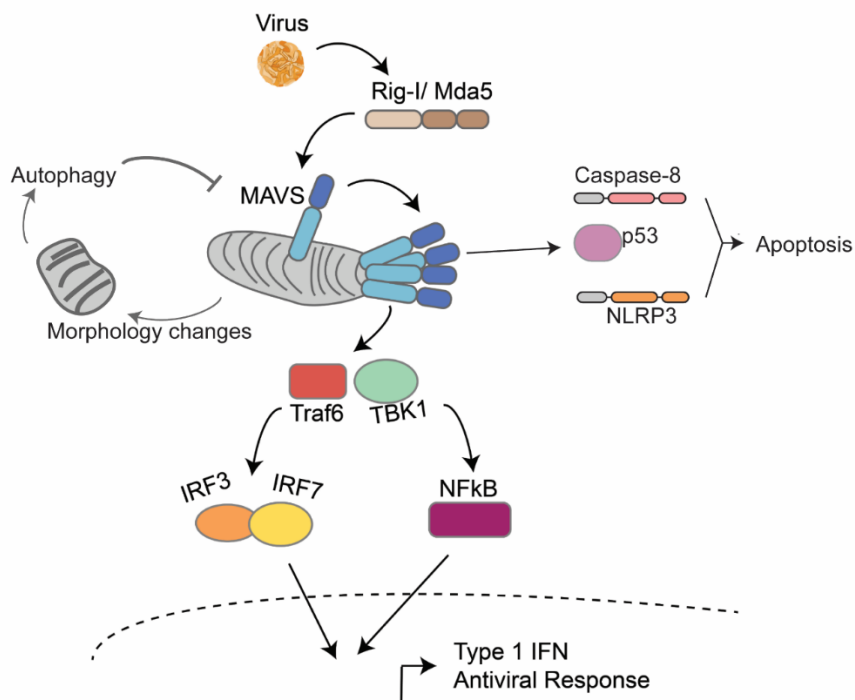


Figure 2. MAVS is the central hub for the Rig-I Like receptor signaling pathway. RLR signaling begins with the recognition of viral RNA PAMPs by the PRRs, RIG-I or MDA5. The RLR will undergo a conformational change allowing its CARDs to bind to corresponding CARD domains on MAVS. MAVS is located on the outer mitochondrial membrane, and upon binding with a RLR, MAVS will form prion-like aggregates which form the central signaling hub for downstream relays. MAVS will recruit and facilitate the phosphorylation of Traf6 and TBK1, which in turn phosphorylate IRF3/7 and NFκB. This ultimately leads to the transcription of Type I IFNs and other antiviral genes. MAVS can also interact with Caspase-8, p53, and the NLRP3 inflammasome to promote apoptosis. MAVS signaling is intricately linked with mitochondrial dynamics, and activation of MAVS can promote mitophagy, which in turn downregulates RLR signaling.

PART 1**Entry of West Nile virus into the central nervous system draining lymphatics precedes differential programming of CD8+ T cells in the brain**

Abigail Vanderheiden^{1,2,¶}, Justin T. O’Neal^{1,2,¶}, Devon J. Eddins^{1,2}, Renan Aguilar-Valenzuela^{1,2}, Jasmine Herz⁴, Jonathan Kipnis⁴, Arash Grakoui^{2,3}, Mehul S. Suthar^{1,2,3 *}

¹Department of Pediatrics, Division of Infectious Disease, Emory University School of Medicine, Atlanta, GA 30322, USA.

²Emory Vaccine Center, Emory University School of Medicine, Atlanta, GA 30329, USA.

³Yerkes National Primate Research Center, Atlanta, GA 30329, USA.

⁴Center for Brain Immunology and Glia (BIG), Washington University in St. Louis, School of Medicine, St. Louis, MO 63110, USA.

¶ These authors contributed equally to this work

*Corresponding Author

This paper has been submitted at Plos Pathogens.

ABSTRACT

Neuroinvasive West Nile virus (WNV) infection requires CD8⁺ T cell responses for virologic control in the central nervous system (CNS). Here, we investigate the contribution of the CNS-draining lymph nodes (LNs) and meninges to WNV pathogenesis and CD8⁺ T cell immunity. We found that the meninges and CNS-draining LNs have detectable WNV RNA early during pathogenesis, prior to parenchymal invasion. Characterization of the immune response in these compartments observed conventional dendritic cell accumulation and activation corresponding to viral kinetics. WNV-specific CD8⁺ T cells in the CNS-draining LNs and meninges were activated and in the effector phase. However, WNV-specific CD8⁺ T cells in the brain and meninges had distinct cytokine and inhibitory marker expression as compared to CNS-draining lymph nodes. A neuronal-CD8⁺ T cell co-culture model demonstrated that this profile contributed to more efficient control of WNV in infected neurons. These findings highlight the early involvement of CNS-draining lymphatics during WNV pathogenesis and how anatomic localization influences CD8⁺ T cell function.

INTRODUCTION

West Nile virus (WNV) is a neurotropic mosquito-borne flavivirus of global importance (6, 83, 158-160). Neuroinvasive WNV infection results in encephalitis and can lead to prolonged neurological impairment or death (6, 158-160). Induction of the host response mediates early virologic control in the periphery and promotes priming of adaptive immunity (161-163). Following early replication and dissemination to secondary lymphoid tissues, the neuroinvasive stage is characterized by brain parenchymal invasion, neuronal infection, neuroinflammation, and neuronal cell death (83, 164).

Meningeal immunity has been demonstrated to play a pivotal role in central nervous system (CNS) defense against pathogen invasion (116, 165, 166). Antigen-presenting cells (APCs), such as dendritic cells (DCs) and border-associated macrophages (MΦs), within the meninges (dura, arachnoid and pia mater), choroid plexus, and perivascular spaces serve in an immune surveillance capacity to protect the CNS from invading pathogens (167-169). Immune cells traffic through meningeal lymphatic vessels, which drain to the superficial and deep cervical lymph nodes (scLNs and dcLNs, respectively) and support interactions between peripheral and CNS-localized immune cell populations (68-71). Conventional DCs (cDCs) excel at initiating T cell responses by presenting antigen on MHC I (major histocompatibility complex class I) and MHC II, and directing T cell polarization through cytokine secretion. In contrast, plasmacytoid DCs (pDCs) are less efficient at antigen presentation, but produce extensive amounts of type I interferon (IFN-I) in response to viral RNA and DNA (170-173). DCs, a key target cell of WNV infection, limit early viral replication and dissemination in the periphery through the production of IFN-I, pro-inflammatory cytokines, and priming of both humoral and cell-mediated responses (84-86, 91, 95,

118). Previous studies indicate that *Batf3*^{-/-} mice, which lack cDC1s, fail to generate optimal WNV-specific effector CD8⁺ T cell responses (91, 103). Furthermore, infected and bystander CD8 α ⁺ CD11c⁺ DCs, but only infected CD11b⁺ CD11c⁻ myeloid cells, have been shown to present the immune-dominant WNV NS4B peptide epitope in complex with MHC I during WNV infection. Thus, supporting that DCs are critical for priming protective CD8⁺ T cell responses (174). Altogether, we have a broad understanding of the kinetics of viral spread in major tissue compartments and the integral role of DCs in virologic control; however, an in-depth examination of viral kinetics and immune cell dynamics within the meninges and CNS-draining lymphatics is notably lacking.

CD8⁺ T cells are essential for control of WNV infection (100, 175). Mice lacking CD8 α or MHC-I exhibit increased mortality, higher viral burden in the CNS and periphery, and exaggerated pathology in the brain compared to wild-type mice (100). During WNV neuroinvasive disease, CD8⁺ T cells enter the brain parenchyma from the meningeal vasculature in a CXCR3 dependent fashion (108, 176). Once in the parenchymal space, CD8⁺ T cells control WNV through the secretion of cytotoxic molecules, and production of antiviral cytokines such as TNF- α and IFN- γ (49, 82, 121, 122, 177-179). CNS-infiltrating antiviral CD8⁺ T cells require a reactivation signal from CNS-localized DC or M Φ populations during WNV infection, and the meninges have been speculated to be the site of these crucial interactions (118, 180). However, the characteristics of meningeal APCs and CD8⁺ T cells has not been assessed during WNV infection.

Differential localization to the parenchyma, meninges, CNS-draining LNs and periphery may impact T cell programming. In the lymphocytic choriomeningitis virus (LCMV) model, splenic

antigen-specific CD8⁺ T cells from white pulp and red pulp of the spleen exhibited phenotypic and functional differences, supporting that anatomic localization can influence antiviral T cell responses via environmental cues (115). During coronavirus infection, CD8⁺ T cells were shown to require a re-activation signal for effective viral clearance after recruitment by CCL19 and CCL21-producing stroma cells in the meninges (116). In the experimental autoimmune encephalitis (EAE) model, CNS-infiltrating auto-reactive CD4⁺ T cells have been shown to contribute to CNS damage following reactivation within the meninges upon stimulation from local APCs presumably presenting myelin antigen (66, 117). Altogether, these findings suggest that localization to the CNS space re-programs antigen specific CD8⁺ T cells; however, whether this process occurs during WNV infection is unknown.

In this study, we investigated how CNS-draining lymphatics and meninges contribute to WNV pathogenesis, and CD8⁺ T cell immunity. We found that WNV RNA was detectable in the CNS-draining lymphatics and meninges prior to infiltration to the parenchyma. cDC activation and accumulation corresponded to peak viral burden in each tissue. Accumulation of WNV-specific CD8⁺ T cells in the CNS-draining LNs occurred prior to meningeal T cells expansion, which increased at later time points concurrent with brain T cell populations. Splenic and brain WNV-specific CD8⁺ T cells exhibited disparate phenotypic profiles, while T cells from CNS-draining LNs and meninges displayed unique intermediate signatures. Substantial transcriptional differences were observed for splenic and CNS-localized WNV-specific CD8⁺ T cells, with CNS-localized WNV-specific CD8⁺ T cells exhibiting high inhibitory receptor and cytokine expression. Most notably, CNS-localized antigen-specific CD8⁺ T cells were more efficient at controlling WNV infection of cortical neurons than splenic antigen-specific CD8⁺ T cells. Thus,

demonstrating that anatomic localization influences the phenotypic signature and functional capacity of WNV-specific CD8⁺ T cells. Our findings represent the first comprehensive analysis of early viral kinetics and immune cell dynamics between peripheral, CNS-draining lymphoid tissues, meninges, and brain during neuroinvasive flavivirus infection.

RESULTS

Viral RNA detection and activated cDC accumulation in CNS-draining lymph nodes precede parenchymal invasion. To determine which components of the CNS and CNS-draining lymphatics, which include the superficial cervical lymph node (scLN) and deep cervical lymph node (dcLN), are seeded by WNV and evaluate viral kinetics, we performed qPCR for viral RNA on CNS-draining LNs, brain, and meninges (**Fig. 1A**). WNV was detectable in the scLN and dcLN by 2 days p.i., with viral RNA peaking between 4-6 days p.i. (**Fig. 1B**). Viral RNA was detectable in the meninges as early as 4 days p.i., preceding the initial spike in viral replication in the brain which occurred between 4 and 6 days p.i. (**Fig. 1B**). Notably, CNS-draining LNs and meninges did not show a decline in viral RNA burden by 6 days p.i. unlike other peripheral compartments (**Fig. 1B**). Analysis of interferon-stimulated genes, IFIT1 and RSAD2, showed an increase in expression by day 2 p.i. and peaking at day 4 p.i. in the scLN. ISG expression in the dcLN began at day 4 p.i. and increased through day 6 p.i. ISG expression in the meninges and brain was undetectable until day 4 p.i. (**Fig. 1C-D**). Thus, WNV seeds the CNS-draining lymphatics and meninges and induces ISG expression prior to parenchymal invasion.

Since DCs and macrophages are important targets of WNV infection, we sought to define the dynamics of antigen presenting cell populations within the CNS-draining lymph nodes and meninges. Monocyte numbers peaked at day 2 p.i. in the scLN and dcLN, declining by day 8 p.i. In contrast, monocyte numbers did not increase in the meninges and brain until 8 days p.i. (Fig. 2A). moDCs peaked between 2-4 days p.i. in the CNS-draining lymph nodes, but did not significantly increase in the meninges (Fig. 2B). cDC1 and cDC2 populations had similar kinetics, peaking in the scLN and dcLN at day 2 p.i., while meningeal and brain cDCs did not increase until

day 8 p.i. (Fig. 2C-D). pDC numbers remained steady in most compartments with a small increase observed in the dcLN at day 8 p.i. (Fig. 2E). In total, APC population dynamics correlated with viral kinetics in the scLN and dcLN, while the meninges and brain had a delayed accumulation of APC populations in response to WNV infection.

As discussed above, cDCs are critical for priming an effective antigen specific T cell response. Therefore, we performed further analysis on the cDC population to determine activation status. We investigated the expression of MHC-I and CD86 on cDCs across CNS tissues during peak viral burden for each respective tissue (see Fig. 1B). cDCs isolated from the scLN, dcLN, and meninges all had increased expression of MHC-I (1.5-2-fold increase over mock) at 4 days p.i. (Fig. 2E-F). CD86 expression was elevated compared to mock in the scLN (~ 2-fold). However, CD86 was not significantly enriched on cDCs in the dcLN or meninges at 4 days p.i., indicating that some tissue-specific effects are impacting activation (Fig. 2E-F). We also noted that both MHC-I and CD86 had much lower expression on day 0 and day 4 p.i. in the meninges as compared to the CNS-draining lymph nodes (Fig. 2F). Altogether, these results support the initiation of an inflammatory response to WNV infection as demonstrated by the accumulation of activated APCs in the CNS-draining LNs and meninges.

Phenotypic differences between WNV specific CD8⁺ T cells based on anatomic localization.

To further examine changes in the cellular composition of CNS-draining LNs and meninges, we evaluated expansion of antigen-specific CD8⁺ T cells during WNV infection. To examine WNV-specific CD8⁺ T cell responses we utilized a tetramer expressing the immunodominant epitope from the NS4B protein of WNV (104). WNV-specific CD8⁺ T cells expand in CNS-draining LNs

and meninges by 7 days p.i., (**Fig. 3A**). By 10 days p.i., WNV-specific CD8⁺ T cells have contracted in the CNS-draining LNs but numbers remained high in the meninges (**Fig. 3A**). Within the brain, WNV-specific CD8⁺ T cell populations increase by 7 days p.i. with variability across mice. However, by 10 days p.i. all mice have consistently high numbers of WNV-specific CD8⁺ T cells (**Fig. 3A**). Notably, WNV-specific NS4B Tetramer⁺ CD8⁺ T cells accounted for roughly 30% of the total CD8⁺ T cell population in the meninges and approximately 45% of total CD8⁺ T cells in the brain at 10 days p.i. (**Fig. 3A**). In total, these data find tissue-specific dynamics of WNV-specific CD8⁺ T cell accumulation with the kinetics in CNS-draining LNs more closely resembling that observed in the periphery rather than the meninges and brain.

The tissue specific immune cell dynamics noted above, prompted investigation into potential differences in CD8⁺ T cell phenotype and function from peripheral lymphoid tissues, CNS-draining lymphoid tissues, meninges, and brain. These analyses could not be performed on bulk CD8⁺ T cell populations as the results would be skewed by the differences in antigen-specific T cell frequencies between tissues (**Fig. 3A**). Therefore, to normalize the WNV-specific CD8⁺ T cell frequencies, we utilized our W4B T cell receptor (TCR)-transgenic mouse model, which have CD8⁺ T cells specific for the immunodominant epitope in the WNV NS4B protein (104). W4B cells were adoptively transferred to wild-type mice of a different congenic background, which were then infected, and tissues harvested at 7 days p.i. for flow cytometry analysis (**Fig. 3B**). We utilized congenic markers to select for the transferred cells, of which >99% were WNV-specific (**Fig. 3B**).

We first compared the expression of various surface markers associated with CD8⁺ T cell activation and effector function between CNS compartments at 7 days p.i.. Bulk, non-WNV specific (NS4B Tet⁻) CD8⁺ T cells, which serve as a negative control, displayed low expression of CD44, a canonical marker of CD8⁺ T cell activation (**Fig. 3C**). Conversely, WNV-specific W4B cells from spleen, scLN, dcLN, meninges and brain were all activated as indicated by upregulated CD44 expression (**Fig. 3C**). Interestingly, there were varying levels of CD44 expression among activated W4B cells across tissues (**Fig. 3C**). Cells isolated from the spleen and the meninges had the lowest MFIs, while cells isolated from the scLN, dcLN and brain had markedly higher MFIs (~ 2-fold higher) (**Fig. 3C**). Previous work has demonstrated that W4B cells residing in highly vascularized tissue have higher CD44 expression during WNV infection (104). Therefore, CD44 is upregulated across anatomic compartments in response to WNV infection, but higher CD44 expression may correlate with tissue vascularization.

Analysis of KLRG1 expression, another marker upregulated on CD8⁺ T cells during the effector phase, found that cells from the spleen (28%) and meninges (27%) had the highest frequency of KLRG1⁺ W4B cells (**Fig. 3D**). In contrast, W4B cells from the CNS-draining LNs and brain had a significantly lower frequency of KLRG1⁺ cells (**Fig. 3D**). This suggests that W4B cells isolated from the spleen and meninges are most likely to be in the effector phase; however, when we examined inducible markers of activation, we did not see the same pattern. ICOS is an activation-induced co-stimulatory marker, and its expression was highest in the scLN, meninges and brain, suggesting that W4B cells in the brain, meninges, and scLN are receiving the most co-stimulatory signals at 7 days p.i. (**Fig. 3C**). Analysis of PD-1, a co-inhibitory marker, found that the meninges (18%) and brain (10%) had the highest percentage of PD-1 expressing W4B cells, whereas the

spleen (2.5%) and CNS-draining LNs (less than 5%) were significantly lower (**Fig. 3D**). PD-1 is upregulated after TCR activation, but its expression is also maintained when cells are receiving inhibitory signals. Therefore, PD-1 upregulation could reflect either recent stimulation with cognate antigen or the presence of immunoregulatory signals in the CNS (181-183). In total, these results demonstrate that CD8⁺ T cells isolated from peripheral and CNS compartments have distinct phenotypes during WNV infection. W4B cells isolated from the CNS-draining LNs displayed extremely similar activation phenotypes, while the meninges and brain shared some but not all phenotypic markers.

WNV-specific CD8⁺ T cells from peripheral and CNS compartments are transcriptionally distinct. To further explore the unique programming of CNS localized CD8⁺ T cells at the transcriptional level, we performed mRNA-seq analysis. We characterized brain W4B cells as representative for the CNS compartment and splenic CD8⁺ T cells for comparison. To analyze transcriptional differences between peripheral and CNS-localized WNV-specific CD8⁺ T cells, we utilized the same transgenic adoptive transfer system described above. W4B cells were transferred into naïve C57BL/6J mice (50,000 cells per mouse), and W4B cells were sorted from the spleen and brain at 7 days p.i. for RNA-seq (**Fig. 4A**).

Differential gene expression analysis found that while there was overlapping gene expression between the two anatomic locations (1746 genes), 934 genes were uniquely expressed in splenic W4B cells and 736 genes in brain W4B cells (the following cutoffs were used: $p < 0.001$, fold-change > 2 or < -2) (**Fig. 4B**). Many downregulated genes (as compared to naïve) were shared by W4B cells from both compartments (**Fig. 4C**). Notably, brain W4B cells upregulated many genes

compared to naïve that were not expressed in the splenic W4B cells (422 genes), suggesting that localization to the CNS imparts many transcriptional changes as compared to splenic W4B cells from both naïve and infected mice (**Fig. 4C**).

Flow cytometry analysis indicated differences in activation status in the CNS compartments (Fig. 3), therefore we next compared the differentiation profiles between the splenic and brain W4B cells. Genes associated with a terminal effector profile, (highlighted in blue) were upregulated compared to mock in both splenic and brain W4B cells, with most of these genes equally expressed in the spleen and brain (**Fig. 4D**). Accordingly, genes associated with a memory precursor profile (highlighted in green) were downregulated compared to mock in both anatomic locations (**Fig. 4D**). Collectively this indicates that brain and splenic W4B cells are firmly in the terminal effector phase of their response.

Closer examination of selected genes related to the terminal effector determine that antiviral cytokines (*Ifng*), cytotoxic receptors (*Fasl*), and cytotoxic molecules (*Gzmb*, *Prf1*) all displayed higher levels of expression in brain W4B cells compared to splenic W4B cells (**Fig. 4E**). Analysis of genes for activation receptors found that several activation receptors (*Cd69*, *Klrk1*) were enriched in brain W4B cells as compared to splenic W4B cells (**Fig. 4F**). Since flow cytometry data found a higher frequency of PD-1 expression for brain and meningeal W4B cells (**Fig. 3D**), we next examined whether other inhibitory receptors were differentially expressed in brain and splenic W4B cells. Strikingly, multiple inhibitory receptors (*Ctla4*, *Lag3*, *Tigit*, *Pdcd1* (PD-1), *Ili10ra*, *Cd244*) displayed increased expression on brain W4B cells (**Fig. 4F**). Altogether taken in

context with the phenotypic and transcriptomic profiles, brain W4B cells appear to be highly activated effector-phase cells with a potent antiviral phenotype

To investigate other potential areas of CD8⁺ T cell function that are altered in the CNS compared to the periphery, we performed gene set enrichment analysis (GSEA) using the Hallmarks data set. Many pathways were highly enriched in the brain W4B cells compared to the splenic W4B cells as indicated by positive normalized enrichment scores (NES). Interestingly, one of the pathways upregulated in the brain W4B cells is signaling through the TGF- β receptor (**Fig. 4G**), which correlates with our increased inhibitory marker expression (**Fig. 4F**). Several pathways enriched in brain W4B cells were related to metabolic signaling, this included; cholesterol homeostasis, glycolysis, mTORC1 signaling, as well as a hypoxia response (**Fig. 4G**). However, 3 of the 4 pathways with the highest enrichment score are related to inflammatory cytokine signaling (IL-2 signaling, IFN γ response, and inflammatory response) (**Fig. 4G**) Examination of genes involved in cytokine receptor signaling and response (highlighted in purple) found that many of these genes were only upregulated in the brain W4B cells but not in the spleen (**Fig. 4H**). Specifically, components of the IL-12R and IL-2R signaling pathway, such as *Il2ra*, *Il12rb1*, and *Stat1* were upregulated in the brain compared to the splenic W4B cells (**Fig. 4I**). Transcription factors induced by these signaling pathways (IRF family members, *Jun*, *Fos*) were also selectively enriched in brain W4B cells (**Fig. 4I**). Overall, brain W4B cells have enrichment of many unique metabolic and cytokine signaling pathways, specifically IL-12 and IL-2 signaling which will promote the production of cytokines and cytotoxic molecules (184).

Transcriptional analysis of brain and splenic W4B cells revealed that WNV-specific CD8⁺ T cells localized to the CNS are terminally differentiated effector cells, feature a highly antiviral profile, and express high levels of activation receptors. Brain W4B cells display signs of a regulatory environment with increased inhibitory receptor expression and TGF- β signaling. CNS localized W4B cells also have enriched expression of cytokine signaling pathways (IL-2, and IL-12) that will promote CD8⁺ T cell effector function. Together these data indicate the brain micro-environment may contribute to a unique CD8⁺ T cell profile.

Meningeal and brain CD8⁺ T cells efficiently control virus via polyfunctional cytokine secretion. Our mRNA-Seq data indicated high expression of effector function molecules in CNS localized CD8⁺ T cells. To investigate differences in the cytokine production capacity of W4B cells across anatomic locations, we performed an *ex vivo* stimulation. Splenocytes isolated at 7 days p.i. were stimulated with their cognate antigen (NS4B peptide), and cytokines were accumulated within the cell via treatment with GolgiStop. As expected, unstimulated splenic W4B cells did not produce cytokines, and nearly all stimulated W4B cells displayed detectable levels of cytokine production (**Fig. 5A**). Thus, demonstrating that W4B cells are activated and able to respond to WNV at 7 days p.i. in the surveyed tissues. While all W4B cells responded to stimulation, we observed dramatically different cytokine profiles between peripheral and CNS tissues. Only 5-20% of W4B cells from peripheral compartments (spleen, scLN, and dcLN) produce either IFN γ or TNF α or both. Conversely, over 60% of meningeal W4B cells and over 85% of brain W4B cells exhibit IFN γ or TNF α production following *ex vivo* stimulation (**Fig. 5A**). In addition to differences in total production, the cytokine profiles were distinct between peripheral and CNS W4B cells. W4B cells from the periphery preferentially produce TNF α , and secrete little

to no IFN γ (**Fig. 5A**). In contrast, brain and meningeal W4B cells are predominantly TNF α and IFN γ double-positive populations (**Fig. 5A**). Of the single-producing populations in the CNS, W4B cells are more likely to be secreting IFN γ than TNF α (**Fig. 5A**). These data find that W4B cells isolated from brain and meningeal compartments have a high-producing, polyfunctional cytokine signature, whereas peripheral W4B cells which have a low-producing, TNF α -dominated signature.

We next hypothesized that brain W4B cells, which exhibit a polyfunctional antiviral phenotype, control WNV more efficiently than splenic W4B cells when co-cultured with cortical neurons. WNV can directly infect neurons and replicate to high levels in the brain (up to 10^8 pfu/g tissue) (82, 121). Therefore, we utilized a cortical neuron co-culture model (82, 121) to determine if the observed phenotypic differences between peripheral and CNS WNV-specific CD8 $^+$ T cells translated to a functional difference. Cortical neuron cultures were derived from WT embryonic mice, differentiated, and then infected with WNV. After virus adsorption, infected cortical neurons were co-incubated with WNV-specific CD8 $^+$ T cells sorted from either the brain or spleen of mice at 7 days p.i. Cortical neurons and CD8 $^+$ T cells were co-cultured for 24 hours at which point viral titers were assessed by focus-forming assay, allowing us to directly compare the capacity of CD8 $^+$ T cells from distinct anatomic compartments to control WNV replication (**Fig. 5B**). The addition of W4B cells from either anatomic compartment resulted in a decrease in viral burden as compared to untreated neurons, supporting previously published findings that CD8 $^+$ T cells help control WNV replication in neurons (82, 121). Interestingly, WNV-specific CD8 $^+$ T cells from the brain were able to decrease viral burden by 2-fold as compared to splenic WNV-specific CD8 $^+$ T cells

(Fig. 5C). Thus, demonstrating that CNS-derived WNV-specific CD8⁺ T cells control WNV infection in cortical neurons more efficiently than splenic WNV-specific CD8⁺ T cells.

DISCUSSION

Here, we provide the first comprehensive analysis of pathogenesis and immune cell dynamics in the CNS-draining lymph nodes and meninges during WNV neuroinvasive disease. We find that these compartments are seeded by WNV at early timepoints, which results in APC accumulation and activation, and subsequent parenchymal invasion. Characterization of the CD8⁺ T cell response found substantial differences in dynamics and phenotype between anatomic compartments, with a sharp divide between the parenchymal space and the periphery. CD8⁺ T cells localized to the meninges had an intermediate phenotype. Antigen-specific CD8⁺ T cells in the parenchyma displayed a distinct anti-viral profile characterized by increased cytokine production and higher levels of activation markers compared to peripheral CD8⁺ T cells. CD8⁺ T cells isolated from the brain were also more efficient than splenic CD8⁺ T cells at controlling WNV replication in neurons. Together these data find substantial differences in viral dynamics and the CD8⁺ T cell responses based on anatomic localization during WNV infection.

These data demonstrate that the meninges and CNS-draining LNs have high levels of viral RNA at 4 days p.i., prior to brain parenchymal invasion and more closely resemble the post-viremic replication kinetics observed in the spleen than in the brain. These findings support the notion that these compartments are seeded with WNV much earlier than previously appreciated and suggest that WNV might be reaching CNS-border regions during the early viremic stage, even prior to peak replication in the spleen, and seeding the scLNs and dcLNs before brain parenchymal invasion. When examining immune cell dynamics within these tissue compartments, we observed accumulation of activated APC populations in the CNS-draining LNs at 4 days p.i. followed by an increase in WNV-specific CD8⁺ T cells by 7 days p.i. which corresponded with viral RNA.

However, despite viral RNA being detectable as early as 4 days p.i. similar to the CNS-draining LNs, the meninges more closely resembled the brain in many respects with APCs and WNV-specific CD8⁺ T cells accumulating at 8 days p.i. and 10 days p.i., respectively. These findings support an early involvement of CNS-draining lymphatics in WNV pathogenesis.

Phenotypic profiling of CD8⁺ T cells across peripheral and CNS tissues identified profound differences based on anatomic location and tissue architecture. Studies in other models of infection have noted a similar phenomenon in mucosal sites or even between the red pulp and white pulp within the spleen (115, 185). However, mechanisms by which tissue specific programming occurs is unclear. Some of these differences could be due to the structural characteristics of each tissue. For example, the expression of CD44, an activation-induced receptor associated with CD8⁺ T cell movement, on W4B cells was inversely correlated with the level of vascularization of the residing tissue (**Fig. 4C**). However, many of the functional and phenotypic differences (IFN γ , TNF α , ICOS, PD-1 expression) were correlated with localization to the CNS, which could be due to the unique microenvironment. For example, many cytokine signaling pathways (IL-2, IL-12, TGF- β) were upregulated only in brain W4B cells (**Fig. 6G-I**). This suggests that CD8⁺ T cells may be experiencing a unique cytokine milieu in the CNS, which could lead to phenotypic and functional differences. W4B cells isolated from the spleen and brain have the most exaggerated differences, while those from the meninges and CNS-draining LNs might be best described as having an intermediate phenotype. Some phenotypic differences, such as the increased ICOS expression on W4B cells from CNS-draining LNs as compared to the spleen, might be due to recent migration from the CNS or differences in antigen load at those later points. Importantly, meningeal CD8⁺ T cell populations may or may not have been subject to environmental cues within the brain

parenchyma. Therefore, it is unclear whether the intermediate phenotype observed for meningeal WNV-specific CD8⁺ T cells results from unique meningeal environmental cues or heterogeneity in exposure across the CD8⁺ T cell population.

Thorough phenotypic and transcriptional profiling of WNV-specific CD8⁺ T cells supports that CD8⁺ T cells adopt a unique and highly antiviral terminal effector phenotype upon entry to the CNS. At 7 days p.i., W4B cells isolated from both the spleen and the brain expressed an activated effector T cell signature; however, brain W4B cells exhibited consistently higher levels of activation markers by both flow cytometry and RNA-seq analysis. Brain W4B cells also had enriched expression of several pathways linked to the effector phase of T cell function, including glycolysis, mTORC signaling, and IL-2/STAT5 signaling (101). Brain W4B cells had particularly enriched *Il2ra* expression, suggesting that cells are continuing to receive effector phase-promoting signals. Notably, IL-2 signaling can promote the formation of short-lived effector cells (SLECs) in a *Prdm1/Tbx21* dependent-manner (186), and indeed we see that *Prdm1* expression is highly upregulated in brain W4B cells (**Fig. 6D**). Furthermore, *Prdm1* drives a terminal effector transcriptional program and promotes the cytotoxic functions of the CD8⁺ T cells (186). It is worth noting that the increase in effector cells could also be a reflection of viral load, as at 7 days p.i. WNV replication in the spleen is declining, but approaching peak viral burden in the brain. Altogether, these findings suggest that brain WNV-specific CD8⁺ T cells are more likely to be in a highly activated short-lived effector phase than cells from the spleen at 7 days p.i. and express high levels of both activating and inhibitory receptors.

Corresponding to the aforementioned effector phenotype, we observed that brain and meningeal W4B cells exhibit a polyfunctional antiviral signature, producing both IFN- γ and TNF- α , whereas W4B cells from the spleen, scLN, and dcLN have a 5-fold lower frequency of producing these cytokines. Brain and meningeal W4B cells favored the production of IFN- γ over TNF- α upon encounter with their cognate antigen, unlike peripheral W4B cells which preferentially produced TNF- α . Interestingly, IFN- γ can directly impact neuronal function and has been shown to promote non-cytolytic clearance of Sindbis virus from infected neurons (187). Therefore, the preferential secretion of IFN- γ by brain W4B cells during WNV infection may be an effective way to clear virus while limiting cytotoxicity. However, recent work has shown that IFN- γ production from antiviral CD8⁺ T cells persisting in the CNS parenchyma promotes microglia-mediated synaptic elimination (188). Therefore, the IFN- γ -dominated signature of the brain W4B cells might be necessary for virologic control, but could cause unintended consequences during recovery.

A major finding to emerge from our analysis of splenic and brain W4B cells was that CNS localization was associated with enhanced expression of inhibitory receptors. Engagement of these receptors serves to dampen the effector functions of CD8⁺ T cells by inhibiting the production of cytokines and cytotoxic molecules. High expression of inhibitory receptors is often associated with an exhausted cell phenotype found in chronic infections (183, 189). However, during an acute infection such as WNV, this is potentially indicative of an immunoregulatory environment where cells are receiving suppressive signals in order to limit pathology (181, 182). Following acute encephalitis from murine cytomegalovirus (MCMV) infection, the PD1:PD-L1 axis has been shown to contribute to the establishment of resident memory T (T_{RM}) cell populations within the CNS (182). A similar observation also has been made following murine polyomavirus (MuPyV)

infection (181). In combination with previously published data that W4B cells express elevated levels of CD103 and CD69 in the brain, this may suggest the establishment of T_{RM} cells in the CNS following WNV infection (104). Additionally, *Il10ra*, the IL-10 receptor gene, is highly upregulated on brain W4B cells (**Fig. 6F**). T regulatory (T_{reg}) cells are the primary producers of IL-10, and previous studies have demonstrated that increased T_{reg} cell numbers during WNV neuroinvasive disease is protective in both humans and mice (190). While the impacts of T_{reg} cells on CD8⁺ T cell function in the CNS has not been directly assessed during WNV infection, this suggests a link between induction of a regulatory environment and protection from immunopathology that requires further investigation.

The CD8⁺ T cell:cortical neuron co-culture system represents a unique model (82, 121). Here we describe the first functional demonstration that CNS-localized WNV-specific CD8⁺ T cells control WNV infection of cortical neurons more efficiently than splenic WNV-specific CD8⁺ T cells. The difference in functional capacity corresponded with phenotypic and transcriptional signatures, which revealed a highly activated and terminal effector phenotype for CNS-localized W4B cells. An important limitation of the co-culture system is that it cannot perfectly recapitulate the microenvironment of the brain, including tissue architecture and multicellular interactions with CNS-resident cells, such as microglia, or other infiltrating peripheral leukocytes. The system, however, could be modified in the future to include other cell types such as microglia or T_{reg} cells to further interrogate the mechanisms of immunoregulation during neuronal infection *ex vivo*.

In this study, we defined the early involvement of CNS-draining lymphatics during WNV pathogenesis and examined phenotypic and functional differences in WNV-specific CD8⁺ T cells

across peripheral and CNS compartments. Accumulation of viral RNA and activated cDCs in CNS-draining LNs occur prior to parenchymal invasion, and WNV-specific CD8⁺ T cell accumulation parallels that of the spleen. Comprehensive phenotypic profiling of WNV-specific CD8⁺ T cells in the spleen, CNS-draining LNs, meninges and brain revealed that brain W4B cells are phenotypically distinct from splenic W4B cells, while cells from the meninges and CNS-draining LNs display unique intermediate phenotypes. An emerging body of evidence implicates CD8⁺ T cells and cytokines in memory formation, learning, or other neurological sequelae following injury or infection. Future therapeutic interventions may require consideration of the unique programming of CD8⁺ T cells in the CNS during neuroinvasive viral infection, as well as the consequences of persisting antiviral CD8⁺ T cells in the CNS. Furthermore, future investigation of the specific cues within the CNS microenvironment that prompt these phenotypic shifts, including those in the brain parenchyma and meninges, could provide valuable insight into the underlying mechanisms of protection within the CNS.

MATERIALS AND METHODS

Viruses and animals. WNV isolate Texas 2002-HC (WNV-TX) has been previously described (191). Viral titers were measured by plaque assay on BHK-21 cells. C57BL/6J and Prtprc mice were obtained commercially from Jackson Laboratories or bred in-house at the Yerkes National Primate Research Center rodent facility at Emory University. W4B transgenic mice were originally obtained from the Bevan laboratory and bred in-house. For viral infections, adult male and female mice (8-12 weeks old) were inoculated subcutaneously in the rear footpad with 100 plaque-forming units (PFU) of WNV-TX (10 μ L). Infected mice were monitored and weighed daily. All experiments adhered to the guidelines approved by the Emory University Institutional Animal Care and Committee.

Focus-forming assays. Focus-forming assays (FFAs) were performed on Vero cells with supernatants from WNV-infected cortical neuron cultures. Vero cells were cultured in DMEM (VWR, #45000-304) supplemented with 5% FBS, antibiotic/antimycotic, sodium pyruvate (VWR, #45000-710), HEPES (VWR, # 45000-690), L-glutamine (VWR, # 25005CI), and nonessential amino acids (VWR, #45000-700). Supernatants were serially diluted 10-fold in 1% FBS-DMEM. Vero cells were then infected with 50 μ L of diluted supernatant for 1 hr at 37°C followed by the addition of a methylcellulose overlay (2% methylcellulose (Sigma, #M0512), 2% FBS, OptiMem). Cells were then incubated for 48 hr at 37°C. Cells were fixed (2% PFA-PBS), permeabilized (0.1% saponin, 0.1% BSA, PBS), washed with PBS, and then incubated with an anti-WNV E16 primary antibody overnight at 4°C. Wells were incubated with HRP conjugated anti-human IgG (Thermo, #62-842-0) for 2 hr at room temperature, and spots were visualized using True Blue Peroxidase Substrate (KPL, #507802) and imaged using an ELISPOT reader.

Measurement of viral load in tissues. Mice were deeply anesthetized using an isoflurane vaporizer, and blood was collected via cheek bleed from each mouse in a BD Microtainer serum separator tube (SST) (VWR, #VT365967) to isolate serum. Mice were transcardially perfused with sterile DPBS. All tissues were collected in Omni Bead Ruptor Tubes (VWR, #10032-358) pre-filled with TRI Reagent (Zymo, #R2050-1-200). Tissues were homogenized using the Omni Bead Ruptor 24 (5.15 ms, 15 seconds) then centrifuged to remove tissue debris. RNA was extracted using the Direct-Zol 96 RNA Kit (Zymo, #R2056), and converted to cDNA using the High-capacity Reverse Transcriptase cDNA Kit (Thermo, #4368813). WNV RNA levels were quantified by qPCR as previously described (192) on an Applied Biosystems QuantStudio 5.

Immunophenotyping by flow cytometry. Mice were anesthetized and intravital labelling was performed by injecting mice with CD45:PE or CD8:APC via the retro-orbital route. After 5 minutes, mice were euthanized via isoflurane overdose. Splenocytes were obtained by mechanical homogenization and filtration through a 70 μm filter (VWR, #10199-657). Brains were mechanically homogenized, digested for 15 min at room temperature in Liberase (Sigma, #540102000, 50 μg) buffer. The tissue was pushed through a filter and pelleted. To remove myelin debris, the cells were resuspended in a 30% Percoll in PBS solution and spun at 2000 rpm for 20 min. Meninges were incubated in dissociation media (0.5 mg/mL DNaseI (Sigma, #DN25-100MG), 8 mg/mL Collagenase D (Sigma, #11088866001) , RPMI) for 40 min at 37°C on a shaker, then processed to a single-cell suspension and filtered. Lymph nodes were digested for 20 minutes at 37°C on a shaker in dissociation media (0.1 mg/mL DNase I, 20 μg /mL Liberase, RPMI). Tissue was passed through a filter to create a single-cell suspension. If cytokines were

measured, samples were stimulated *ex vivo* with NS4B peptide (1 $\mu\text{g}/\text{mL}$) and GolgiStop (BD, #52-2092KZ) for 5 hr (104). For all samples, cells were resuspended in anti-CD16/32 antibody (Biolegend, #101302) for 20 min at room temperature, followed by surface staining for 30 min at 4°C. Cells were washed in FACS buffer, then fixed with BD FACS/Lyse buffer (#349202) for 10 min. For intracellular stains, cells were permeabilized with FoxP3 Fix/Perm buffer for 30 min at 4°C (Tonbo, #1020-L050), then stained with intracellular antibodies (30 min, 4°C). Cells were resuspended in 200 μL of FACS Buffer supplemented with Precision Count Beads (Biolegend, #424902) for acquisition. Data were collected using an LSRII instrument and analyzed using FlowJo software.

Adoptive transfer experiments. Spleens from naïve W4B mice were homogenized, treated with red blood cell lysis buffer (Lonza, #10-548E), and processed to a single-cell suspension. CD8⁺ T cells were isolated using the Mojo Sort CD8⁺ T cell Negative Selection Kit (Biolegend, #480035). CD8⁺ T cells isolated from W4B mice were >95% NS4B tetramer-positive (193). W4B cells were resuspended in DMEM and 5,000 or 50,000 W4B cells were transferred to each recipient via retro-orbital route.

Bulk mRNA sequencing (RNA-seq). Brains and spleens from infected mice were processed to single-cell suspension as described above. Cells were stained with CD45.2(PE-Cy7), CD45.1(Bv450), CD8(AF700), CD3(PerCpCy5.5), and Live/Dead (BV510). Transferred W4B cells were sorted using congenic markers ($n = 4$), 10,000 viable cells were sorted into 100 μL RLT buffer (Qiagen) with β 2-mercaptoethanol (1:100). mRNA sequencing libraries were prepared, quality assessed, and sequenced at Yerkes Genomics Core

(http://www.yerkes.emory.edu/nhp_genomics_core/), and reads were mapped to the GENCODE mouse reference genome (GRCm38.p5, release M16) all as previously described (192). Reads were normalized and differential expression analysis performed using DESeq2 (194). Normalized reads were expressed as fold change over mock values. Gene set enrichment analysis was performed using software from the Broad institute and gene sets from the MSigDB database.

Culture of cortical neurons. Embryos were harvested from pregnant dams at day 13-15 of gestation. Cortical hemispheres were isolated from the brain, and meningeal tissue was removed. The cortices were homogenized, digested in a 1% Trypsin- DNaseL solution (15 min, RT), and processed to a single-cell suspension. Cells were plated in DMEM supplemented with 5% Hi-Horse Serum (Thermo, #26050070), 5% FBS, antibiotics, non-essential amino acids, and HEPES. The next day media was changed to B27 (Thermo, #A3582801) supplemented Neurobasal Media (Thermo, #21103049). Neurons were monitored for axonal outgrowth and were determined ready for experimental use 4-5 days post plating. Cortical neurons were infected with WNV-Tx at the indicated MOI via adsorption for 1 hour, followed by three washes.

Antibodies. The following antibodies were used in this paper for flow cytometry. CD8⁺ T cell panel: anti-CD8:AF700 (Clone 53.67), anti-CD8:APC (2.43), anti-CD3:PerCpCy5.5 (145-2C11), anti-CD45.2:PE-Cy7 (104), Ghost Dye Violet 510, anti-KLRG1:BV605 (2F1), anti-CD44:APC-Cy7 (IM7), anti-ICOS:BUV395 (C398.4A), anti-CD127:FITC (A7R34), anti-IFN γ :PE-Dazzle (XMG1.2), anti-TNF α : BV711 (MP6-XT22), anti-GrazymeB:BV450 (NGZB), anti-PD1:BV650 (J43). Myeloid cell panels: CD11c:BV650 (N418), CD26:PE-Cy7 (H194-112), I-A/I-E (MHC II):AF700 (M5/114.15.2), XCR1:PE (ZET), CD172a (SIRP α):BV510 (P84), Siglec H:AF647

(551), H2kb (MHC I):PacBlue (AF6-88.5), CD86:BV605 (GL-1), CD64:PerCP-Cy5.5 (X54-5/7.1), CD3:FITC (145-2C11), NK1.1:FITC (PK136), B220:FITC (RA3-6B2), CD45.2:PE-Dazzle594 (104), F4/80:FITC (BM8), Siglec H:BV421 (440c), CD45:PE (30-F11), XCR1:AF647 (ZET), CD45.2:BV605 (104), Ly6C:BV510 (HK1.4), CD11c:BUV737 (HL3), CD11b:BUV395 (M1/70), CD86:PE-Dazzle594 (GL-1), Ly6C:APC-Cy7 (HK1.4).

Statistical analysis and software. Statistical analyses and graphical presentation of data was performed using Prism 8 (GraphPad) software. One-way ANOVA with Tukey's multiple comparison correction and the multiple t tests were used to evaluate significant differences depending on the experiment.

FIGURE LEGENDS

Figure 1. WNV seeds the CNS-draining lymph nodes and meninges prior to parenchymal invasion. Mice were infected with WNV (100 PFU) by subcutaneous footpad inoculation, and tissues collected at the indicated time points (n = 4). (A) Schematic of CNS tissues examined in this study. The meninges encompass the brain and meningeal lymphatic vessels drain to the scLN and dcLN. (B) Relative WNV RNA was measured by qPCR where C_T values were normalized to the reference gene *Gapdh* and represented as fold change over time-matched mock values. Fold change over mock at the indicated timepoint and tissue for (C) *Ifit1* (D) *Rsad2*.

Figure 2. Activated dendritic cell kinetics differ between the CNS-draining lymph nodes, meninges, and parenchyma. Mice were infected with WNV-TX (100 PFU) by subcutaneous footpad inoculation, and tissues collected at the indicated time points. (A) Total cell numbers for (A) $CD11b^{hi} Ly6C^{hi}$ monocytes, (B) $MHC II^+$ moDCs, $CD11b^{hi}$ (C) $MHC II^+ CD26^+ XCR1^+ CD172a^-$ cDC1, (D) $MHC II^+ CD26^+ XCR1^- CD172a^+$ cDC2, (E) $B220^+ SiglecH^+$ pDCs. (F-G) $MHC I$ and $CD86$ marker expression was represented by MFI for $MHC II^+ CD11c^+ CD26^+$ cDCs. (F) Representative histograms for cDCs isolated from the indicated tissue at 0 and 4 days p.i., and the (G) corresponding MFIs. Results are representative of two independent experiments with 4-6 mice per group. t tests were performed to test significance (*ns* = not significant; $*p < 0.05$; $**p < 10^{-2}$; $***p < 10^{-3}$).

Figure 3. Localization to the meninges, brain, and CNS-draining lymphoid tissues changes WNV-specific $CD8^+$ T cell activation. Mice were infected with WNV-TX (100 PFU) by

subcutaneous footpad inoculation, and tissues collected at the indicated time points. (A) Total number and frequency of NS4B Tet⁺ CD8⁺ T cells were quantified for the CNS-draining LNs, meninges and brain at the indicated days p.i. W4B cells from naïve CD45.1 mice were adoptively transferred (5000 cells/mouse) to a CD45.2 naïve mouse. 1 day post transfer mice were infected with WNV-Tx, and tissues were harvested at 7 days p.i. for flow cytometry analysis. (B) Experimental schematic, and gating strategy to identify W4B cells. (C) Expression of CD44 and ICOS on W4B cells across tissues. CD44 and ICOS MFI are shown as representative histograms. Non-WNV-specific NS4B Tet⁻ CD8⁺ T cells were used as a negative control (grey). Quantification of the MFI for each receptor is below. The legend for conditions depicted on bar graphs can be found at the bottom. (D) KLRG1 and (E) PD-1 expression shown as percentages of total W4B cells. Representative flow plots for the gating strategy are depicted with NS4B Tet⁻ CD8⁺ T cells used as a negative control (grey). Data are representative of two independent experiments (5 mice per group) . One-way ANOVA was performed to test significance (*ns* = not significant; **p* < 0.05; ***p* < 10⁻²; ****p* < 10⁻³; *****p* < 10⁻⁴).

Figure 4. CNS-localized W4B cells are transcriptionally distinct from splenic T cells. (A) Experimental schematic. Adoptive transfers were performed as described in Fig. 3A. At 7 days p.i., W4B cells were sorted from spleen and brain and total RNA was extracted for RNA-seq analysis. Naïve splenic W4B cells were sorted as a control (n = 4-5 per group). (B) Heat map showing mean gene expression values normalized and represented as log₂-transformed fold change over mock spleen values. Expression fold change values correspond to the color gradient (right). The Venn diagram at the bottom highlights the total number of differentially expressed genes for W4B cells from the spleen (red) or brain (blue), as well as overlapping genes (yellow).

(C) A scatter plot of log₂-transformed expression fold change (FC) values is shown for comparison of up-regulated and down-regulated genes in W4B cells from infected spleen (green) and brain (red). Cutoff values were as follows: ± 2 fold change and $p < 0.001$. (D) Shown in grey is a scatter plot of all significantly up or down regulated log₂-transformed expression fold change values compared to mock. Genes highlighted in color correspond to a selected gene list specified above the plot and particular genes of interest are labelled. (E-F) Normalized read count values (log₂) are shown for the indicated genes from day 7 p.i. splenic and brain W4B cells. (G) Normalized enrichment scores of selected pathways as calculated by GSEA software. Positive NES indicates enrichment in brain, negative NES indicates enrichment in splenic cells. (H) Scatter plot of selected gene list (cytokine response) highlighted in purple. (I) Heatmaps of fold-change over mock (log₂) for splenic and brain W4B cells for the indicated genes. Statistical significance was determined using one-way anovas, ($*p < 0.05$; $**p < 10^{-2}$; $***p < 10^{-3}$; $****p < 10^{-4}$).

Figure 5. W4B Cells from the CNS have polyfunctional cytokine secretion and efficiently control WNV. Adoptive transfers were performed as described in Fig. 3A. After tissue isolation, cells were stimulated *ex vivo* with NS4B peptide (1 $\mu\text{g}/\text{mL}$) for 5 h at 37°C. Cells were then permeabilized and stained for cytokines. (A) Representative flow plots are shown for TNF- α and IFN- γ gating on CD45.1⁺ CD3⁺ CD8⁺ cells (W4B cells). Unstimulated splenic W4B cells were used to define the negative population (grey). Populations were divided into quadrants (labeled 1-4) to identify double-negative cells (Q1), TNF- α single producers (Q2), IFN- γ single producers (Q3), and TNF- α /IFN- γ double producers (Q4). Bar graphs are shown for the percentage of cells in Q1-4 across tissues (n = 4). (B) Experimental schematic. Cortical neurons were generated from embryonic day 13-15 fetal mice after culturing for 4 days in neuronal growth medium. Cortical

neurons were infected with WNV (MOI of 0.01) and co-incubated for 24 h with W4B cells sorted from the spleen or brain of WNV-infected mice at 7 days p.i. Supernatants were collected and viral titers determined by FFA. (C) Viral titers of supernatants represented as focus-forming units (FFU) per mL in log₁₀ scale. Relative reduction percentage normalizes the viral titer data to the untreated control. Data are representative of three independent experiments. One-way ANOVA was performed to test significance (*ns* = not significant; **p* < 0.05; ***p* < 10⁻²; ****p* < 10⁻³; *****p* < 10⁻⁴).

ACKNOWLEDGEMENTS

We would like to thank the Yerkes Genomics Core for their assistance in processing the RNA-Seq samples. We'd also like to thank the Yerkes Flow Cytometry Core and the Emory Pediatrics Flow core for their help in sorting and analyzing cells via flow cytometry.

AUTHOR CONTRIBUTIONS

J.T.O. and A.V. contributed equally to this work. Both authors were involved in experimental design and execution, data analysis, figure generation, and manuscript preparation. D.J.E. provided valuable scientific discussion with regard to experimental design and assisted with tissue collection and RNA purification, as well as tissue collection, processing, and staining for flow cytometry to evaluate APC activation and immune cell accumulation. R.A. performed adoptive transfer experiments and tissue collection for bulk RNA-seq. J.H. and J.K. provided technical expertise and advice on collection of CNS-draining tissues and meninges. M.S.S. and A.G. provided mentorship, expertise in virology and immunology, and guidance for experimental design and manuscript preparation.

Figure 1

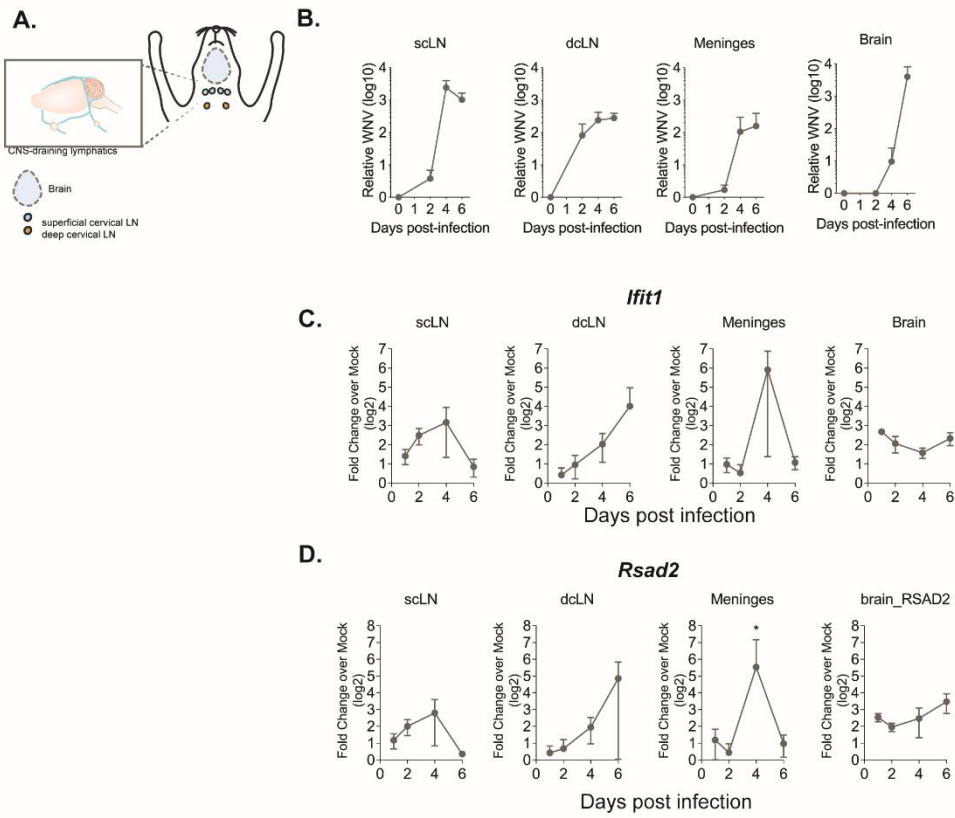


Figure 2

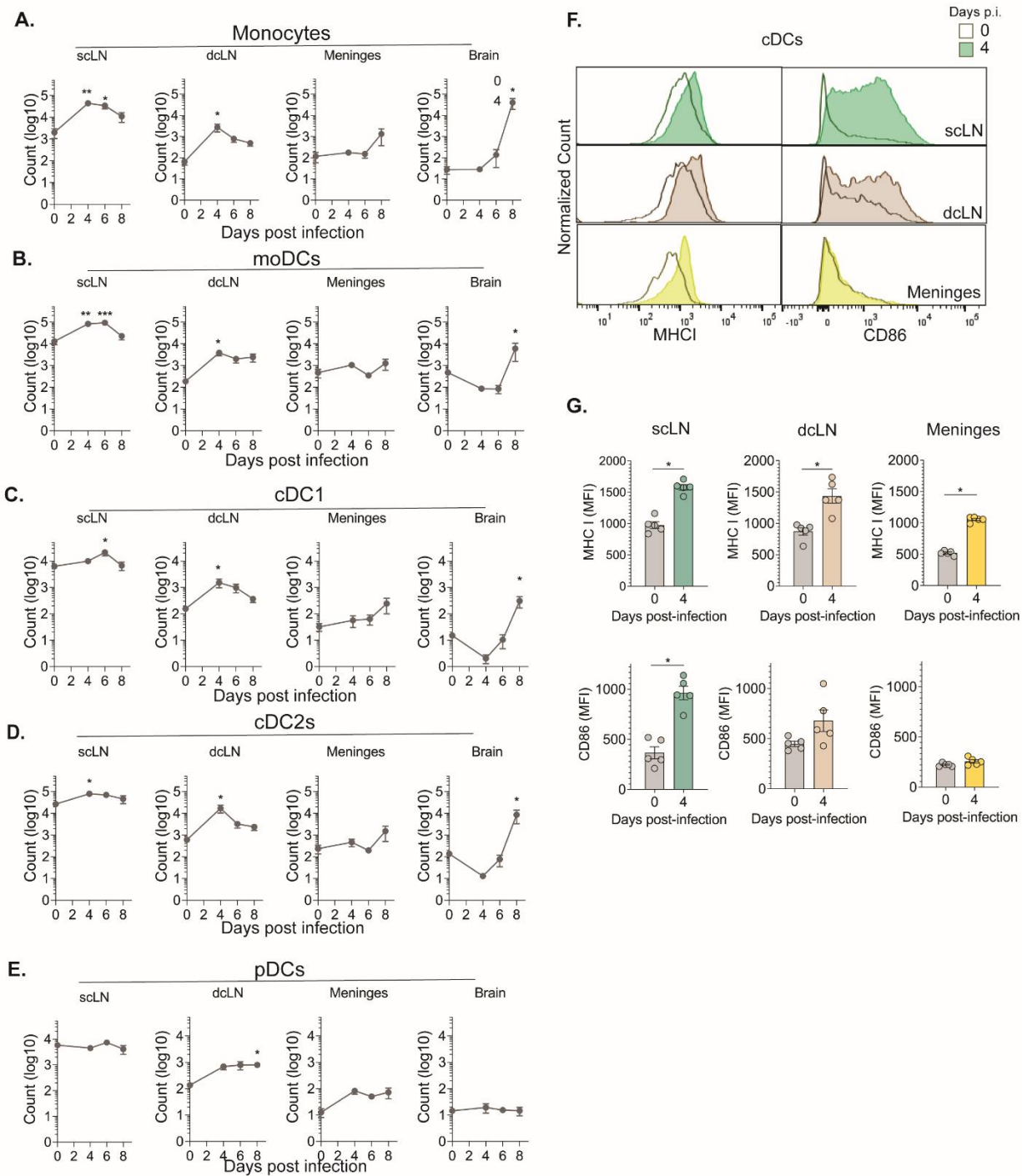


Figure 3

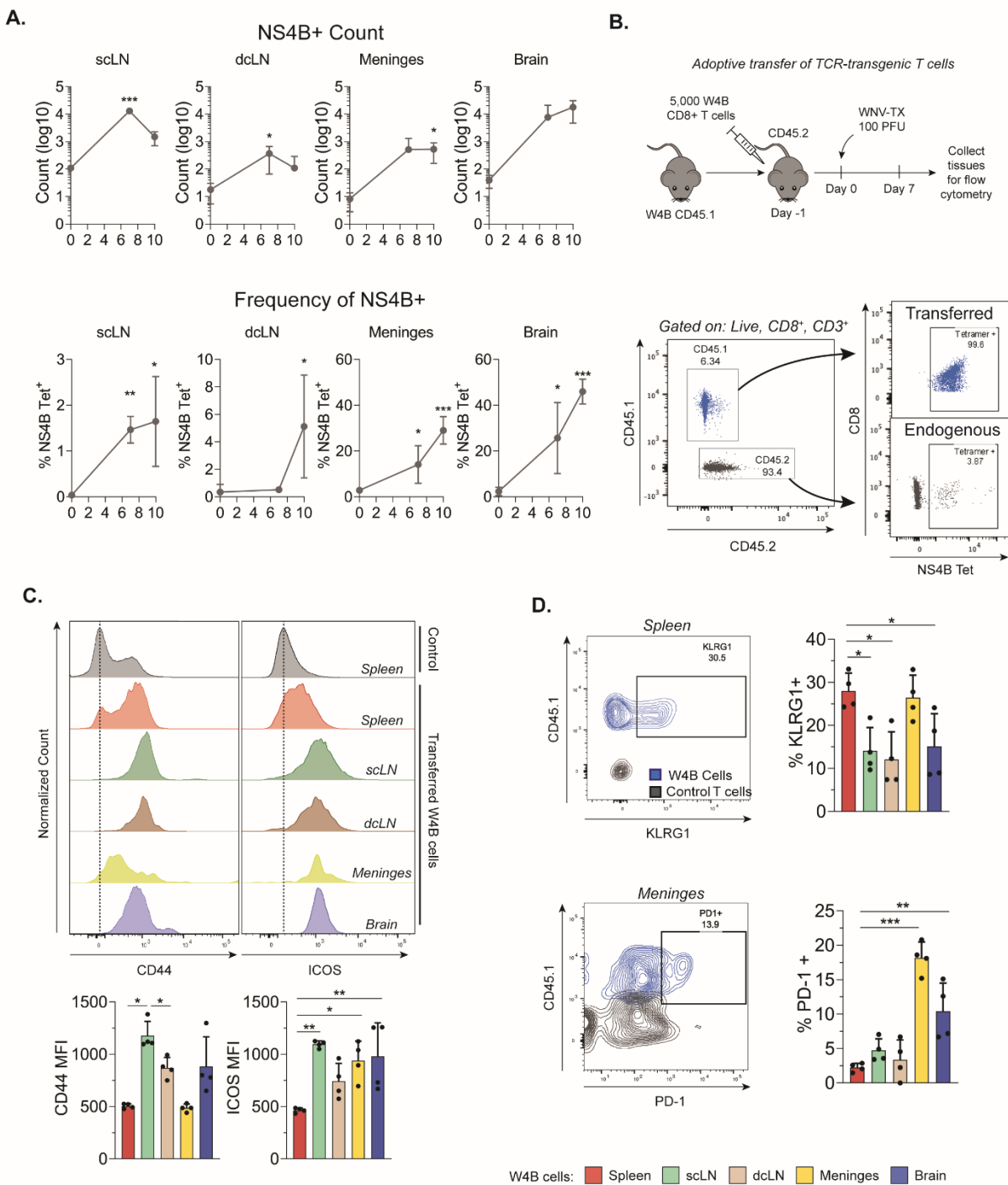


Figure 4

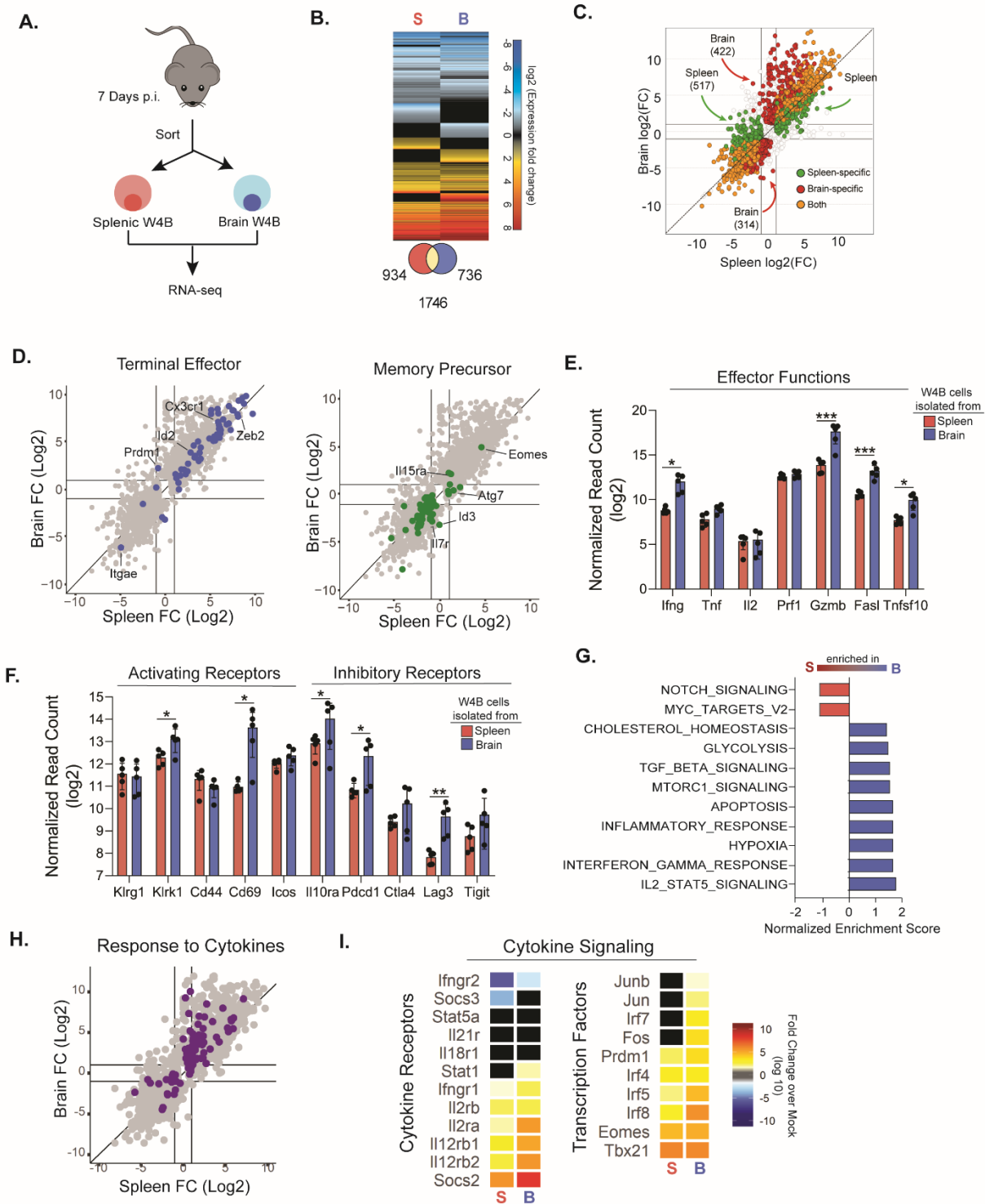
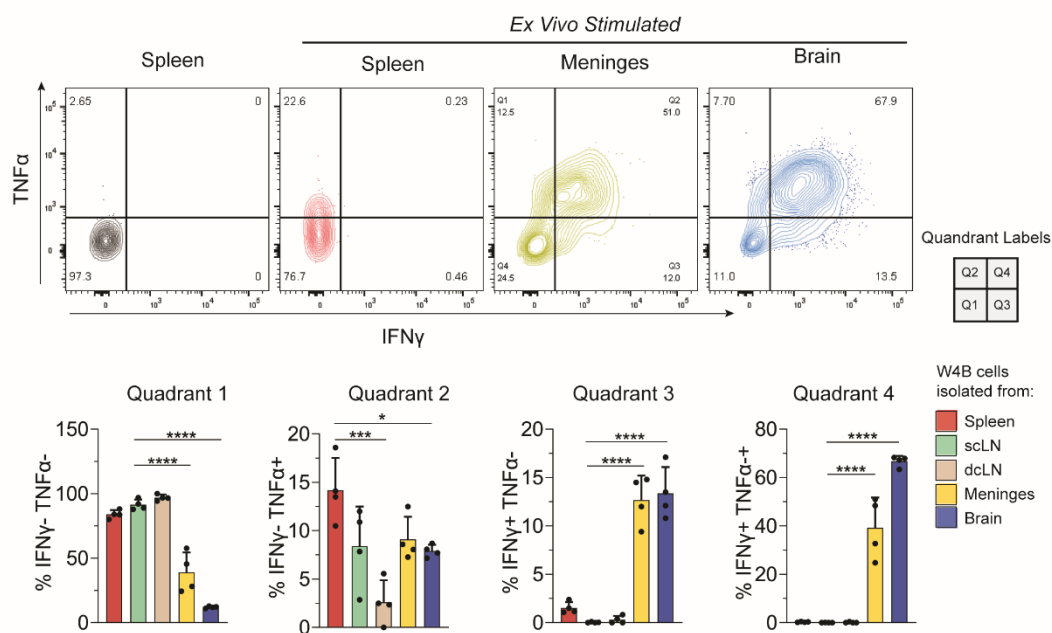
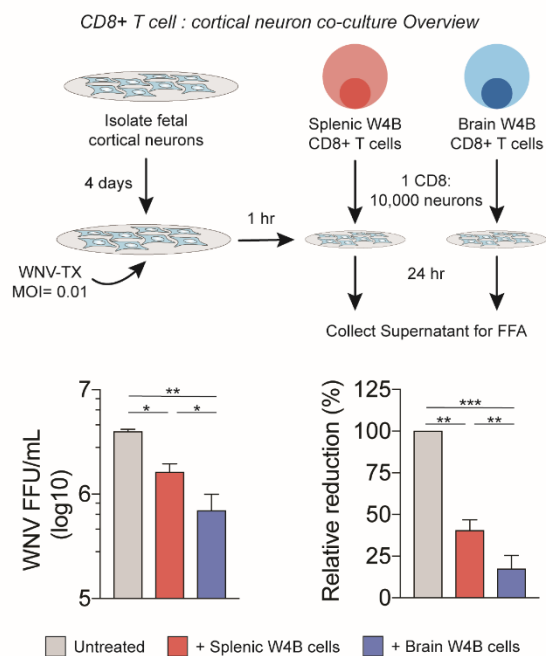


Figure 5

A.



B.



PART 2**Cell-intrinsic MAVS regulates mitochondrial metabolism to promote CD8+ T cell proliferation**

One sentence summary: Cell-intrinsic MAVS promotes mitochondrial elongation and oxidative phosphorylation to facilitate antigen-specific CD8+ T cell proliferation during viral infection.

Abigail Vanderheiden^{a,b,c}, Renan Aguilar-Valenzuela^{a,b,c}, Hans Verkerke^{a,b,c}, Fengzhi Jin^{b,c,d}, ,
Madeline Price^d, Jeremy M. Boss^d, Arash Grakoui^{b,c,d}, Mehul S. Suthar^{a,b,c,d}

^aDepartment of Pediatrics, Division of Infectious Disease, Emory University School of Medicine, Atlanta, Georgia, USA

^bEmory Vaccine Center, Emory University School of Medicine, Atlanta, Georgia, USA

^cYerkes National Primate Research Center, Atlanta, Georgia, USA

^dDepartment of Microbiology and Immunology, Emory University School of Medicine, Atlanta, Georgia, USA

Under review at Science Immunology

SUMMARY

Mitochondrial antiviral signaling (MAVS) protein, the central adaptor protein for RIG-I like receptor (RLR) signaling, is essential for promoting innate immunity against RNA virus infections. MAVS is expressed in nearly every cell and is localized on the mitochondria. Here, we find that MAVS is found within CD8⁺ T cells and functions in a cell-intrinsic manner to promote mitochondrial respiration and cell proliferation. We demonstrate that ablation of MAVS in antigen-specific CD8⁺ T cells leads to dysregulated oxidative phosphorylation transcriptional profiles and decreased mitochondrial potential *in vivo* during virus infection. Through adoptive transfer experiments, we determine that MAVS is required for expansion of antigen-specific CD8⁺ T cells. Mechanistically, we found that MAVS functions in CD8⁺ T cells by positively regulating cell proliferation during virus infection. Our findings identify a non-canonical role for MAVS as a positive regulator of mitochondrial respiration and cell proliferation of antigen-specific CD8⁺ T cells during viral infection.

INTRODUCTION

The RIG-I-like receptor (RLR) signaling pathway is essential for initiating the immune response against RNA viruses (195). This pathway includes the pattern recognition receptors (PRRs), RIG-I and MDA5, which upon detection of a virus bind to MAVS (mitochondrial associated anti-viral signaling protein), to induce oligomerization of MAVS on the mitochondria (141). Aggregated MAVS forms the central signaling hub for the RLR pathway by recruiting TBK1 or TRAF proteins to initiate downstream activation of NF- κ B and IRF-3/7, culminating in the production of Type I interferon (IFN) and pro-inflammatory cytokines (85, 195). MAVS also regulates additional cellular processes, including induction of caspase-mediated cell death, p53 signaling, and formation of inflammasomes (144-146). MAVS has also been linked to the regulation of mitophagy and mitochondrial dynamics. Activation of the RLR pathway promotes mitochondrial elongation and the initiation of autophagy (147, 148). Ectopic expression of MAVS results in a disruption of the mitochondrial membrane potential and induces LC3-dependent mitophagy, which initiates a feedback-loop mechanism to prevent excess RLR signaling (148). MAVS physically interacts with several key regulators of mitochondrial dynamics, including; mitofusin-1 and -2 (MFN1/2), and Tom70 (149-152).

Dynamic regulation of mitochondrial metabolism is crucial for the initiation of CD8⁺ T cell responses and subsequent differentiation into terminal effector or memory cells. Naïve CD8⁺ T cells rely on fatty acid oxidation and oxidative phosphorylation for their homeostatic needs, while activated CD8⁺ T cells will rapidly increase both oxidative phosphorylation and glycolysis (196, 197). Mitochondria are part of the TCR signaling cascade, as CD3-dependent mitochondrial reactive oxygen species (ROS) release promotes NFAT activation, and ultimately is required for

antigen-specific CD8⁺ T cell expansion *in vivo* (196). CD28 conjugation increases mitochondrial spare respiratory capacity, which is inessential for initial antigen-specific T cell activation, but necessary to respond to increased bioenergetic demand in the effector or memory phase (198). After initial TCR-induced activation, CD8⁺ T cells rely primarily on glycolysis for energy and the promotion of IFN γ production, while oxidative phosphorylation is redundant during the effector phase (199) (197). However, differentiation into memory CD8⁺ T cells is accompanied by a metabolic switch from glycolysis to a reliance on fatty acid oxidation and oxidative phosphorylation (200). This shift is supported by Opa-1 dependent mitochondrial fusion resulting in tight cristae structures which promote mitochondrial respiration (201). Thus, mitochondrial dynamics and metabolism regulate CD8⁺ T cell function and fate, however the impact of RLR signaling on these metabolic shifts is unknown.

In viral models of infection, the RLR signaling pathway was found to contribute to the regulation of CD8⁺ T cell responses. West Nile Virus (WNV) is a mosquito borne single-stranded, positive-sense, RNA virus of the Flaviviridae family, which causes annual outbreaks of encephalitis across North America (158, 159, 202). WNV can cross the blood-brain barrier (BBB) and replicate in neurons, causing encephalitis, long-term neurological damage, or even death (6, 160, 202). WNV has an excellent mouse model that recapitulates the pathogenesis of neuroinvasive disease in humans (52, 202). CD8⁺ T cells are essential for the control of WNV infection in the periphery and central nervous system (CNS) as mice lacking CD8 α or MHC-I exhibit complete mortality, higher viral burden, and increased pathology (100). Cell-intrinsic LGP2, a RLR that has a regulatory function, was found to promote CD8⁺ T cell fitness and survival by regulating sensitivity to CD95-dependent apoptosis (157). Adoptive transfer studies identified MDA5 as

necessary for CD8⁺ T cell control of virus in the CNS but not the periphery (154). Finally, global loss of MAVS signaling results in 100% mortality, increased viral burden, and an exaggerated influx of CD8⁺ T cells into the parenchyma (84). However, the cell-specific impact of MAVS signaling on CD8⁺ T cell function during viral infection has not been addressed.

In this study, we investigate the impact of MAVS on CD8⁺ T cell metabolism and function during viral infection. We find that MAVS is expressed within CD8⁺ T cells and functions in a cell-intrinsic manner to promote mitochondrial elongation, oxidative phosphorylation, and T cell receptor (TCR) induced proliferation. We demonstrate that ablation of MAVS in antigen-specific CD8⁺ T cells leads to dysregulated metabolic transcriptional profiles, including oxidative phosphorylation and fatty acid oxidation, as well as decreased mitochondrial potential *in vivo* during virus infection. Through adoptive transfer experiments, we determine that MAVS is required for the expansion of antigen-specific CD8⁺ T cells. Mechanistically, we found that MAVS functions in CD8⁺ T cells to positively regulate cell proliferation during virus infection. Our findings identify a non-canonical role for MAVS as a positive regulator of mitochondrial respiration and proliferation of antigen-specific CD8⁺ T cells during viral infection.

RESULTS

MAVS regulates mitochondrial number and elongation in activated CD8⁺ T cells. The RLR pathway is essential for the detection of RNA viruses and the initiation of a Type I IFN response (195). We have previously shown that the RLRs, RIG-I, LGP2, MDA-5, are upregulated after T-cell receptor (TCR) stimulation, and that LGP2 plays a crucial role in promoting CD8⁺ T cell responses during WNV infection (157). We next determined whether MAVS is expressed in CD8⁺ T cells. CD8⁺ T cells were isolated from naïve C57Bl6 or *Mavs*^{-/-} spleens and *in vitro* stimulated using α -CD3/CD28 for 18, 24, or 48 hours. Western blot analysis showed that CD8⁺ T cells express MAVS at the protein level, but expression does not change following TCR stimulation (Fig. 1A). We next evaluated the role of MAVS on CD8⁺ T cell activation. *Mavs*^{-/-} CD8⁺ T cells had similar frequencies of activated (CD44⁺CD62L⁻) and naïve (CD44⁻CD62L⁺) cells at 48 hours post stimulation (Fig. 1B). Together these data find that MAVS does not impact TCR induced activation and is constitutively expressed in CD8⁺ T cells.

MAVS has been previously linked to the regulation of mitochondrial dynamics and mitophagy, thus to test if MAVS is involved in the regulation of CD8⁺ T cell mitochondria we examined mitochondrial structure and morphology in WT and *Mavs*^{-/-} CD8⁺ T cells. Unstimulated and stimulated WT and *Mavs*^{-/-} CD8⁺ T cells were generated using the *in vitro* system described above, and analyzed via transmission electron microscopy (TEM) for mitochondrial morphology at 0 and 24 hours post stimulation. Unstimulated WT and *Mavs*^{-/-} CD8⁺ T cells had predominantly round mitochondria with loose cristae structures. Upon stimulation, WT CD8⁺ T cells had a mix of round and elongated mitochondria with more tightly packed cristae. However, *Mavs*^{-/-} CD8⁺ T cells maintained mostly round mitochondria with disorganized cristae (Fig. 1C). Interestingly, *Mavs*^{-/-}

CD8⁺ T cells had an increased number of mitochondria per cell both before and after stimulation. Both WT and *Mavs*^{-/-} mitochondria increased in size after stimulation, however the increase in WT cells was associated with an increase in elongation (as measured by the aspect ratio) (Fig. 1D). These data find that MAVS is important in the control of mitochondrial number and elongation after TCR stimulation.

MAVS promotes oxidative phosphorylation after TCR stimulation in CD8⁺ T cells.

Mitochondrial respiration is intricately linked to the morphology of mitochondria. Round, small mitochondria are associated with low levels of oxidative phosphorylation, while elongated, large mitochondria with distinct cristae are associated with increased respiration (201). We next investigated whether the altered mitochondrial dynamics and morphology observed in *Mavs*^{-/-} CD8⁺ T cells was also associated with changes in oxidative phosphorylation by utilizing an *in vitro* Seahorse assay system (147, 148). CD8⁺ T cells from WT or *Mavs*^{-/-} mice were isolated and stimulated *in vitro* using α -CD3/CD28 for 24 hours. Equal numbers of stimulated cells and unstimulated control cells (freshly isolated the day of the assay) were subjected to a mitochondrial stress test. A seahorse analyzer was used to measure the oxygen consumption rate (OCR) of the CD8⁺ T cells before and after the addition of oligomycin, carbonyl cyanide-4-(trifluoromethoxy)phenylhydrazone (FCCP), and rotenone/atinomycin, to provide measures of the mitochondrial function of each genotype. Naïve WT and *Mavs*^{-/-} CD8⁺ T cells had low OCRs, and there was no discernable difference between the two genotypes. However, 24 hours after activation, WT CD8⁺ T cells doubled their basal OCR and tripled their maximal OCR while *Mavs*^{-/-} CD8⁺ T cells displayed similar OCR to naïve cells (Fig.2A-B). Stimulated WT CD8⁺ T cells also had 4 times higher rates of ATP production and 2 times more spare respiratory capacity as

compared to *Mavs*^{-/-} CD8⁺ T cells (Fig. 2B). Thus, *Mavs*^{-/-} CD8⁺ T cells poorly upregulate mitochondrial respiration after TCR stimulation. To determine if MAVS also plays a role in glycolysis, we performed a glycolytic flux test using the same *in vitro* system. The extracellular acidification rate (ECAR) of stimulated and unstimulated WT and *Mavs*^{-/-} cells were measured before and after the addition of glucose, oligomycin, and 2-deoxyglucose. Unstimulated CD8⁺ T cells showed little to no glycolytic activity, but stimulated CD8⁺ T cells had an increase of 100-fold in ECAR after the addition of glucose (Fig. 2C). However, no significant differences in basal glycolysis, total glycolytic capacity, or glycolytic reserves were observed between stimulated WT and *Mavs*^{-/-} CD8⁺ T cells (Fig. 2D). Together these data find that MAVS specifically promotes oxidative phosphorylation, but not glycolysis.

MAVS mediated metabolism promotes CD8⁺ T cell proliferation. Our *in vitro* studies show a defect in TCR stimulation-induced mitochondrial respiration in *Mavs*^{-/-} CD8⁺ T cells. CD8⁺ T cells utilize both glycolysis and oxidative phosphorylation to provide the necessary ATP and small molecules needed for proliferation and cell growth (200). Given our findings that MAVS does not impact the glycolytic pathway, we hypothesized that if forced to utilize oxidative phosphorylation *Mavs*^{-/-} CD8⁺ T cells would exhibit a proliferation and/or activation defect. To test this hypothesis, we stimulated CTV-stained WT and *Mavs*^{-/-} CD8⁺ T cells and cultured them in conditions of limiting glucose concentrations (Fig. 3A). WT CD8⁺ T cells cultured in no glucose or limited glucose (0-0.5 mM glucose) proliferate, but have a higher percentage of cells in division 0 or 1 as compared to cells cultured in excess glucose (5mM glucose) (Fig. 3B). However, in conditions of limited glucose, *Mavs*^{-/-} CD8⁺ T cells have a three-fold increase in the number of undivided cells as compared to WT CD8⁺ T cells, and significantly reduced frequency of cells that have undergone

one or more divisions (Fig. 3C). This proliferation defect can be rescued with the addition of glucose in a dose-dependent manner, as culturing *Mavs*^{-/-} CD8⁺ T cells in 0.5 mM glucose as compared to no glucose reduced the frequency of undivided cells by half (Fig. 3D). Thus, MAVS promotes activation induced proliferation of CD8⁺ T cells through non-glycolytic metabolism.

Loss of MAVS induces metabolic dysfunction in CD8⁺ T cells *in vivo*. To confirm our *in vitro* observations, we evaluated the expression of MAVS in antigen-specific CD8⁺ T cells during a viral infection. We utilized our previously described WNV-specific transgenic mouse model, W4B mice, in which >98% of CD8⁺ T cells express a TCR specific for the immunodominant epitope (SSVWNATTAI) of the NS4B protein of WNV (104). To evaluate the CD8⁺ T cell-intrinsic role of MAVS, we crossed *Mavs*^{-/-} mice to the transgenic W4B mice to generate *Mavs*^{-/-} W4B mice (86). Naïve CD8⁺ T cells were isolated from WT and *Mavs*^{-/-} W4B mice, and adoptively transferred into congenically marked CD45.1⁺ C57Bl/6 mice (50,000 WT or *Mavs*^{-/-} W4B cells per mouse) (Supplemental Fig. 1A). At 7 days p.i., W4B cells were sorted from the spleen of naïve mice or from the spleen and brain of WNV infected mice. Transferred W4B cells were identified as Live, CD8⁺, CD3⁺, NS4B⁺ and distinguished from endogenous populations using congenic markers (Supplemental Fig. 1B). Naïve WT and *Mavs*^{-/-} W4B cells were found to have similar phenotypes, as determined via flow cytometry analysis of CD62L and CD44 staining (Supplemental Fig. 1C), and this was confirmed in our RNA-Seq data. Differential gene expression analysis found 43 differentially expressed genes (DEG thresholds: $p < 0.01$, fold-change > 2 or < -2) between WT and *Mavs*^{-/-} W4B cells (Supplemental Fig. 1D). These findings indicate that MAVS does not play a role in quiescent CD8⁺ T cell homeostasis.

We next compared antigen-experienced WT and *Mavs*^{-/-} W4B cells isolated on day 7 p.i. as compared to naïve cells isolated from mock-infected mice. Similar to our protein expression data, we found that *Mavs* is expressed at the transcriptional level and is slightly upregulated in cells isolated from infected mice (Fig. 4A). WNV does not infect CD8⁺ T cells, but signaling components of the RLR pathway, including MDA5 (*Ifih1*), LGP2 (*Dhx58*), *Tbk1*, *Traf6*, *Irf3*, and *Irf7* are expressed basally and show changes in expression during virus infection. Moreover, Type I IFN transcripts (*Ifna2*, *Ifnb1*) were not expressed in cells isolated from either naïve or WNV-infected mice (Fig. 4B).

WNV infection induced significant transcriptional changes in W4B CD8⁺ T cells as compared to naïve W4B cells. While many of these genes were expressed in WT and *Mavs*^{-/-} W4B cells (2043 DEGs), a substantial number of unique DEGs were present only in WT (441 DEGs) or *Mavs*^{-/-} W4B cells (1571 DEGs) (Fig. 4C). To evaluate the metabolic signatures in W4B cells, we performed gene set enrichment analysis (GSEA) between WT and *Mavs*^{-/-} W4B cells using the Hallmarks data-set from the MSigDB database. GSEA identified significant enrichment of genes related to glycolysis, oxidative phosphorylation, and fatty acid oxidation in WT W4B cells as compared to *Mavs*^{-/-} W4B cells. Additionally, genes related to hypoxia were enriched in *Mavs*^{-/-} W4B cells, suggesting metabolic stress (Fig. 4D). In support, heatmap analysis identified genes associated with both ER stress (*Atf5*, *Hspa1b*, *Ddit3*) and hypoxia-induced stress (*Hif1a*) as more highly expressed in *Mavs*^{-/-} as compared to WT W4B cells (Fig. 4E).

To confirm these observations, WT and *Mavs*^{-/-} W4B cells were adoptively transferred, harvested at 8 days p.i., and mitochondrial potential was assessed using MitoTracker Orange staining, a cell

permeable dye that will be retained in active mitochondria. WT W4B cells from the brain had a distinct population of cells exhibiting high MitoTracker Orange staining, indicating either greater numbers of mitochondria or increased membrane potential in each mitochondrion. However, *Mavs*^{-/-} W4B cells completely lacked this population, with <1% of cells exhibiting high mitochondrial potential (Fig. 4F). Combined, these data demonstrate that MAVS functions in a T cell-intrinsic manner to regulate cell stress responses, metabolic profiles, and mitochondrial potential in CD8⁺ T cells during viral infection.

Cell-intrinsic MAVS promotes antigen-specific CD8⁺ T cell accumulation and cytotoxicity during infection. We next determined whether CD8⁺ T cell intrinsic MAVS plays a role in supporting T cell function during viral infection. WT and *Mavs*^{-/-} W4B cells were adoptively transferred (5000 cells/mouse) to congenically distinct (CD45.1) WT mice, infected with WNV-TX, and spleens and brains were harvested for flow cytometry analysis at 8 days p.i. We utilized congenic markers to distinguish transferred vs endogenous NS4B⁺ cells and found that *Mavs*^{-/-} W4B cells had decreased frequency (9.7%) compared to WT W4B cells (41%) in the brain (Fig. 5A). Additionally, the total number of *Mavs*^{-/-} W4B cells in the brain was 100-fold lower than WT W4B cells (Fig. 5A). *Mavs*^{-/-} W4B cells were also assessed in the spleen and found to have a similar defect in accumulation, with 40-fold fewer *Mavs*^{-/-} as compared to WT W4B (Fig. 5B). Thus, MAVS promotes the systemic accumulation of antigen-specific CD8⁺ T cells during viral infection.

We next examined if MAVS impacted CD8⁺ T cell activation during viral infection. There were no differences in the frequency of naïve (CD62L⁺ CD44⁻) or activated (CD62L⁻ CD44⁺) WT or *Mavs*^{-/-} W4B in the brain (Fig. 5C). The expression of other activation induced receptors, such as PD-1, and ICOS, were similarly unchanged between WT and *Mavs*^{-/-} W4B cells (Supplemental Fig. 2A-B). However, the mean fluorescent intensity (MFI) of CD44 was slightly elevated on *Mavs*^{-/-} W4B cells (Supplemental Fig. 2C). The differentiation status of WNV-specific CD8⁺ T cells was not affected by MAVS as frequencies of short-lived effector cells (SLEC) and memory precursor effector cells (MPEC) populations were similar between WT and *Mavs*^{-/-} W4B cells (Supplemental Fig. 2D). Transcriptional analysis of W4B cells from the brain at 7 days p.i., found that both WT and *Mavs*^{-/-} W4B cells had increased expression of genes related to a terminal effector profile (highlighted in purple, Fig. 5D), such as *Tbx21* or *Zeb2*, as compared to cells from naïve mice. However, there was no substantial difference in expression of terminal effector genes between WT and *Mavs*^{-/-} W4B cells, with most genes falling along the asymptote. Accordingly, WNV infection induced an equal downregulation of genes associated with a memory precursor profile in both WT and *Mavs*^{-/-} W4B cells (highlighted in pink, Fig. 5D). Heatmap analysis of activating receptors or effector functions found that most of the selected genes were equally upregulated in WT and *Mavs*^{-/-} W4B cells (*Fasl*, *Gzmb*, *Klrg1*, *Icos*, *Cd69*) as compared to naïve W4B cells. However, several genes were more highly expressed in the WT W4B cells (*Il2*, *Prf1*, *Il2ra*) while *Mavs*^{-/-} W4B cells had higher expression of *Tnf* and *Itgax* (Fig. 5E). Therefore, at 7 days p.i., W4B cells are most likely to be in the terminal effector phase and this differentiation is largely unaffected by MAVS. However, MAVS may play a role in regulating the expression of select genes associated with CD8⁺ T cell effector functions.

To evaluate the functional capacity of WT and *Mavs*^{-/-} WNV-specific CD8⁺ T cells, brain lymphocytes were stimulated *ex vivo* with NS4B peptide for 5 hours to measure intracellular cytokine production. Previous studies have identified TNF α , IFN γ , and perforin as important for the control of WNV in the brain, therefore we analyzed the frequency of W4B cells producing one or more of these molecules (49, 82, 179). As published previously, W4B cells in the brain primarily produced both TNF α and IFN γ in response to WNV, but there was no difference in the frequencies of TNF α ⁺ (Q2), IFN γ ⁺ (Q3), or double-positive (Q4) producers between WT and *Mavs*^{-/-} W4B cells (Fig. 5F, (104)). Perforin expression was significantly decreased in *Mavs*^{-/-} W4B cells from the brain, with WT W4B cells displaying 3-fold higher MFIs (Fig. 5G). Analysis of W4B cells isolated from the spleen yielded similar results (Supplemental Fig. 3). Cumulatively, these adoptive transfer experiments defined a cell-intrinsic role for MAVS in promoting antigen-specific CD8⁺ T cell accumulation and cytotoxic function.

MAVS promotes proliferation in a CD8⁺ T cell-intrinsic manner during viral infection. Our *in vitro* data identified a role for MAVS-mediated metabolism in promoting proliferation of CD8⁺ T cells when subjected to nutrient limiting conditions. To explore if the accumulation defect observed in mice that received *Mavs*^{-/-} W4B cells was due to a loss of proliferative ability, we performed GSEA between WT and *Mavs*^{-/-} W4B cells isolated from the brain at 7 days p.i. and subjected to mRNA-Seq. Through this analysis, we observed significant enrichment of genes associated with the G to M checkpoint and targets of E2F transcription factors in WT W4B cells (Fig. 6A). To characterize which transcription factors were important in controlling the disparate phenotypes of WT and *Mavs*^{-/-} W4B cells, we used iRegulon analysis (Cytoscape software) to identify the most common transcription factor motifs in DEGs from both samples, WT only, or

Mavs^{-/-} only. In agreement with our GSEA, a large number of the DEGs expressed only in WT W4B cells were targets of cell cycle regulators, including E2F1 (121 transcripts) and E2F3 (81 transcripts). In contrast, DEGs expressed only in *Mavs*^{-/-} W4B cells were targets of BCL-3 (144 transcripts) and ATF-4 (48 transcripts) regulation (Fig. 6B). Heatmap analysis of genes related to the formation of the mitotic spindle confirmed that most of these genes (*Bub1*, *Tpx2*, *Cdk1*) were more highly upregulated in WT W4B cells (Fig. 6C). Similar transcriptional phenotypes were observed in WT and *Mavs*^{-/-} W4B cells isolated from the spleen (Supplemental Fig. 4). Combined, these data indicate that MAVS plays an important role in promoting positive regulation of cell cycle genes in antigen-specific CD8⁺ T cells.

Based on our mRNA-Seq data, we next decided to test if MAVS impacts CD8⁺ T cell proliferation during virus infection. We infected C57Bl/6J mice with WNV-TX, and at 5 days p.i. performed adoptive transfers of WT or *Mavs*^{-/-} W4B cells labelled with the proliferation tracking dye, Cell Trace Violet (CTV). Given the global similarity of WT and *Mavs*^{-/-} W4B cells isolated from the brain and spleen (Supplemental Fig. 3&4), we analyzed splenic W4B cells via flow cytometry for CTV dilution at 7 days p.i. (2 days post transfer, Supplemental Fig. 5A). Flow cytometry analysis demonstrated that W4B cells were partially activated at 2 days post transfer, with 40-50% of W4B cells expressing both CD62L and CD44. Interestingly, *Mavs*^{-/-} W4B cells had slightly higher expression of CD44 compared to WT, indicating higher levels of activation (Supplemental Fig. 5B). Despite similar or even higher activation, *Mavs*^{-/-} W4B cells had significantly reduced frequencies of cells that had entered division as compared to WT W4B cells. Up to 80% of WT W4B cells had undergone one or more divisions, while only 50-60% of *Mavs*^{-/-} W4B cells had divided. This resulted in a lower percentage of *Mavs*^{-/-} W4B cells in each subsequent division, and

a reduced overall division index (Fig. 6D). The lack of proliferation did not correlate to an increase in apoptosis, as Annexin V staining was comparable between both WT and *Mavs*^{-/-} W4B cells (Supplemental Fig. 5C). The higher frequencies of undivided *Mavs*^{-/-} W4B cells, unchanged apoptosis, and lower expression of cell-cycle associated genes demonstrate that the reduced number of *Mavs*^{-/-} W4B cells during WNV infection is attributable to decreased initiation of proliferation in response to antigen.

DISCUSSION

Our study identifies a cell-intrinsic and non-canonical role for MAVS in promoting mitochondrial respiration to facilitate antigen specific CD8⁺ T cell proliferation during viral infection. MAVS is constitutively expressed in CD8⁺ T cells and promotes mitochondrial elongation and oxidative phosphorylation in activated CD8⁺ T cells. MAVS-mediated metabolism supports proliferation of CD8⁺ T cells after TCR stimulation. *In vivo* studies identify a role for MAVS in regulating antigen-specific CD8⁺ T cell metabolism and mitochondrial potential. Adoptive transfer experiments determined that CD8⁺ T cell intrinsic MAVS promotes antigen-specific cell accumulation and cytotoxicity. Mechanistically, MAVS promotes entry into proliferation, and positive regulation of the cell cycle. Thus, MAVS is an essential component of the metabolic signaling networks that support the expansion of antigen-specific CD8⁺ T cell responses during viral infection.

The RLR signaling pathway has been previously linked to changes in mitochondrial dynamics. In models of viral infection, the propagation of RLR signaling requires mitochondrial potential and is promoted by mitochondrial fusion, and reactive oxygen species release (147, 152, 173, 203).

Activation of RLR pathway signaling in turn promotes mitochondrial fusion, suggesting a feedback loop between RLR signaling and mitochondrial fusion/fission (147). In this study we find that *Mavs*^{-/-} CD8⁺ T cells have increased numbers of more circular mitochondria as compared to WT cells, a phenotype that is characteristic of cells with a defect in mitochondrial fusion (201). Accordingly, MAVS has been demonstrated via immunoprecipitation assays to physically interact with MFN1 and MFN2, which are key regulators of mitochondrial fission and fusion (150, 152). Together these data warrant further studies into the role of MAVS in mitochondrial turnover and fusion/fission. In our study, we focused primarily on the role of MAVS at the mitochondria, however MAVS can also be found in the mitochondrial-associated-membrane subdomain of the ER and peroxisomes (204, 205). RNA-Seq analysis of *Mavs*^{-/-} CD8⁺ T cells found increased levels of ER stress related genes, and ATF-4 targets as compared to WT cells (Fig. 4). Whether this phenotype is a secondary consequence of dysregulated mitochondrial dynamics and respiration or another direct function of MAVS is a subject for further studies.

These data add to a growing body of literature identifying roles for innate immune signaling components, including MAVS, in regulating adaptive immunity. A mixed bone-marrow chimera model found cell-extrinsic MAVS signaling promotes expansion of T regulatory cells in response to WNV infection. (156). Studies in a model of systemic lupus erythematosus identified B-cell intrinsic MAVS signaling as necessary for autoantibody production (206). Thus, MAVS has both extrinsic and intrinsic signaling functions in B and T cells, as in our study we find that cell-intrinsic MAVS promotes the expansion of antigen-specific CD8⁺ T cells. Similar functions have been found for other innate immune molecules in CD8⁺ T cells, such as MyD88, a critical adaptor protein for the toll-like receptor pathway, which promotes the expansion of naïve but not memory

CD8⁺ T cells during lymphocytic choriomeningitis viral (LCMV) infection (207-209). The RLR pathway component, LGP2, functions in a cell-intrinsic manner to promote CD8⁺ T cell survival by modulating the levels of Fas-ligand expression (157). CD8⁺ T cell intrinsic MAVS supports proliferation through the promotion of mitochondrial metabolism, joining a variety of innate immune molecules that have been implicated in the regulation of CD8⁺ T cell metabolism. For example, C1q, an initiator of the complement pathway, promotes mitochondrial metabolism upon internalization by CD8⁺ T cells specifically in MPECs (210). Additionally, the viral sensor, STING, can regulate ER stress and calcium homeostasis in response to TCR signaling independently of Type I IFN in CD8⁺ T cells (211). Combined with our data, these studies highlight the interactions of innate immune sensors and metabolic pathways which together influence CD8⁺ T cell expansion and function.

The metabolic networks that regulate CD8⁺ T cell function and differentiation are just beginning to be characterized, and in this study we identify MAVS-mediated mitochondrial metabolism as part of this system. Mitochondrial respiration is essential for the establishment and maintenance of memory CD8⁺ T cells, and limited mitochondrial spare respiratory capacity inhibits the ability of memory T cells to respond to antigen (198, 201). Tissue resident memory CD8⁺ T cells in the CNS are established in response to viral infection, and respond to new antigen primarily through the production of IFN γ (212). A WNV-specific CD8⁺ T cell population in the CNS is necessary to control viral replication and prevent death (100). However, IFN γ production by T cell populations persisting in the CNS after the resolution of WNV infection contributes to neurological sequelae during recovery (8). Thus, CD8⁺ T cell intrinsic MAVS signaling is part of a complex network that orchestrates the balance between viral clearance, resident memory formation, and

pathology in the CNS. Consideration of MAVS signaling in promoting effective resident T cell memory populations will be important for vaccine design targeting the CNS.

MATERIALS AND METHODS

Viruses and animals. WNV isolate Texas 2002-HC (WNV-TX) has been previously described. WNV-TX stock titers were measured by plaque assay on BHK-21 cells. C57BL/6J and Prtprc mice were bought from Jackson Laboratories or bred in-house at the Yerkes National Primate Research Center rodent facility at Emory University. W4B transgenic mice were originally generated by the Bevan laboratory and bred in-house. *Mavs*^{-/-} mice have been previously described and were bred in-house (84). For WNV-TX infections, adult male and female mice (8-12 weeks old) were inoculated subcutaneously in the rear footpad with 100 plaque-forming units (PFU) of WNV-TX, and infected mice were monitored and weighed daily. All experiments adhered to the guidelines approved by the Emory University Institutional Animal Care and Committee.

CD8⁺ T cell *in vitro* stimulation. Spleens were dissected from naïve WT or *Mavs*^{-/-} mice, and mechanically homogenized. Tissue suspension was collected in 1% FBS-HBSS and spun down. Cells were lysed with ACK lysis buffer (Lonza) for 5 minutes at 4°C. Lysis was stopped with 10 mLs of FBS-HBSS and suspension was passed through a 70 µM filter. CD8⁺ T cells were isolated using the MojoSort Negative Selection Kit (Biolegend, 480035) according to the manufacturer's instructions. After isolation, cells were washed, counted, and resuspended at 2 x 10⁶ CD8⁺ T cells/mL in complete T cell media (10% FBS, Non-essential amino acids, glutamine, HEPES, antibiotics, sodium pyruvate, RPMI). Cells were processed immediately for use, or stimulated with

anti- CD3 (1 $\mu\text{g}/\text{mL}$, Tonbo Biosciences) and anti- CD28 (1 $\mu\text{g}/\text{mL}$, Tonbo Biosciences) at 37°C for the indicated time.

Adoptive transfer experiments. Spleens from naïve WT or *Mavs*^{-/-} W4B mice were processed to a single-cell suspension, red-blood cells were lysed, and CD8⁺ T cells were isolated using a negative-selection kit. Cells were counted and resuspended in sterile PBS at 5 x 10³ cells/ 100 μL (unless stated otherwise). Mice were anesthetized using an isoflurane vaporizer, and 100 μL of cell suspension was administered via the retro-orbital route to each recipient. At 8 days p.i. (unless otherwise indicated), mice were anesthetized and intravital labeling was performed by injecting 100 μL of CD8-APC or CD8-PE (1:20 dilution in PBS) via the retro-orbital route. After 5 minutes, mice were euthanized via isoflurane overdose. Spleens and brains were collected in 1% FBS-HBSS and placed on ice for processing. Spleens were mechanically homogenized, lysed in ACK lysis buffer for 5 minutes at 4°C, and passed through a 70 μM to obtain a single cell-suspension. Brains were mechanically homogenized, digested for 15 min at room temperature in Liberase (Sigma, #540102000, 50 μg) diluted in PBS, and pushed through a filter to obtain a single-cell suspension. Cells were resuspended in a 30% Percoll-PBS (GE Healthcare) solution and spun at 2000 rpm for 20 min. The top layer was discarded to remove any myelin debris, and the pellet was collected. Brain and spleen single cell suspensions were resuspended in 10% FBS-DMEM and stored on ice until ready for staining for flow cytometry analysis.

Flow cytometry analysis. Single-cell suspensions were spun down, and resuspended in anti-CD16/32 (Tonbo, Clone 2.4G2) blocking solution for 20 minutes at 4°C. If indicated, tetramer

staining was performed after the blocking step by resuspending cells in NS4B tetramer (Yerkes Tetramer Core) diluted 1:250 in FACS (1%FBS-PBS) buffer. If indicated, MitoTracker Orange (ThermoFisher) staining was performed after blocking; a fresh vial of MitoTracker Orange was resuspended in DMSO, and diluted 1:10,000 in sterile PBS. Cells were resuspended in MitoTracker:PBS solution (1 million cells/ 1 mL), and incubated for 15 min at 37°C. After incubation cells were washed with 10% FBS-RPMI. For all experiments; cell suspensions were spun down, and stained with Live/Dead Ghost Dye stain (Tonbo Biosciences) for 20 minutes at 4°C. Cells were washed, and resuspended in the indicated surface stain in FACS buffer for 20 minutes at 4°C. After staining, cells were washed and fixed in 2%PFA-PBS for 20 minutes at room temperature. Precision count beads (Biolegend) were added to samples to obtain counts. Samples were run on a BD FACS Symphony A5 or a LSRII.

The following antibodies were used in this study: CD45.2-PE-Cy7 (Tonbo, Clone:104), CD45.1-vF450 (Tonbo, A20), CD3-BUV737C (BD Biosciences, 1452C11), CD8-APC, CD8-AF700 (BD Pharmingen, 52-6.7), CD44-APC-Cy7(Tonbo, IM7), CD62L-PerCpCy5.5 (BD Biosciences, MEL-14), PD-1-BV650 (BD Biosciences, J43), ICOS-BUV395 (Fisher Scientific, C398.4A), IFN γ -PE-Dazzle (Biolegend, XMG1.2), TNF α -BV711 (BD Biosciences, MP6-XT22), Perforin-PE (Biolegend, S1600A), KLRG1-BV605 (BioLegend, MAFA), IL-7R-FITC (Biolegend, A7R34).

Ex vivo stimulation for cytokine analysis. Freshly isolated single cell suspensions were incubated with NS4B tetramer (1 μ g/mL) and Golgi-Plug (1 μ g/mL, BD Biosciences) for 5 hours at 37°C.

Cells were washed, and surface staining for flow cytometry was performed as described above. Cells were fixed in 2% PFA-PBS for 30 min at 4°C. After fixation, cells were permeabilized using a FoxP3 Fix/Perm Kit (Tonbo). Permeabilized cells were stained for intracellular cytokine analysis in FACS Buffer containing the following antibodies : IFN γ , TNF α , Perforin

Immunoblotting. Cells were lysed in cold, modified radioimmunoprecipitation assay buffer (1.2% Tris, 8.7% NaCl, 10% Na-deoxycholate, 10% Triton X-100) supplemented with Halt Protease Inhibitor Cocktail (ThermoFisher) and phosphatase inhibitor cocktail II (Calbiochem) on ice for 30 minutes. Lysates were spun down at 15,000 rpm for 10 minutes at 4°C to clear cell debris, and the supernatant was removed. Protein concentration was measured using a Bradford Assay and 10 μ g of protein sample was mixed with loading dye and boiled at 95°C for 15 minutes. Samples underwent SDS-PAGE and western blot analysis as previously described to detect MAVS (Cell Signaling, #4983S), and Tubulin (Cell Signaling, #3873(157)).

RNA-Sequencing. As described above, brains and spleens from 7 day p.i. mice or naïve mice were processed to single cell suspensions. Cells were stained with CD45.2(PE-Cy7), CD45.1(Bv450), CD8(AF700), CD3(PerCpCy5.5), and Live/Dead (BV510) for 30 min at 4°C. Transferred W4B cells were sorted using congenic markers (n = 4-5 per group), 10,000 viable cells were sorted into 100 μ l RLT buffer (Qiagen) with β 2-mercaptoethanol (1:100). mRNA sequencing libraries were prepared and sequenced at Yerkes Genomics Core (http://www.yerkes.emory.edu/nhp_genomics_core/). Reads were mapped to the GENCODE mouse reference genome (GRCm38.p5, release M16) as previously described (192). Reads were

normalized and differentially expressed gene analysis was performed using DESeq2 (194). Normalized read counts were expressed as fold change over mock values. Gene set enrichment analysis was performed using software from the Broad institute and the Hallmarks gene set from the MSigDB database. Identification of transcription factor networks was performed using the iRegulon plug-in for Cytoscape software. The data provided in this paper will be deposited in NCBI's Gene Expression Omnibus and will be available through a GEO accession number.

Cell-Trace Violet proliferation tracking. Naïve W4B WT and *Mavs*^{-/-} CD8⁺ T cells were isolated from spleens as described above. Isolated W4B cells were stained with Cell Trace Violet (1 μ L/ 10 million cells, Thermo Fisher) for 20 minutes at 37°C, then washed and spun down. Stained cells were resuspended at 1×10^6 cells/ 100 μ L in sterile PBS. CTV-labelled W4B cells were adoptively transferred into C57Bl/6 mice at day 5 post WNV-TX infection via the retro-orbital route (100 μ L cells/mouse). Mice were euthanized at day 7 post infection (2 days after transfer) and spleens were collected for flow cytometry analysis as described above.

Seahorse Assays. As described above, CD8⁺ T cells from WT and *Mavs*^{-/-} mice were isolated and stimulated for 24 hours. Naïve and stimulated CD8⁺ T cell numbers were counted and 200,000 cells were added to each well of a Poly-D-Lysine (Sigma-Aldrich) coated Seahorse cell culture plate and spun down at 400 \times g for 5 minutes to create an adherent monolayer. The supernatant was removed and replaced with XF assay media (150 μ L total, Agilent Technologies), and the cells were equilibrated for 30 minutes in an XF prep station. Mitochondrial stress assays were performed in a Seahorse Extracellular 96 well analyzer (Agilent Technologies) by measuring

oxygen consumption rate before and after the addition of oligomycin (2 μ M, Sigma-Aldrich), FCCP (2.5 μ M), and Rotenone/Atinomycin (1.25 μ M, Sigma-Aldrich). Glycolytic flux tests were performed by measuring extracellular acidification rate before and after the addition of glucose (10 mM, Sigma-Aldrich), oligomycin (2 μ M), and 2-DG (50 mM, Sigma-Aldrich). Greater than 6 technical replicates were used for each condition.

Transmission electron microscopy. WT and *Mavs*^{-/-} CD8⁺ T cells were isolated and stimulated as described above. For each sample, 3 million cells were collected and washed 3 times with PBS. To remove excess salts, cells were washed 2 times with cocodyllate fix buffer (pH 7.4) twice before post-fixation in 1% osmium tetroxide for 1 hour. After additional buffer rinses, samples were dehydrated through an ethanol series and then with three additional, 15-minute, 100% ethanol exchanges. Samples were initially infiltrated with a mixture of propylene oxide and Eponate 12 resin (Ted Pella Inc., Redding, CA), then embedded in pure Eponate 12 resin in BEEM capsules (Ted Pella Inc., Redding, CA), and finally placed in a 60°C oven for polymerization. 80-90 nm ultrathin sections were cut with a Leica EM CU6 ultramicrotome (Leica Microsystems Inc., Buffalo Grove, IL), and placed on 200 mesh copper grids. Sections were stained with uranyl acetate for 15 minutes followed by lead citrate for 15 minutes. Sections were imaged on a JEOL JEM-1400 transmission electron microscope (Tokyo, Japan) operated at 80 kV. Images were acquired at magnifications ranging from 2000x to 5000x using a Gatan US1000 CCD camera (Gatan Inc., Pleasanton, CA).

ACKNOWLEDGEMENTS

The research reported in this publication was supported in part by the National Institutes of Health ORIP/OD P51OD011132, R21AI154352 (M.S.S), U19AI00625 (M.S.S), 1R56AI147623 (M.S.S), Children's Healthcare of Atlanta, Emory Vaccine Center, and The Georgia Research Alliance (M.S.S). The Yerkes NHP Genomics Core is supported in part by NIH P51OD011132, and an equipment grant, NIH S10 OD026799. We also thank the Yerkes and Emory Pediatrics Flow Cytometry Core. We acknowledge the NIH Tetramer Core Facility (contract HHSN272201300006C) for provision of tetramers. This study was supported by the Robert P. Apkarian Integrated Electron Microscopy Core (RPAIEMC), which is subsidized by the Emory University School of Medicine and the Emory College of Arts and Sciences. Additional support was provided by the Georgia Clinical & Translational Science Alliance of the National Institutes of Health under award number UL1TR000454. The data described here was collected on the JEOL JEM-1400, 120kV TEM supported by the National Institutes of Health Grant S10 RR025679. The Flow Cytometry Core is generously supported by Children's Healthcare of Atlanta, Winship Cancer Institute, and Emory University. The funders had no role in study design, data collection and analysis, decision to publish, or preparation, the manuscript.

AUTHOR CONTRIBUTIONS

A.V. contributed to the acquisition, analysis, and interpretation of the data, as well as the conception and design of the work, and writing the manuscript. R.A. contributed to the acquisition, analysis of the data, and conception of the work. H.V. contributed to the acquisition, analysis, and interpretation of the data. F.Z. and M.P. contributed to the methodology and acquisition of the data. J.B. contributed to the interpretation of data and conception of the work. A.G. and M.S.S.

contributed to the interpretation of data, conception and design of the work, and writing the manuscript.

FIGURES

Figure 1.

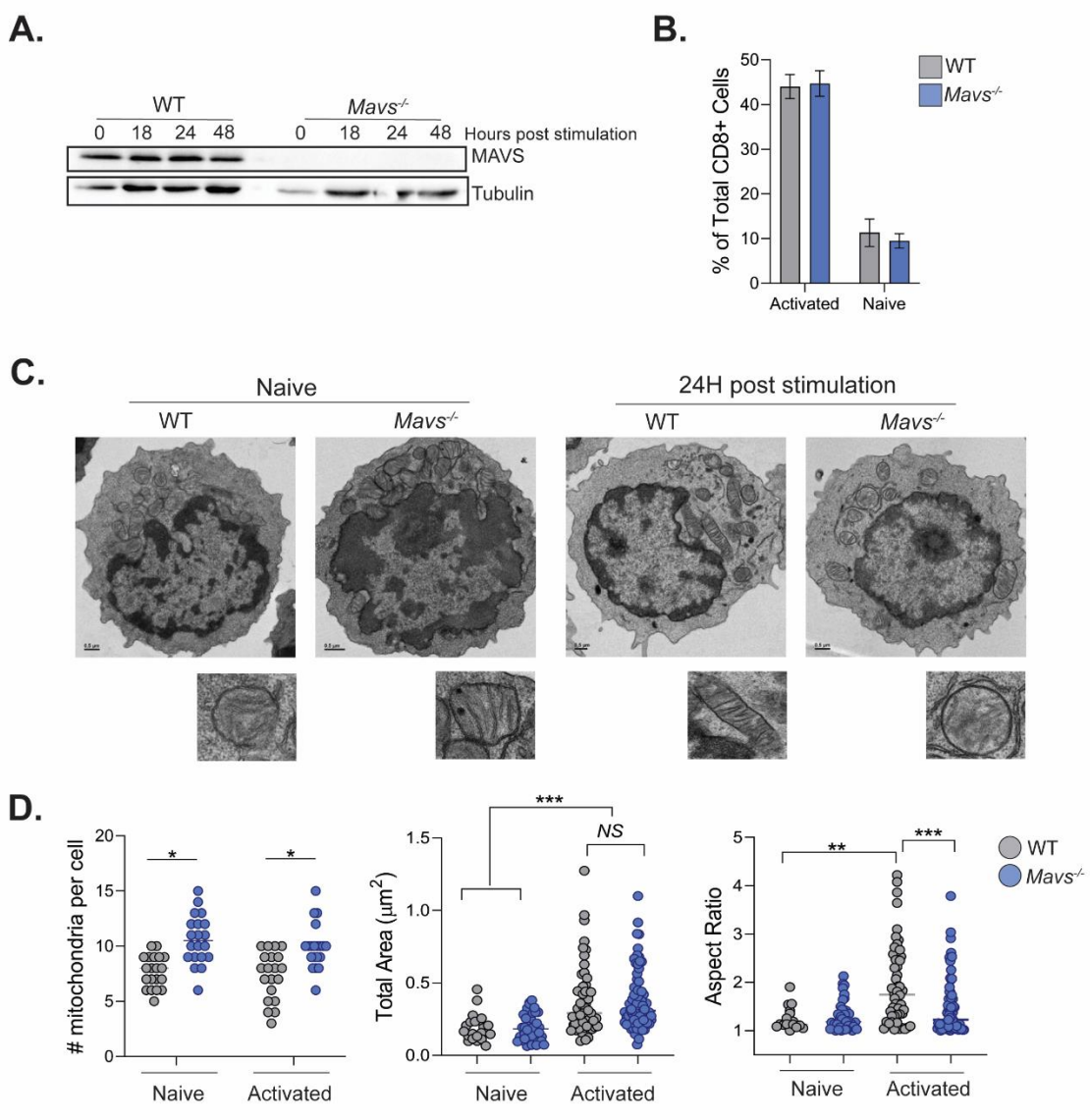


Figure 1. MAVS regulates mitochondrial number and elongation in activated CD8+ T cells.

WT or *Mavs*^{-/-} CD8+ T cells were isolated from naïve spleens, and used immediately for assays or stimulated with anti-CD3/CD28 for up to 48 hours. A) Samples were collected at the indicated timepoints and analyzed via western blot for MAVS expression. B) Frequency of naïve (CD62L+ CD44-) or activated (CD62L- CD44+) WT or *Mavs*^{-/-} CD8+ T cells at 48 hours post activation. C) Transmission electron microscopy (TEM) was performed on naïve and stimulated WT or *Mavs*^{-/-} CD8+ T cells. Representative images are shown for each condition, below each image are magnified images of a representative mitochondria from the above cell. D) 30-50 cells per group were used to quantify the following measurements of mitochondria; total number, total surface area, aspect ratio. Results are representative of 3 independent experiments. Statistical significance was determined using unpaired student's t-tests or two-way ANOVA. * = p<0.05, **= p<0.01, ***= p<0.001, ****= <0.0001.

Figure 2.

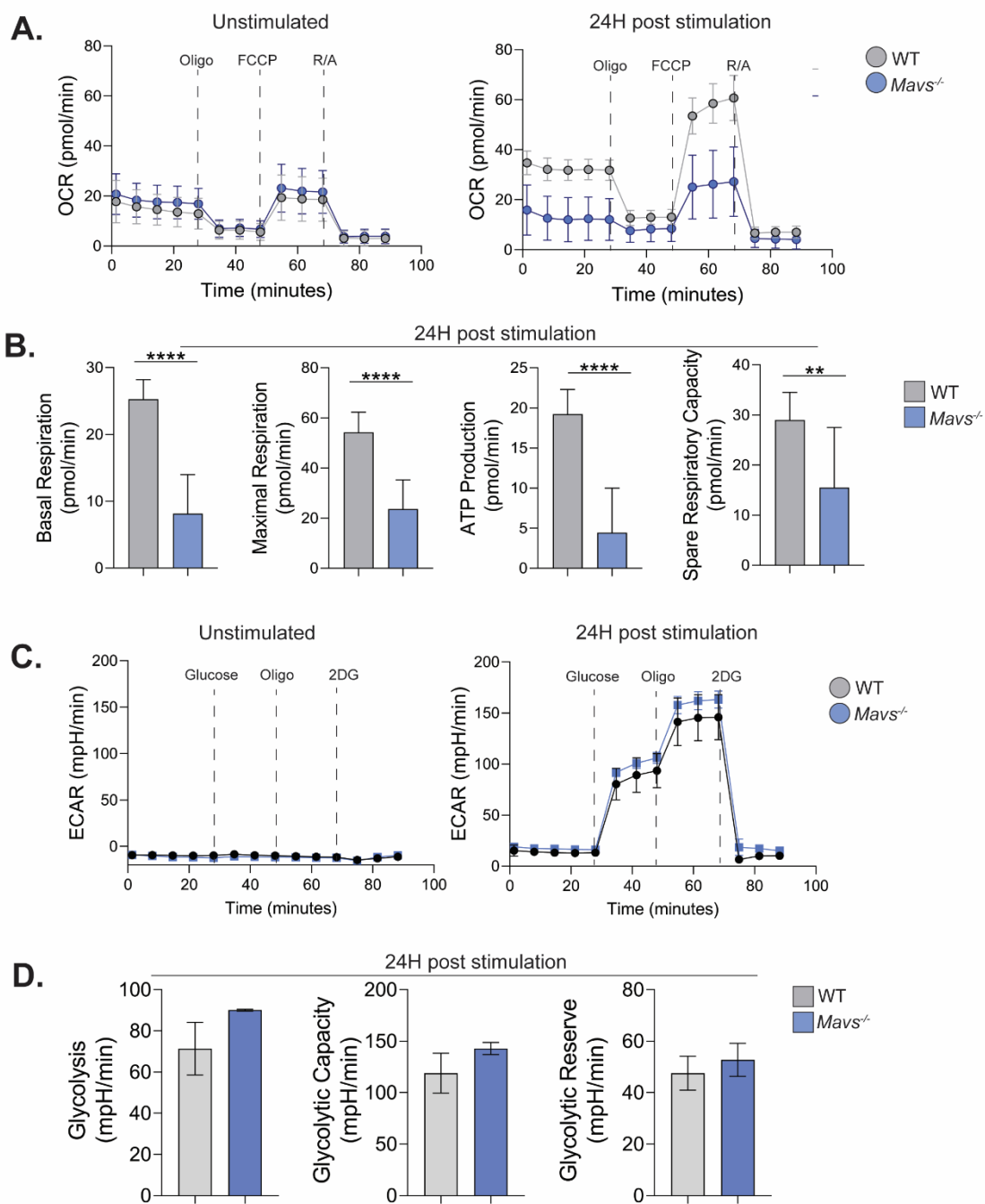


Figure 2. MAVS promotes oxidative phosphorylation in activated CD8⁺ T cells. A) A Seahorse oxidative stress test was performed for the indicated samples. Representative oxygen consumption rates (OCR) are shown (average of 6+ technical replicates) for one biological replicate before and after the addition of oligomycin (oligo), FCCP, and rotenone/atinomycin (R/A). B) The indicated measure of mitochondrial function as determined by seahorse assay at 24 hours post stimulation (3-4 biological replicates per group). C) A Seahorse glycolytic flux test was performed for the indicated samples. Representative extracellular acidification rates (ECAR) are shown (average of 6+ technical replicates) for one biological replicate before and after the addition of glucose, oligomycin (oligo), and 2-deoxyglucose (2DG). D) The indicated measure of glycolytic flux as determined by seahorse assay (3-4 biological replicates per group). Results are representative of 3 independent experiments. Statistical significance was determined using unpaired student's t-tests. * = $p < 0.05$, ** = $p < 0.01$, *** = $p < 0.001$, **** = $p < 0.0001$.

Figure 3.

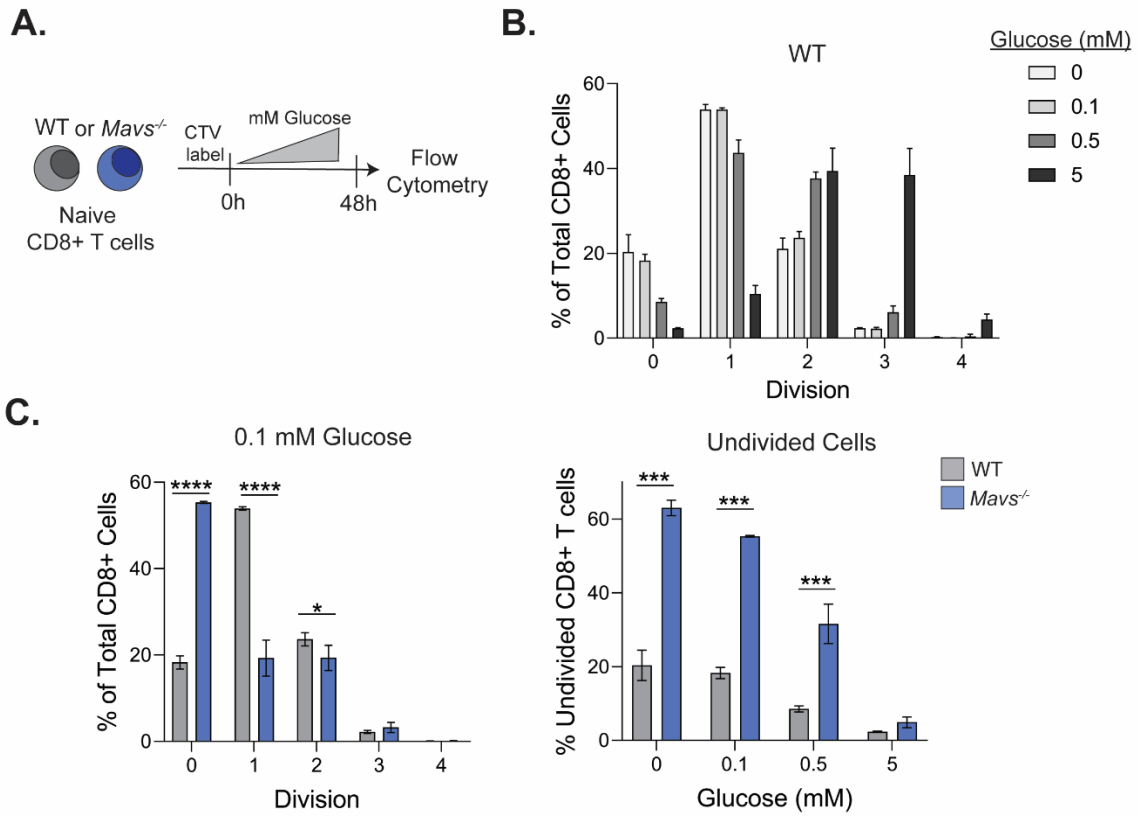


Figure 3. MAVS-mediated metabolism promotes CD8+ T cell proliferation. A) Experimental schematic. WT or *Mavs*^{-/-} CD8+ T cells were isolated from naïve mice, labelled with cell trace violet (CTV), and stimulated with (α CD3/CD28) for 48 hours with varying concentrations of added glucose. Proliferation was analyzed by tracking CTV dilutions via flow cytometry. B) The percentage of WT cells in each division at varying concentrations of added glucose. C) The percentage of WT or *Mavs*^{-/-} cells in each division with 0.1 mM glucose, or on the right, the percentage of undivided cells from each genotype at varying concentrations of glucose. Results are representative of 3 independent experiments. Statistical significance was determined using unpaired student's t-tests or two-way ANOVA. * = $p < 0.05$, ** = $p < 0.01$, *** = $p < 0.001$, **** = $p < 0.0001$.

Figure 4.

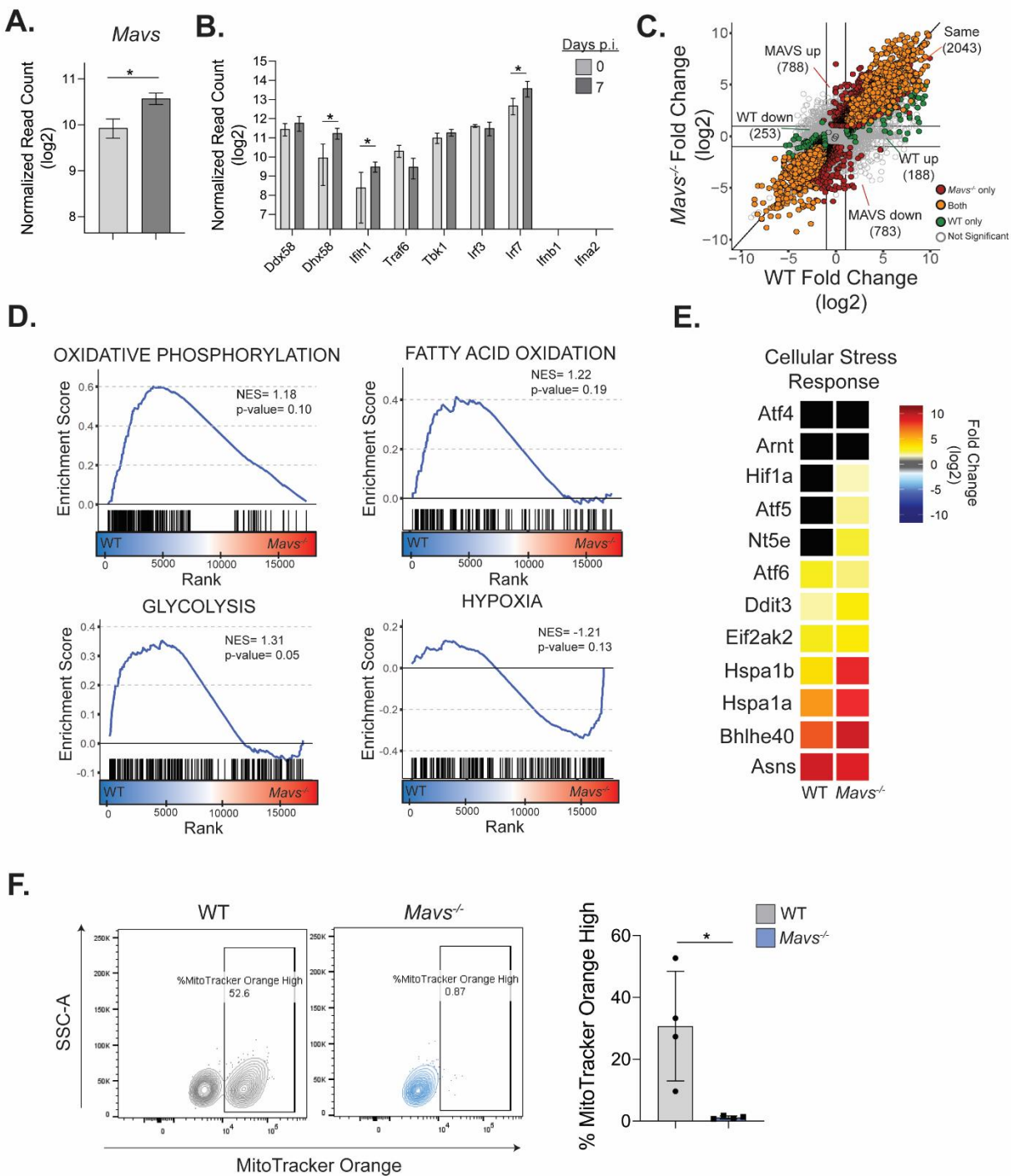


Figure 4. *Mavs*^{-/-} W4B cells have dysregulated metabolic profiles during WNV infection. WT or *Mavs*^{-/-} W4B cells were adoptively transferred via the retro-orbital route to congenically distinct WT mice (50,000 cells/mouse). 1 day post transfer, mice were infected with WNV-TX (100 pfu) via subcutaneous footpad inoculation and at 7 days p.i., sorted from the brain for mRNA-Seq analysis (n=4-5) A) Normalized read counts for *Mavs* are shown for WT W4B cells from the spleens of naive (grey) and infected (black) mice. B) Normalized read counts in WT W4B cells sorted from spleens at day 0 and 7 days p.i. for selected RLR pathway genes. C) DEG analysis was performed by comparing WT and *Mavs*^{-/-} genes to their respective naive controls. WT and *Mavs*^{-/-} fold change over naive were plotted against each other to highlight DEGs expressed in both (orange), WT only (green), or *Mavs*^{-/-} only (red). Non-significant genes are highlighted in grey (cutoffs: fold-change <-2 or > 2, p-value < 0.01). D) GSEA using Hallmarks data set of WT over *Mavs*^{-/-} for the indicated gene sets. E) Heatmap of the indicated gene set for WT and *Mavs*^{-/-} fold change over mock. D) Adoptively transferred WT or *Mavs*^{-/-} W4B cells were analyzed via flow cytometry from the brain at 8 days p.i. for mitochondrial potential. Left; representative flow plots of MitoTracker orange staining in the two genotypes, Right; percentage of each genotype that was MitoTracker Orange High. Results are representative of 2 independent experiments with 4-6 mice each. Statistical significance was determined using unpaired student's t-tests or two-way ANOVA.

* = p<0.05.

Figure 5.

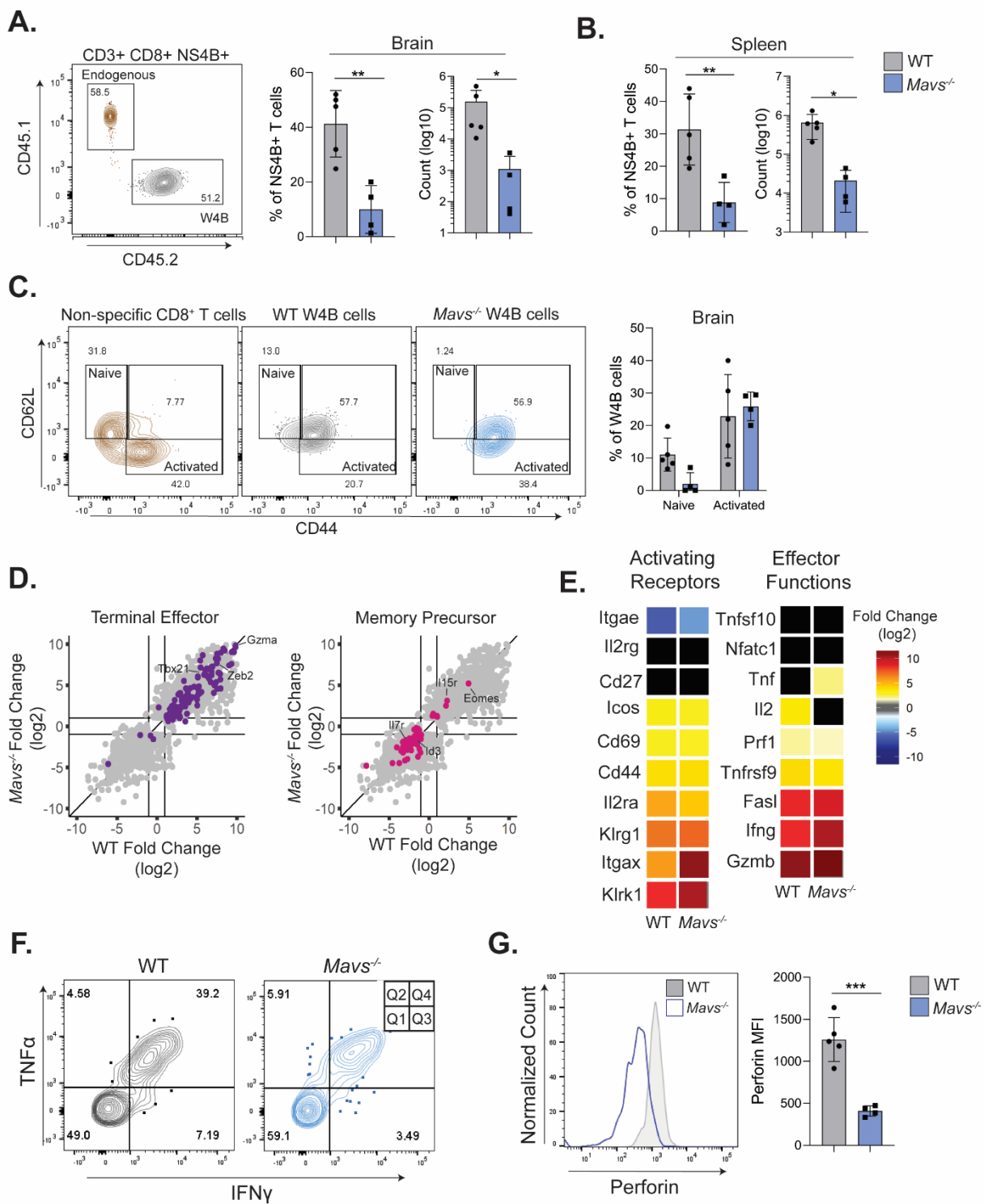


Figure 5. Cell-intrinsic MAVS promotes antigen-specific CD8+ T cell accumulation and cytotoxicity during WNV infection. W4B cells were isolated from WT or *Mavs*^{-/-} mice, adoptively transferred and on day 8 p.i. with WNV-TX, brains were collected for flow cytometry analysis. A) Representative flow plot illustrating the gating strategy to identify transferred WT W4B cells. Quantification of the frequency (of total NS4B tetramer+ cells) and count of WT and *Mavs*^{-/-} W4B cells in the brain on the right. B) Frequency and total count of WT and *Mavs*^{-/-} W4B cells in the spleen. C) Representative flow plots illustrating the percentage of naïve (CD62L+ CD44-) and activated (CD62L- CD44+) W4B cells of each genotype. Non-specific (NS4B tetramer-) CD8+ T cells are illustrated as a control. Frequencies are quantified on the right. D-E) mRNA-Seq analysis was performed on WT or *Mavs*^{-/-} W4B cells isolated from the brain as described in Fig. 3. D) All significant DEGs are highlighted in grey, genes included in the indicated gene set are highlighted in purple (Terminal Effector) or pink (Memory Precursor). E) Heatmap of the indicated gene sets in WT and *Mavs*^{-/-} cells. F-G) Cells were isolated from the brain and stimulated *ex vivo* with NS4B peptide (1 ug/mL) and GolgiStop for 5 hours at 37°C. Intracellular staining was used to analyze cytokine and cytotoxic molecule production. F) Representative flow plots of IFN γ and TNF α production by WT or *Mavs*^{-/-} W4B cells from the brain or spleen, illustrating the frequency of W4B cells in each quadrant (Q1: IFN γ ⁻TNF α ⁻, Q2: IFN γ ⁻TNF α ⁺, Q3: IFN γ ⁺TNF α ⁻, Q4: IFN γ ⁺TNF α ⁺). G) Representative histograms of perforin expression in WT or *Mavs*^{-/-} W4B cells from the brain, with the mean fluorescent intensity (MFI) quantified on the right. Results are representative of 2 independent experiments with 4-6 mice each. Statistical significance was determined using unpaired student's t-tests or two-way ANOVA. * = p<0.05, **= p<0.01, ***= p<0.001.

Figure 6.

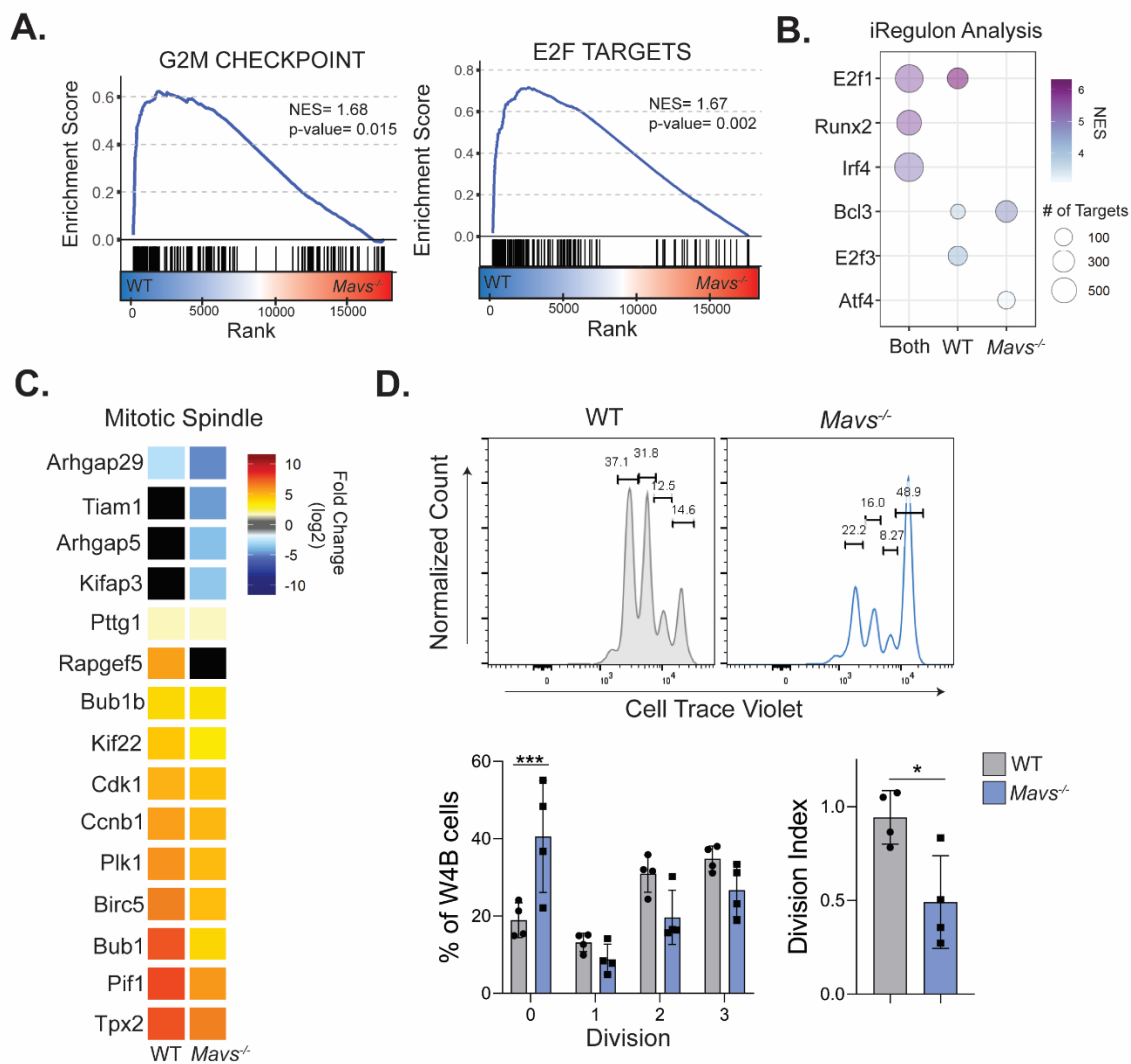
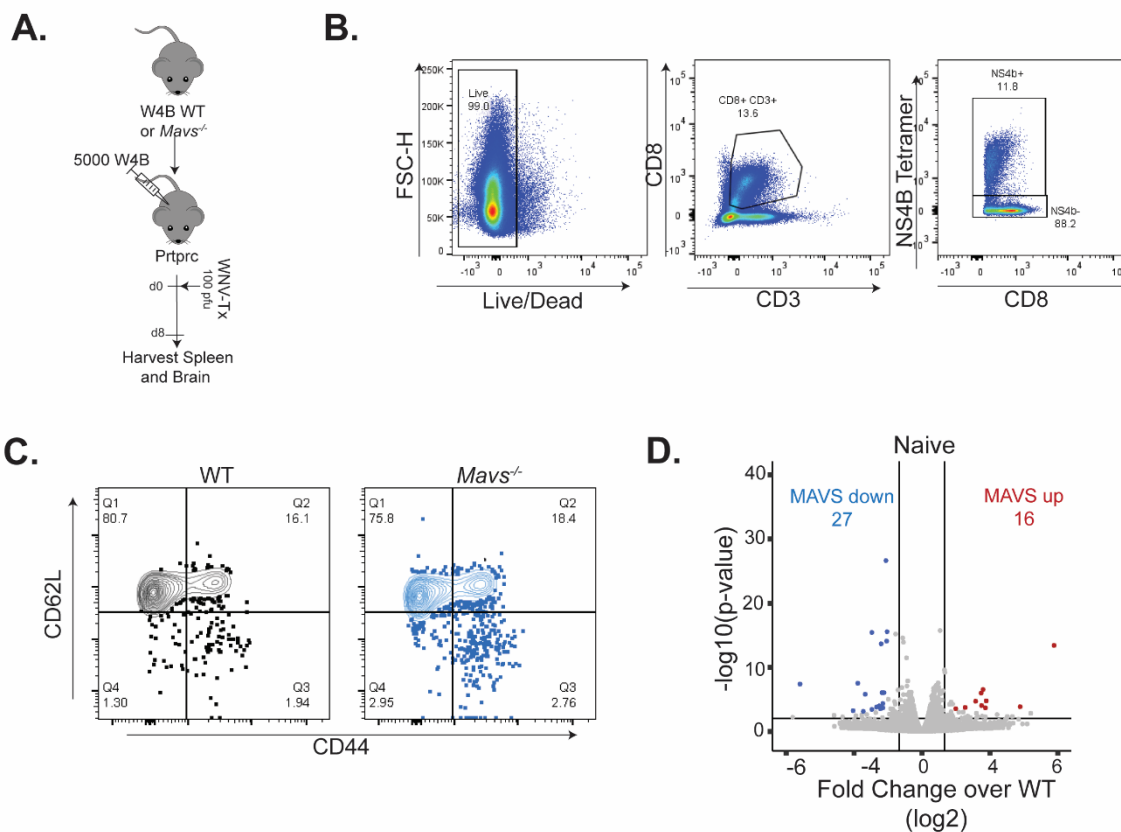


Figure 6. MAVS promotes proliferation of antigen-specific CD8⁺ T cells during viral infection. mRNA-Seq analysis was performed on WT or *Mavs*^{-/-} W4B cells isolated from the brain as described in Fig. 3. A) GSEA of WT (left, blue) over *Mavs*^{-/-} (red, right) for the indicated gene sets from the Hallmarks collection (MSigDB). B) The iRegulon plug-in for cytoscape software was used to identify the transcription factors driving DEGs in both genotypes, WT only, or *Mavs*^{-/-} only. Bubble size indicates the number of targets for the indicated transcription factor, bubble color indicates the normalized enrichment score (NES). C) Heatmap of the indicated genes related to the mitotic spindle. D) WT mice were infected with WNV-TX, and at 5 days p.i. received CTV labelled naïve WT or *Mavs*^{-/-} W4B cells. At 7 days p.i., spleens were analyzed via flow cytometry for CTV expression. Representative histograms of CTV dilutions in W4B cells, the corresponding percentages in each division, and division index below. Results are representative of 2 independent experiments with 4-5 mice each. Statistical significance was determined using unpaired student's t-tests or two-way ANOVA. * = p<0.05, **= p<0.01, ***= p<0.001.

SUPPLEMENTAL FIGURES

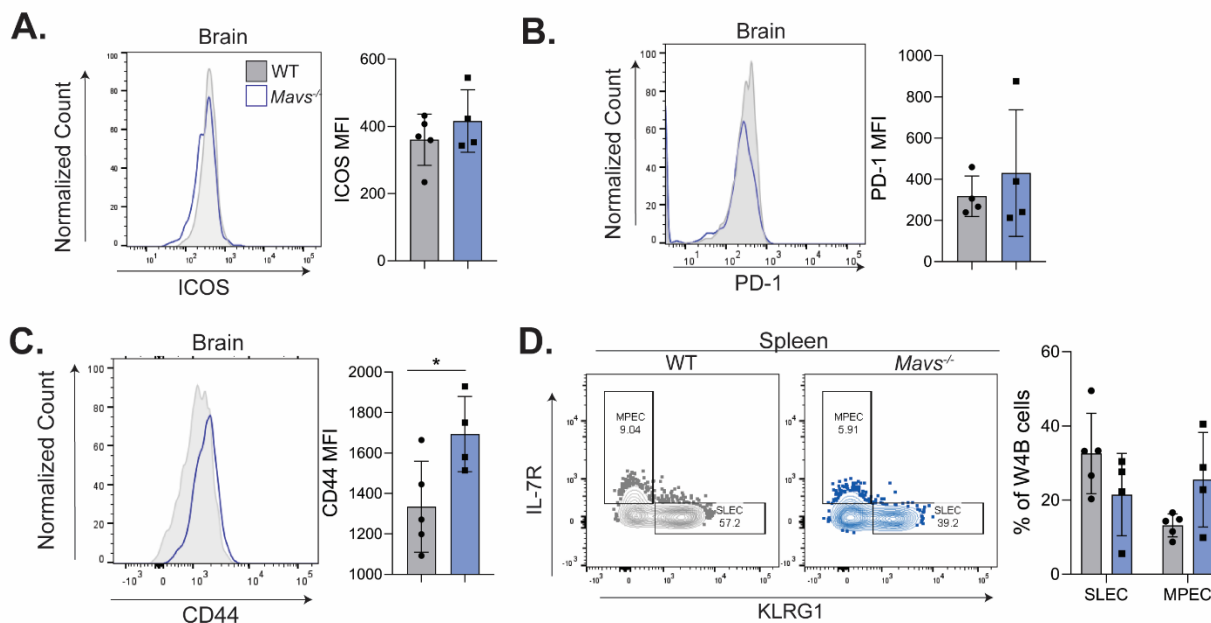
Supplemental Figure 1.



Supplemental Figure 1. Naive CD8⁺ T cell function is not impacted by MAVS. CD8⁺ T cells were isolated from naïve WT or *Mavs*^{-/-} spleens and adoptively transferred (50,000 cells/mouse) to a congenically distinct WT recipient. One day post transfer mice were infected with WNV-TX (100 pfu/mouse) and at day 7 post infection brains and spleens were harvested, processed to single cell suspension, and W4B cells were sorted then subjected to mRNA-Seq. A) Experimental schematic. B) Gating strategy to identify W4B cells. C) Representative flow plots showing the expression of CD62L and CD44 on Singlet, Live, CD3⁺, CD8⁺ cells from naïve WT or *Mavs*^{-/-} W4B cells. D) W4B cells were sorted from the spleens of naïve WT or *Mavs*^{-/-} mice and analyzed via RNA-seq (n=4). Volcano plot illustrating the fold change (log₂) of genes from *Mavs*^{-/-} W4B cells over WT (lines indicate cutoff values, FC <-2 or >2, p-value <0.01). Highlighted in red are

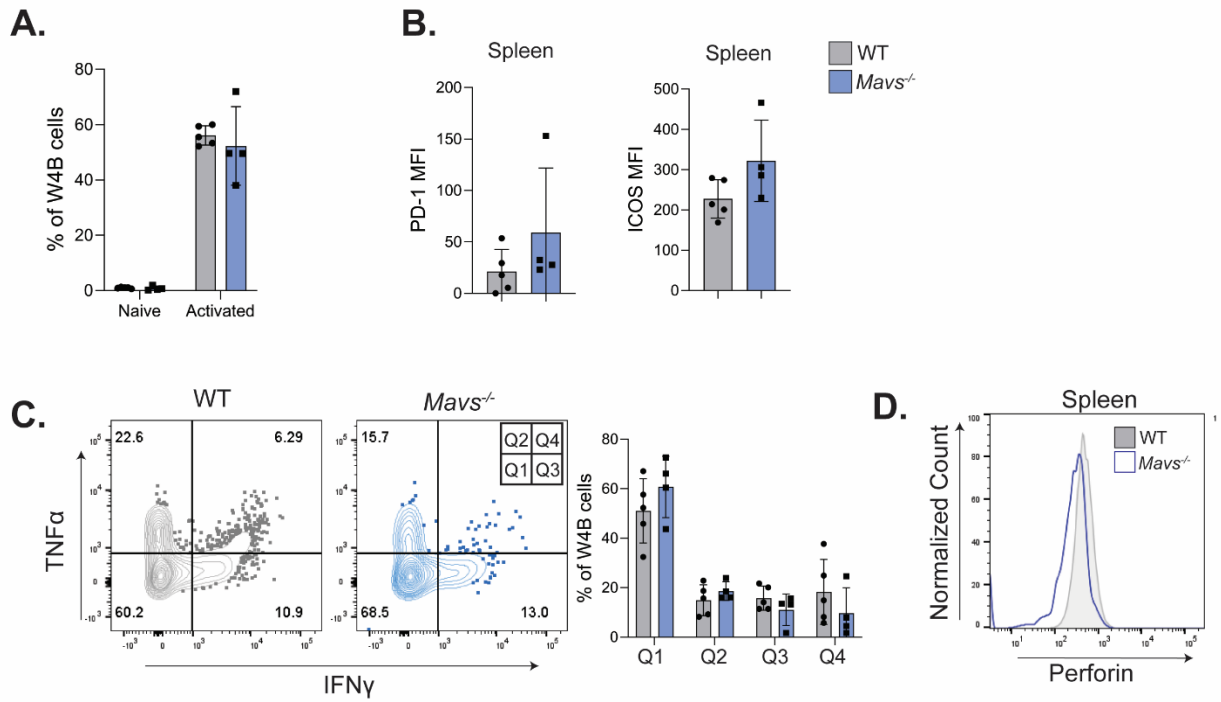
genes significantly upregulated (16 transcripts), in blue significantly downregulated (27 transcripts) in *Mavs*^{-/-} compared to WT.

Supplemental Figure 2.



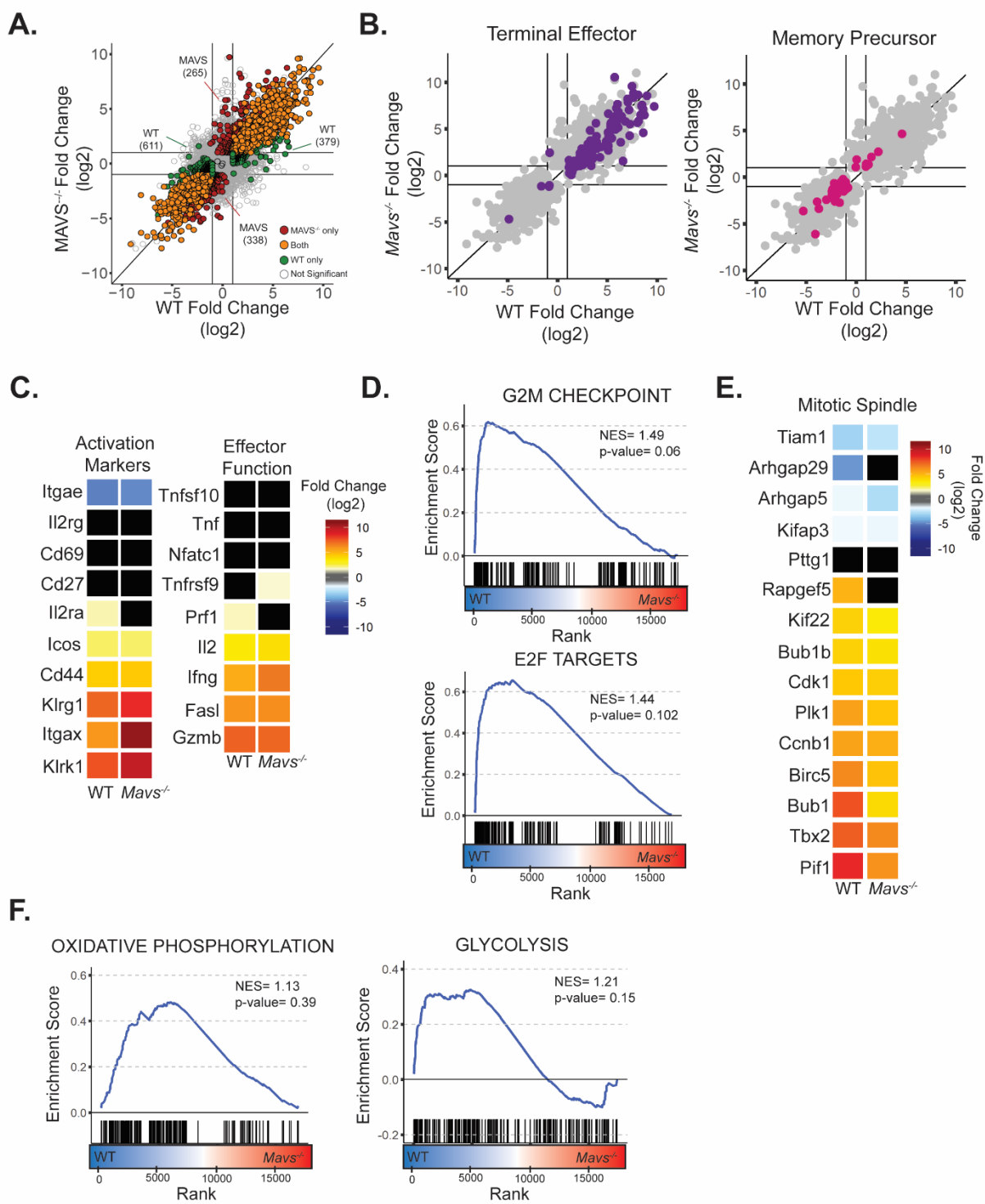
Supplemental Figure 2. MAVS does not impact activation or differentiation of CD8⁺ T cells during viral infection. WT or *Mavs*^{-/-} W4B cells were adoptively transferred to WT mice, infected with WNV-TX, and harvested at 8 days p.i. and analyzed via flow cytometry. Histograms and the corresponding MFIs of A) ICOS expression, B) PD-1 expression or C) CD44 expression on WT or *Mavs*^{-/-} W4B cells from the brain. D) Representative flow plots of MPEC (IL-7R^{hi}, KLRG1^{lo}) and SLEC (IL-7R^{lo}, KLRG1^{hi}) populations, and the corresponding quantification on the right, in WT and *Mavs*^{-/-} W4B cells from the spleen. Results are representative of 2 independent experiments with 4-6 mice each. Statistical significance was determined using unpaired student's t-tests or two-way ANOVA. * = p<0.05

Supplemental Figure 3.



Supplemental Figure 3. MAVS promotes cytotoxicity in splenic W4B cells. WT or *Mavs*^{-/-} W4B cells were adoptively transferred to WT mice, infected with WNV-TX, harvested at 8 days p.i., and analyzed via flow cytometry. A) Quantification of the percentage of naïve (CD62L⁺ CD44⁻) and activated (CD62L⁻ CD44⁺) W4B cells from the spleen. B) Quantification of the MFI of PD-1 and ICOS on splenic W4B cells. C) Representative flow plots of IFN γ and TNF α production by WT or *Mavs*^{-/-} W4B cells from the spleen. The percentage of W4B cells in each quadrant is quantified on the right (Q1: IFN γ ⁻TNF α ⁻, Q2: IFN γ ⁻TNF α ⁺, Q3: IFN γ ⁺TNF α ⁻, Q4: IFN γ ⁺TNF α ⁺). D) Representative histograms of perforin expression in WT or *Mavs*^{-/-} W4B cells from the spleen. Statistical significance was determined using unpaired student's t-tests or two-way ANOVA. * = p<0.05, ** = p<0.01.

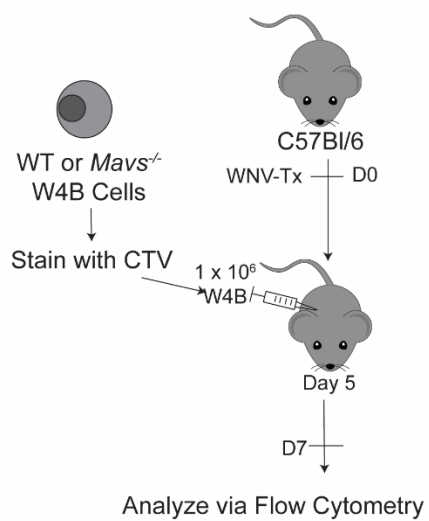
Supplemental Figure 4.



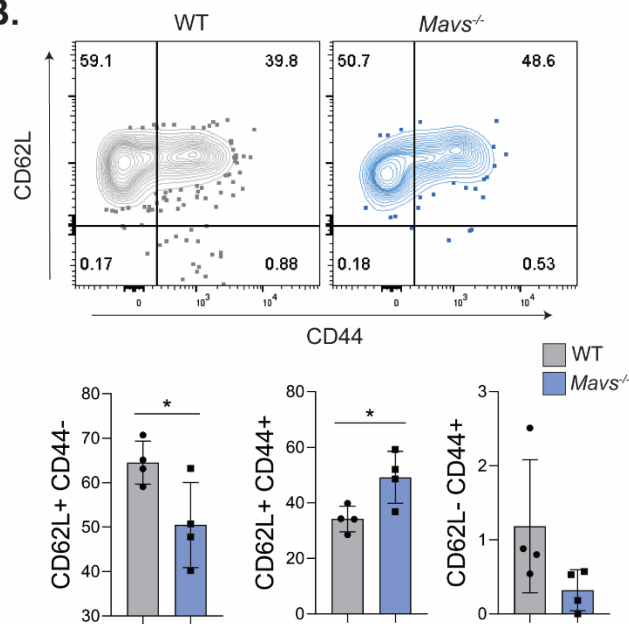
Supplemental Figure 4. MAVS promotes cell cycle transcript expression and metabolism in splenic CD8+ T cells during viral infection. RNA-Seq analysis was performed on WT or *Mavs*^{-/-} W4B cells isolated from the spleen as described in Fig. 3. A) WT and *Mavs*^{-/-} fold change over mock were plotted against each other to highlight DEGs expressed in both (orange), WT only (green), or *Mavs*^{-/-} only (red). Non-significant genes are highlighted in grey (cutoffs: FC < or > 2, p-value < 0.01). B) All significant DEGs are highlighted in grey, genes included in the indicated gene set are highlighted in purple (Terminal Effector) or pink (Memory Precursor). C) Heatmap of the indicated gene sets in WT and *Mavs*^{-/-} cells. D) GSEA of WT (left, blue) over *Mavs*^{-/-} (red, right) for the indicated gene sets from the Hallmarks collection (MSigDB). E) Heatmap of the indicated genes related to the mitotic spindle. F) GSEA of WT over *Mavs*^{-/-} for the indicated Hallmarks Gene sets.

Supplemental Figure 5.

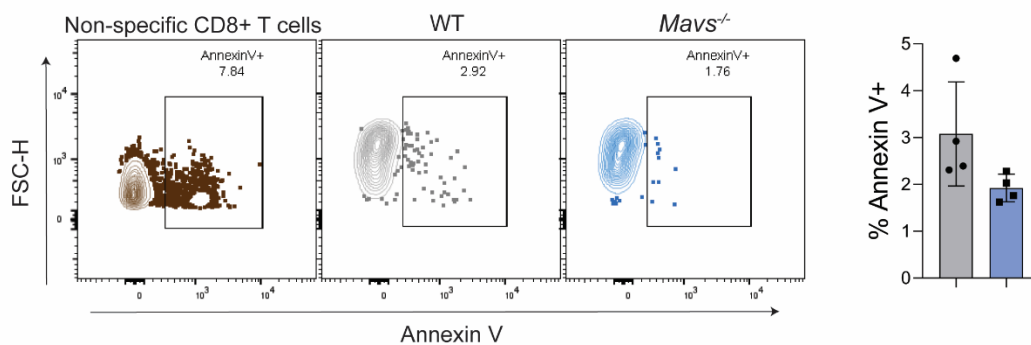
A.



B.



C.



Supplemental Figure 5. MAVS does not impact apoptosis of antigen-specific CD8⁺ T cells.

A) Experimental schematic of proliferation tracking experiment. WT and *Mavs*^{-/-} W4B cells were isolated from naïve mice and stained with cell-trace violet (CTV). 1×10^6 W4B cells were transferred into congenically distinct WT mice at Day 5 p.i. with WNV-TX. 48 hours post transfer (Day 7 p.i.) spleens were harvested and analyzed via flow cytometry to track CTV dilution. B) Representative flow plots of CD62L vs CD44 staining and the corresponding quantification below in WT and *Mavs*^{-/-} W4B. C) Representative Annexin V flow plots on WT and *Mavs*^{-/-} W4B cells, using NS4b Tetramer- non-specific CD8⁺ T cells as a gating control, results are quantified on the right. Results are representative of 2 independent experiments with 4-5 mice each. Statistical significance was determined using unpaired student's t-tests or two-way ANOVA. * = $p < 0.05$

DISCUSSION

CD8+ T cell programming differs based on anatomic location.

In part 1, we find that CD8+ T cell phenotype and function is influenced by anatomic localization. Despite identical clonality, WNV-specific CD8+ T cells isolated from the spleen, dcLN, scLN, meninges, and brain all had distinct kinetics, phenotypic, transcriptional, and functional profiles. Splenic, dcLN, and scLN localized CD8+ T cells peaked 2 days earlier than meningeal or brain localized CD8+ T cells. CD8+ T cell kinetics thus track roughly with WNV kinetics with a 1-2 day delay. Dye tracking studies have demonstrated that CD8+ T cells from the brain parenchyma extravasate into meningeal lymphatic vessels, which if located in the olfactory bulb drain to the scLN or in the cortex/cerebellum to the dcLN (68, 71). Interestingly during WNV infection we found that expansion of CD8+ T cells to the dcLN and scLN occurs prior to accumulation in the parenchyma and meninges. CD8+ T cells can be locally primed in the CNS-draining lymph nodes by parenchymal antigen as demonstrated in models of multiple sclerosis (68, 213). Thus, dcLN or scLN localized CD8+ T cells could be proliferating locally in response to viral antigen. Alternatively, CD8+ T cells can also be primed in the periphery and then migrate into the CNS, even in the absence of CNS infection (214). Whether CNS localized CD8+ T cells during WNV infection are primed in the periphery or the CNS-draining lymph nodes is not clear. Since studies in the gut have demonstrated that priming in different lymph nodes can affect the programming of T cells as tolerogenic or proinflammatory, this will be an important topic for future studies. (215)

Our study found that dcLN and scLN CD8+ T cell phenotypes were distinct from meningeal or parenchymal CD8+ T cells, as well as splenic CD8+ T cells. While similar in cytokine expression, dcLN and scLN localized CD8+ T cells did have differences in CD44 and

ICOS expression. These differences in WNV-specific CD8⁺ T cells in the dcLN as compared to the scLN, could be due to the different regions drained by each respective lymph nodes (68, 71). At later timepoints, when CNS-draining lymph nodes are controlling viral infection, the parenchyma still has high WNV burden. As the dcLN primarily receives lymph from the cortices, the dcLN may be experiencing a mixed population of dcLN resident CD8⁺ T cells and those draining from the parenchyma that are still experiencing antigen (68, 71). Thus the disparate phenotypes between CNS-draining LNs could be due to environmental cues obtained while passing through different regions of the CNS.

Our study observed substantial differences between peripheral and brain/meningeal localized CD8⁺ T cells. Interestingly, meningeal localized CD8⁺ T cells had an ‘intermediate’ phenotype between peripheral and brain parenchymal cells with respect to activation markers and cytokine expression. The meningeal phenotype could be due to distinct meninges-specific signaling. In models of multiple sclerosis, CD4⁺ T cells are reactivated by meningeal APCs, which promote CNS damage (66). In coronavirus infection, meningeal CCL19 and CCL21 help recruit and reactivate CD8⁺ T cells to promote protection (116). Differences between meningeal and brain parenchymal programming could also represent a sequential ‘reprogramming’, as previous studies have identified that movement from the brain vasculature to the parenchyma has additional layers of regulation. In WNV models of infection, CD8⁺ T cells localized to the vasculature require CXCR3 and downregulation of CXCR4 to move from the brain vasculature into the parenchyma (108, 113, 176). Last, CD8⁺ T cells localized to the brain parenchyma not only enter but also egress through the meninges (68). Thus, the ‘intermediate’ phenotype of meningeal CD8⁺ T cells could be independent of meningeal signals but instead represent a mix of infiltrating and egressing parenchymal CD8⁺ T cells.

In our model of WNV infection we noted that brain parenchyma localized CD8⁺ T cells have a distinct phenotype. One possible mechanism for this differential programming could be exposure to unique cell types only present in the brain parenchyma such as neurons, astrocytes, and microglia. Microglia have been previously implicated in the regulation of CD8⁺ T cell responses as they can directly present antigen on MHC-I to CD8⁺ T cells, and this interaction is essential for CD8⁺ T cell mediated viral control (216). Microglia can also secrete a variety of cytokines in response to WNV infection that influence CD8⁺ T cell responses, including CXCL10, CCL2, and TNF α (217). Beyond distinct cellular composition, the brain parenchyma also has altered nutrient availability and bioenergetic demands compared to peripheral organs. For example, asparagine cannot cross the blood brain barrier, therefore CNS resident cells must synthesize this amino acid, and accordingly we see that asparagine synthetase (*Asns*) is highly expressed in brain W4B cells compared to splenic during WNV infection (218). Studies in a model of multiple sclerosis also noted distinct metabolic profiles in CNS resident cells, with a prevalence of highly glycolytic CD8⁺ T cells in the brain parenchyma (219). Thus, the unique environment and cellular composition of the brain parenchyma likely influence CD8⁺ T cell programming during WNV infection.

A unexpected finding from our analysis in part 1 was that CNS localized CD8⁺ T cells had high expression of inhibitory receptors. Engagement of inhibitory receptors inhibits the release of cytokines and cytotoxic molecules by CD8⁺ T cells. High expression of inhibitory receptors is associated with an exhaustion of CD8⁺ T cells induced by chronic infections (183, 189). However, upregulation of inhibitory receptors can also occur during acute infection in response to TCR stimulation or when cells are receiving suppressive signals in order to limit pathology (181, 182). PD-1 expression in particular has been associated with the regulation of CD8⁺ T cells in the CNS.

PD1:PD-L1 interactions promote the establishment of resident memory T (T_{RM}) cell populations within the CNS following encephalitis from murine cytomegalovirus infection or murine polyomavirus infection (181, 182). PD-1 expression was particularly elevated on CD8⁺ T cells localized to the meninges, and previous studies suggest that most brain resident CD8⁺ T cells reside near blood vessels, likely in the meninges (212). Previously published data found that W4B cells express elevated levels of CD103 and CD69 in the brain. Combined with high PD-1 expression, these data may suggest the establishment of T_{RM} cells in the CNS, particularly in the meninges, following WNV infection (104). *Il10ra*, the IL-10 receptor gene, is also upregulated on brain W4B cells. IL-10 is primarily produced by T regulatory (T_{reg}) cells and previous studies have found a correlation between T_{reg} cell numbers during and protection during WNV neuroinvasive disease both humans and mice (190). This suggests a link between a regulatory environment and protection from immunopathology in the CNS. Further studies are needed to assess the impact of T_{reg} cells and PD-1 on WNV-specific CD8⁺ T cell function.

In addition to environmental regulation, WNV-specific CD8⁺ T cells in the brain are subject to cell-intrinsic CNS-specific regulation as well. LGP2 was identified to promote CD8⁺ T cell survival during WNV infection, but only in the CNS, as the receptor had a minimal role in the peripheral T cell response (157). In a model of EAE, the expression of DNA binding molecule TOX, was found to be essential for the acquisition of encephalitogenic potential by CD8⁺ T cells (220). Tissue specific regulation has also been noted in other tissues. For example, *Runx3* promotes CD8⁺ T cell resident memory formation in specifically non-lymphoid tissues (221). In part 2, we identified another unique regulator of CD8⁺ T cell function, MAVS. While MAVS promotes CD8⁺ T cell proliferation and metabolism both in the periphery and CNS, we noted a stronger phenotype in the CNS. *Mavs*^{-/-} CD8⁺ T cells in the brain parenchyma had more

pronounced metabolic dysregulation and expansion deficits. As our *in vitro* data found that MAVS played a role in promoting proliferation during nutrient-limited conditions, this could lead to a larger role for MAVS in CD8⁺ T cells in nutrient restricted environments, such as the brain parenchyma.

MAVS and the mitochondrion

In part 2, we identified a novel CD8⁺ T cell intrinsic role for MAVS in promoting metabolism and proliferation that was dependent on TCR signaling. Canonical RLR signaling requires the activation of MAVS by RIG-I or MDA5 after recognition of an RNA virus, however it's unlikely this mechanism occurs in CD8⁺ T cells. (195). First, previous studies have shown that MDA5 does not have a T-cell intrinsic signaling function during WNV infection, while the role of RIG-I is unknown (154, 157). Second, CD8⁺ T cells are not targets of WNV infection, and our data found that MAVS regulates metabolism in a virus free model of T cell activation. However, alternate methods of MAVS activation have been described; in murine embryonic fibroblasts the release of reactive-oxygen species (ROS) was sufficient to induce MAVS aggregation independently of viral infection (173). As part of the TCR signaling cascade, ROS seems a likely candidate for the incorporation of MAVS signaling into CD8⁺ T cell activation. Whether ROS-induced aggregation of MAVS is dependent on RIG-I is unknown. Additionally, it's possible that the role of MAVS in CD8⁺ T cells is not dependent on aggregation. Future studies will delineate the precise connections between TCR signaling, RIG-I, ROS, and MAVS function.

The RLR signaling pathway is connected with changes in mitochondrial dynamics. Mitochondrial potential is required for RLR signaling and signal propagation is further promoted

by reactive oxygen species release (147, 152, 173, 203). A feedback loop mechanism exists between mitochondrial fusion and the RLR pathway, where mitochondrial fusion enhances RLR signaling, which in turn promotes mitochondrial fusion (147). In part 2, we find that *Mavs*^{-/-} CD8⁺ T cells have increased numbers of mitochondria as compared to WT cells and these mitochondria are circular with disorganized cristae. This is a phenotype that is characteristic of cells with a defect in mitochondrial fusion (201). Disordered cristae is particularly associated with an accumulation of dysfunctional mitochondria, suggesting a defect in mitophagy, which has previously been linked to the RLR pathway (148). MFN1 and MFN2 are key regulators of mitochondrial fission and fusion and both molecules have been demonstrated to physically interact with MAVS by immunoprecipitation assays (150, 152). Together these data warrant further studies into the role of MAVS in mitochondrial dynamics and autophagy. In part 2, we focused on MAVS at the mitochondria, however MAVS is also located at the mitochondrial-associated-membrane subdomain of the ER and peroxisomes (204, 205). Comparison of the transcriptomes of WT and *Mavs*^{-/-} CD8⁺ T cells identified differences in genes related to ER stress genes and ATF-4. This suggests a role for MAVS in CD8⁺ T cells at the ER, but future studies are needed to determine if this is a primary function of MAVS or a secondary consequence of dysregulated mitochondria.

Dynamic regulation of metabolic pathways is crucial for the initiation of CD8⁺ T cell responses and subsequent differentiation into terminal effector or memory cells. Naïve CD8⁺ T cells are relatively metabolically quiescent, and rely on fatty acid oxidation and oxidative phosphorylation for their homeostatic needs (200). After activation, CD8⁺ T cells will increase both oxidative phosphorylation and glycolysis (196, 197). Our study found no role for MAVS in the upregulation of glycolysis, but dramatically reduced levels of oxidative phosphorylation. The upregulation of mitochondrial metabolism and the release of mitochondrial ROS is essential for

T cells to exit quiescence, and accordingly, we see that *Mavs*^{-/-} CD8⁺ T cells have lower levels of entry into the proliferative cycle, that was dependent on their inability to perform non-glycolytic metabolism (196). However, after initial activation, CD8⁺ T cells rely primarily on glycolysis and oxidative phosphorylation is dispensable during the effector phase (199). Changes in glycolysis can also affect T cell function, as the engagement of glycolysis is needed for IFN γ production (197). Our *in vitro* data found that MAVS functions independently of glycolysis, and accordingly we find no defect in the activation status (CD44, ICOS expression) or IFN γ expression in *Mavs*^{-/-} CD8⁺ T cells in mice. Thus the promotion of oxidative phosphorylation by MAVS is essential during the initial proliferative burst after antigen recognition in CD8⁺ T cells, but may be dispensable during the effector phase.

Mitochondrial respiration is essential for the establishment and maintenance of memory CD8⁺ T cells, and limited mitochondrial spare respiratory capacity inhibits the ability of memory T cells to respond to antigen (198, 201). Rapid recall responses in memory CD8⁺ T cells are supported by elongated, super-complexed mitochondria (201). MAVS was necessary for mitochondrial remodeling and increased spare respiratory capacity after TCR stimulation and thus could impact memory formation. Additionally, tissue resident memory T cells have unique metabolic programs as compared to effector or central memory T cells (222). As the impact of MAVS was more pronounced in the brain, and the role of MAVS in promoting proliferation was dependent on nutrient limiting conditions; MAVS may be important for the maintenance of CNS-resident T cells. Future studies will determine if MAVS promotes the effector to memory switch and the persistence of memory CD8⁺ T cells in the CNS.

Mitochondrial dynamics and oxidative phosphorylation have been linked to T cell dysfunction in other models of disease. During chronic LCMV infection, CD8⁺ T cells display

mitochondrial dysregulation characterized by a PD-1 dependent depolarization of the mitochondrion (223). In cancer models, tumor-infiltrating lymphocytes (TILs) show profound metabolic dysfunction. Analysis of TILs found decreased mitochondrial function attributable to a decrease in mitochondrial biogenesis (224). The tumor microenvironment has unique nutrient availability, and accordingly one study identified that in glucose derived cells the ER-stress response was inappropriately activated and repressed mitochondrial function, ultimately leading to T cell exhaustion (225). This study highlights the importance of different nutrient environments on T cell function, a phenomenon we noted with MAVS as well. One feature of exhausted TILs is a defect in mitophagy that was dependent on both TCR and PD-1 signaling (226). However, blockade of PD-1 signaling could re-invigorate TIL mitochondrial metabolism in a *Bhlhe40* dependent mechanism (227). These studies highlight the potentially wide-ranging effects of TCR and microenvironment dependent MAVS-mediated mitochondrial respiration in various models of T cell exhaustion and cancer.

T cells and CNS function

As neurons are a non-renewing cell, during CNS infections CD8⁺ T cells balance a critical line between clearing pathogens from the brain while simultaneously limiting neuronal damage. In section 1, we demonstrated that brain CD8⁺ T cells are highly efficient at controlling viral infection in neurons and preferentially secrete IFN γ in response to WNV antigen. Studies in a model of Sindbis virus have demonstrated that both IFN γ and the IFNGR1 promote the clearance of virus with non-redundant effects (187). Interestingly, IFN γ promoted viral control without cytolysis of infected neurons in a JAK/STAT dependent manner (119, 187). Other *in vitro* studies have identified that in neurons, but not in fibroblasts, IFN γ can signal through

ERK1/2 to block caspase-3 dependent apoptosis (228). This mechanism of non-cytolytic IFN γ dependent viral clearance has also been observed in an *in vivo* model of lymphochoriomeningitis (LCMV) infection. Therapeutically administered LCMV-specific CD8 $^+$ T cells were able to non-cytolytically control a persistent viral infection in the brain by upregulating the expression of STAT1 in microglia and other CNS-resident cells (229). This pathway has also been noted in non-viral models of disease, as during T cell driven autoimmune encephalitis, CNS-infiltrating CD8 $^+$ T cells secrete IFN γ which drives expression of STAT1 in neurons (230). Thus, CD8 $^+$ T cell derived IFN γ is an important common mechanism to restrict infection of neurons with minimal damage.

In section 1, we observed high levels of IFN γ secretion not only in the brain parenchyma, but also in meningeal localized CD8 $^+$ T cells. While anti-viral T cells in the meninges could be important for controlling viral replication in APCs located in that compartment, other models of disease have noted pathologic effects of T cells in the meninges. Meningitis severity has been linked to increased levels of cytokines, including TNF α and IFN γ (231). In a model of HIV-cryptococcal meningitis, low levels of cytokine secretion in the meninges was beneficial for pathogen control but high cytokine levels drove negative disease outcome (232). Immunity in the meningeal space can also drive cognitive dysfunction, as meningitis has been associated with defects in neurogenesis, synaptic coupling, and neuronal circuitry (233-235). In a model of LCMV viral infection, CD8 $^+$ T cell derived IFN γ , but not perforin or FasL, specifically promoted the loss of neuronal dendrites (235). In the absence of infection, most CNS resident T cells are located in the meninges, and studies of immunodeficient mice have demonstrated that even during homeostasis meningeal T cells can impact neurological function (65) (236). For example, IL-17 production by meningeal $\gamma\delta$ -T cells was found to impact cortical neurons and

regulate anxiety behavior under steady state conditions (237). Studies of tissue resident memory CD8⁺ T cells in the CNS suggest Trm primarily reside in regions close to blood vessels in the meninges after the resolution of infection (212). Our work in section 1 suggests that meningeal and parenchymal Trm cells could have different properties however, current studies have not delineated between the two Trm populations. Future studies are needed to explore the role of specifically meningeal CD8⁺ T cells on regulating cognition and behavior during homeostasis, infection and recovery.

While IFN γ -secreting CD8⁺ T cells are necessary for the resolution of CNS infections, parenchymal T cells may also drive cognitive dysfunction. In studies of tuberculosis meningitis, T cells were found to persist in the brain even after the clearance of bacteria, and T cell counts were directly correlated with post-infection clinical symptoms (238). Mechanistically, T_H1 derived IFN γ was found to promote both survival and post-infection neurological sequelae (239). Similarly, studies in mice found that elevated numbers of CD8⁺ T cells could be found up to 16 weeks post infection with WNV, well after WNV infection is controlled in the parenchyma (240). Post-recovery from WNV or Zika virus infection, CD8⁺ T cells in the hippocampus were found to still secrete IFN γ , which in turn activated microglia. IFNGR signaling on microglia promoted phagocytosis of pre- and post-synaptic termini of neurons resulting in spatial learning defects in recovering mice (241). Thus, CD8⁺ T cells play contrasting roles in controlling virus but also promoting post-recovery pathology during CNS infections. Anatomic localization and CD8⁺ T cell intrinsic MAVS signaling are part of a complex network that orchestrates the balance between viral clearance and pathology in the CNS. Consideration of tissue-specific programming and MAVS signaling in promoting effective resident T cell memory populations will be important for vaccine design targeting the CNS.

REFERENCES

1. Smithburn KC, Hughes, T.P., Burke, A.W., Paul, J.H. 1940. A neurotropic flavivirus isolated from the blood of a native of Uganda. *Am J Trop Med Hyg* 20:471-492.
2. Anonymous. 2018. WNV, Statistics and Maps, on Center for Disease Control and Prevention. <https://www.cdc.gov/westnile/statsmaps/index.html>. Accessed 11/26/18.
3. Mostashari F, Bunning ML, Kitsutani PT, Singer DA, Nash D, Cooper MJ, Katz N, Liljebjelke KA, Biggerstaff BJ, Fine AD, Layton MC, Mullin SM, Johnson AJ, Martin DA, Hayes EB, Campbell GL. 2001. Epidemic West Nile encephalitis, New York, 1999: results of a household-based seroepidemiological survey. *Lancet* 358:261-4.
4. Guarner J, Shieh WJ, Hunter S, Paddock CD, Morken T, Campbell GL, Marfin AA, Zaki SR. 2004. Clinicopathologic study and laboratory diagnosis of 23 cases with West Nile virus encephalomyelitis. *Hum Pathol* 35:983-90.
5. Leis AA, Stokic DS, Polk JL, Dostrow V, Winkelmann M. 2002. A Poliomyelitis-like Syndrome from West Nile Virus Infection. *New England Journal of Medicine* 347:1279-1280.
6. Sejvar JJ, Haddad MB, Tierney BC, Campbell GL, Marfin AA, Van Gerpen JA, Fleischauer A, Leis AA, Stokic DS, Petersen LR. 2003. Neurologic manifestations and outcome of West Nile virus infection. *JAMA* 290:511-5.
7. Ahmed S, Libman R, Wesson K, Ahmed F, Einberg K. 2000. Guillain-Barré syndrome: An unusual presentation of West Nile virus infection. *Neurology* 55:144-6.
8. Garber C, Soung A, Vollmer LL, Kanmogne M, Last A, Brown J, Klein RS. 2019. T cells promote microglia-mediated synaptic elimination and cognitive dysfunction during recovery from neuropathogenic flaviviruses. *Nature Neuroscience* 22:1276-1288.
9. Lanciotti RS, Roehrig JT, Deubel V, Smith J, Parker M, Steele K, Crise B, Volpe KE, Crabtree MB, Scherret JH, Hall RA, MacKenzie JS, Cropp CB, Panigrahy B, Ostlund E, Schmitt B, Malkinson M, Banet C, Weissman J, Komar N, Savage HM, Stone W, McNamara T, Gubler DJ. 1999. Origin of the West Nile virus responsible for an outbreak of encephalitis in the northeastern United States. *Science* 286:2333-7.
10. Root JJ, Bosco-Lauth AM. 2019. West Nile Virus Associations in Wild Mammals: An Update. *Viruses* 11:459.
11. Kramer LD, Styer LM, Ebel GD. 2008. A global perspective on the epidemiology of West Nile virus. *Annu Rev Entomol* 53:61-81.
12. Aliota MT, Jones SA, Dupuis AP, II, Ciota AT, Hubalek Z, Kramer LD. 2012. Characterization of Rabensburg Virus, a Flavivirus Closely Related to West Nile Virus of the Japanese Encephalitis Antigenic Group. *PLOS ONE* 7:e39387.
13. Brault AC, Huang CYH, Langevin SA, Kinney RM, Bowen RA, Ramey WN, Panella NA, Holmes EC, Powers AM, Miller BR. 2007. A single positively selected West Nile viral mutation confers increased virogenesis in American crows. *Nature Genetics* 39:1162-1166.
14. Del Amo J, Llorente F, Figuerola J, Soriguer RC, Moreno AM, Cordioli P, Weissenböck H, Jiménez-Clavero MÁ. 2014. Experimental infection of house sparrows (*Passer domesticus*) with West Nile virus isolates of Euro-Mediterranean and North American origins. *Veterinary Research* 45:33.
15. Fang Y, Reisen WKJTAjotm, hygiene. 2006. Previous infection with West Nile or St. Louis encephalitis viruses provides cross protection during reinfection in house finches. *75:480-485*.
16. Turell MJ, Dohm DJ, Sardelis MR, Oguinn ML, Andreadis TG, Blow JA. 2005. An update on the potential of north American mosquitoes (Diptera: Culicidae) to transmit West Nile Virus. *J Med Entomol* 42:57-62.
17. Vogels CB, Göertz GP, Pijlman GP, Koenraadt CJ. 2017. Vector competence of European mosquitoes for West Nile virus. *Emerg Microbes Infect* 6:e96.

18. Girard YA, Klingler KA, Higgs S. 2004. West Nile Virus Dissemination and Tissue Tropisms in Orally Infected *Culex pipiens quinquefasciatus*. *Vector-Borne and Zoonotic Diseases* 4:109-122.
19. Paradkar PN, Duchemin J-B, Voysey R, Walker PJJNTD. 2014. Dicer-2-dependent activation of *Culex Vago* occurs via the TRAF-Rel2 signaling pathway. 8:e2823.
20. Paradkar PN, Trinidad L, Voysey R, Duchemin J-B, Walker PJJPotNAoS. 2012. Secreted Vago restricts West Nile virus infection in *Culex* mosquito cells by activating the Jak-STAT pathway. 109:18915-18920.
21. Colpitts TM, Cox J, Vanlandingham DL, Feitosa FM, Cheng G, Kurscheid S, Wang P, Krishnan MN, Higgs S, Fikrig EJPP. 2011. Alterations in the *Aedes aegypti* transcriptome during infection with West Nile, dengue and yellow fever viruses. 7:e1002189.
22. Styer LM, Kent KA, Albright RG, Bennett CJ, Kramer LD, Bernard KA. 2007. Mosquitoes inoculate high doses of West Nile virus as they probe and feed on live hosts. *PLoS Pathog* 3:1262-70.
23. Davis CW, Nguyen HY, Hanna SL, Sánchez MD, Doms RW, Pierson TC. 2006. West Nile virus discriminates between DC-SIGN and DC-SIGNR for cellular attachment and infection. *J Virol* 80:1290-301.
24. Martina BE, Koraka P, van den Doel P, Rimmelzwaan GF, Haagmans BL, Osterhaus AD. 2008. DC-SIGN enhances infection of cells with glycosylated West Nile virus in vitro and virus replication in human dendritic cells induces production of IFN-alpha and TNF-alpha. *Virus Res* 135:64-71.
25. Cheng G, Cox J, Wang P, Krishnan MN, Dai J, Qian F, Anderson JF, Fikrig E. 2010. A C-type lectin collaborates with a CD45 phosphatase homolog to facilitate West Nile virus infection of mosquitoes. *Cell* 142:714-25.
26. Jemielity S, Wang JJ, Chan YK, Ahmed AA, Li W, Monahan S, Bu X, Farzan M, Freeman GJ, Umetsu DT, Dekruyff RH, Choe H. 2013. TIM-family proteins promote infection of multiple enveloped viruses through virion-associated phosphatidylserine. *PLoS Pathog* 9:e1003232.
27. Bogachek MV, Zaitsev BN, Sekatskii SK, Protopopova EV, Ternovoi VA, Ivanova AV, Kachko AV, Ivanisenko VA, Dietler G, Loktev VB. 2010. Characterization of glycoprotein E C-end of West Nile virus and evaluation of its interaction force with alphaVbeta3 integrin as putative cellular receptor. *Biochemistry (Mosc)* 75:472-80.
28. Lee JW, Chu JJ, Ng ML. 2006. Quantifying the specific binding between West Nile virus envelope domain III protein and the cellular receptor alphaVbeta3 integrin. *J Biol Chem* 281:1352-60.
29. Medigeshi GR, Hirsch AJ, Streblow DN, Nikolich-Zugich J, Nelson JA. 2008. West Nile virus entry requires cholesterol-rich membrane microdomains and is independent of alphavbeta3 integrin. *J Virol* 82:5212-9.
30. Chu JJ, Ng ML. 2004. Infectious entry of West Nile virus occurs through a clathrin-mediated endocytic pathway. *J Virol* 78:10543-55.
31. Krishnan MN, Sukumaran B, Pal U, Agaisse H, Murray JL, Hodge TW, Fikrig E. 2007. Rab 5 is required for the cellular entry of dengue and West Nile viruses. *J Virol* 81:4881-5.
32. Allison SL, Schalich J, Stiasny K, Mandl CW, Kunz C, Heinz FX. 1995. Oligomeric rearrangement of tick-borne encephalitis virus envelope proteins induced by an acidic pH. *J Virol* 69:695-700.
33. Brinton MA. 2013. Replication cycle and molecular biology of the West Nile virus. *Viruses* 6:13-53.
34. Wengler G, Czaya G, Färber PM, Hegemann JH. 1991. In vitro synthesis of West Nile virus proteins indicates that the amino-terminal segment of the NS3 protein contains the active centre of the protease which cleaves the viral polyprotein after multiple basic amino acids. *J Gen Virol* 72 (Pt 4):851-8.

35. Avirutnan P, Fuchs A, Hauhart RE, Somnuk P, Youn S, Diamond MS, Atkinson JP. 2010. Antagonism of the complement component C4 by flavivirus nonstructural protein NS1. *J Exp Med* 207:793-806.
36. Chung KM, Liszewski MK, Nybakken G, Davis AE, Townsend RR, Fremont DH, Atkinson JP, Diamond MS. 2006. West Nile virus nonstructural protein NS1 inhibits complement activation by binding the regulatory protein factor H. *Proc Natl Acad Sci U S A* 103:19111-6.
37. Macdonald J, Tonry J, Hall RA, Williams B, Palacios G, Ashok MS, Jabado O, Clark D, Tesh RB, Briese T, Lipkin WI. 2005. NS1 protein secretion during the acute phase of West Nile virus infection. *J Virol* 79:13924-33.
38. Malet H, Egloff MP, Selisko B, Butcher RE, Wright PJ, Roberts M, Gruez A, Sulzenbacher G, Vonrhein C, Bricogne G, Mackenzie JM, Khromykh AA, Davidson AD, Canard B. 2007. Crystal structure of the RNA polymerase domain of the West Nile virus non-structural protein 5. *J Biol Chem* 282:10678-89.
39. Selisko B, Dutartre H, Guillemot JC, Debarnot C, Benarroch D, Khromykh A, Desprès P, Egloff MP, Canard B. 2006. Comparative mechanistic studies of de novo RNA synthesis by flavivirus RNA-dependent RNA polymerases. *Virology* 351:145-58.
40. Gillespie LK, Hoenen A, Morgan G, Mackenzie JM. 2010. The endoplasmic reticulum provides the membrane platform for biogenesis of the flavivirus replication complex. *J Virol* 84:10438-47.
41. Welsch S, Miller S, Romero-Brey I, Merz A, Bleck CK, Walther P, Fuller SD, Antony C, Krijnse-Locker J, Bartenschlager R. 2009. Composition and three-dimensional architecture of the dengue virus replication and assembly sites. *Cell Host Microbe* 5:365-75.
42. Mackenzie JM, Khromykh AA, Parton RG. 2007. Cholesterol manipulation by West Nile virus perturbs the cellular immune response. *Cell Host Microbe* 2:229-39.
43. Roosendaal J, Westaway EG, Khromykh A, Mackenzie JM. 2006. Regulated cleavages at the West Nile virus NS4A-2K-NS4B junctions play a major role in rearranging cytoplasmic membranes and Golgi trafficking of the NS4A protein. *J Virol* 80:4623-32.
44. Youn S, Ambrose RL, Mackenzie JM, Diamond MS. 2013. Non-structural protein-1 is required for West Nile virus replication complex formation and viral RNA synthesis. *Virology* 453:339.
45. Stadler K, Allison SL, Schalich J, Heinz FX. 1997. Proteolytic activation of tick-borne encephalitis virus by furin. *J Virol* 71:8475-81.
46. Mukhopadhyay S, Kim BS, Chipman PR, Rossmann MG, Kuhn RJ. 2003. Structure of West Nile virus. *Science* 302:248.
47. Samuel MA, Diamond MS. 2006. Pathogenesis of West Nile Virus Infection: a Balance between Virulence, Innate and Adaptive Immunity, and Viral Evasion. *Journal of Virology* 80:9349.
48. Johnston LJ, King NJC, Halliday GM. 2000. Langerhans Cells Migrate to Local Lymph Nodes Following Cutaneous Infection with an Arbovirus. *Journal of Investigative Dermatology* 114:560-568.
49. Shrestha B, Wang T, Samuel MA, Whitby K, Craft J, Fikrig E, Diamond MS. 2006. Gamma interferon plays a crucial early antiviral role in protection against West Nile virus infection. *J Virol* 80:5338-48.
50. Appler KK, Brown AN, Stewart BS, Behr MJ, Demarest VL, Wong SJ, Bernard KA. 2010. Persistence of West Nile virus in the central nervous system and periphery of mice. *PloS one* 5:e10649-e10649.
51. Samuel MA, Wang H, Fau - Siddharthan V, Siddharthan V, Fau - Morrey JD, Morrey Jd, Fau - Diamond MS, Diamond MS. 2007. Axonal transport mediates West Nile virus entry into the central nervous system and induces acute flaccid paralysis. *Proceedings of the National Academy of Sciences of the United States of America* 104:17140-17145.
52. Diamond MS, Shrestha B, Marri A, Mahan D, Engle M. 2003. B cells and antibody play critical roles in the immediate defense of disseminated infection by West Nile encephalitis virus. *J Virol* 77:2578-86.

53. Daniels BP, Holman DW, Cruz-Orengo L, Jujjavarapu H, Durrant DM, Klein RS. 2014. Viral Pathogen-Associated Molecular Patterns Regulate Blood-Brain Barrier Integrity via Competing Innate Cytokine Signals. *mBio* 5:e01476-14.
54. Wang P, Dai J, Bai F, Kong KF, Wong SJ, Montgomery RR, Madri JA, Fikrig E. 2008. Matrix metalloproteinase 9 facilitates West Nile virus entry into the brain. *J Virol* 82:8978-85.
55. Lazear HM, Daniels BP, Pinto AK, Huang AC, Vick SC, Doyle SE, Gale M, Jr., Klein RS, Diamond MS. 2015. Interferon- λ restricts West Nile virus neuroinvasion by tightening the blood-brain barrier. *Sci Transl Med* 7:284ra59.
56. Dai J, Wang P, Bai F, Town T, Fikrig E. 2008. Icam-1 participates in the entry of west nile virus into the central nervous system. *J Virol* 82:4164-8.
57. Miner JJ, Daniels BP, Shrestha B, Proenca-Modena JL, Lew ED, Lazear HM, Gorman MJ, Lemke G, Klein RS, Diamond MS. 2015. The TAM receptor MERTK protects against neuroinvasive viral infection by maintaining blood-brain barrier integrity. *Nature Medicine* 21:1464-1472.
58. Bai F, Kong KF, Dai J, Qian F, Zhang L, Brown CR, Fikrig E, Montgomery RR. 2010. A paradoxical role for neutrophils in the pathogenesis of West Nile virus. *J Infect Dis* 202:1804-12.
59. Paul AM, Acharya D, Duty L, Thompson EA, Le L, Stokic DS, Leis AA, Bai F. 2017. Osteopontin facilitates West Nile virus neuroinvasion via neutrophil "Trojan horse" transport. *Scientific Reports* 7:4722.
60. Maximova OA, Bernbaum JG, Pletnev AG. 2016. West Nile Virus Spreads Transsynaptically within the Pathways of Motor Control: Anatomical and Ultrastructural Mapping of Neuronal Virus Infection in the Primate Central Nervous System. *PLOS Neglected Tropical Diseases* 10:e0004980.
61. Samuel MA, Wang H, Siddharthan V, Morrey JD, Diamond MS. 2007. Axonal transport mediates West Nile virus entry into the central nervous system and induces acute flaccid paralysis. *Proc Natl Acad Sci U S A* 104:17140-5.
62. Hunsperger E, Roehrig JT. 2005. Characterization of West Nile viral replication and maturation in peripheral neurons in culture. *J Neurovirol* 11:11-22.
63. McGavern DB, Homann D, Oldstone MB. 2002. T cells in the central nervous system: the delicate balance between viral clearance and disease. *J Infect Dis* 186 Suppl 2:S145-51.
64. Alves de Lima K, Rustenhoven J, Kipnis J. 2020. Meningeal Immunity and Its Function in Maintenance of the Central Nervous System in Health and Disease. *Annu Rev Immunol* 38:597-620.
65. Van Hove H, Martens L, Scheyltjens I, De Vlaminck K, Pombo Antunes AR, De Prijck S, Vandamme N, De Schepper S, Van Isterdael G, Scott CL, Aerts J, Berx G, Boeckxstaens GE, Vandenbroucke RE, Vereecke L, Moechars D, Guillemins M, Van Ginderachter JA, Saeys Y, Movahedi K. 2019. A single-cell atlas of mouse brain macrophages reveals unique transcriptional identities shaped by ontogeny and tissue environment. *Nature Neuroscience* 22:1021-1035.
66. Bartholomaeus I, Kawakami N, Odoardi F, Schlager C, Miljkovic D, Ellwart JW, Klinkert WE, Flugel-Koch C, Issekutz TB, Wekerle H, Flugel A. 2009. Effector T cell interactions with meningeal vascular structures in nascent autoimmune CNS lesions. *Nature* 462:94-8.
67. Schläger C, Körner H, Krueger M, Vidoli S, Haberl M, Mielke D, Brylla E, Issekutz T, Cabañas C, Nelson PJ, Ziemssen T, Rohde V, Bechmann I, Lodygin D, Odoardi F, Flügel A. 2016. Effector T-cell trafficking between the leptomeninges and the cerebrospinal fluid. *Nature* 530:349-353.
68. Louveau A, Herz J, Alme MN, Salvador AF, Dong MQ, Viar KE, Herod SG, Knopp J, Setliff JC, Lupi AL, Da Mesquita S, Frost EL, Gaultier A, Harris TH, Cao R, Hu S, Lukens JR, Smirnov I, Overall CC, Oliver G, Kipnis J. 2018. CNS lymphatic drainage and neuroinflammation are regulated by meningeal lymphatic vasculature. *Nat Neurosci* 21:1380-1391.

69. Absinta M, Ha SK, Nair G, Sati P, Luciano NJ, Palisoc M, Louveau A, Zaghoul KA, Pittaluga S, Kipnis J, Reich DS. 2017. Human and nonhuman primate meninges harbor lymphatic vessels that can be visualized noninvasively by MRI. *Elife* 6.
70. Aspelund A, Antila S, Proulx ST, Karlsen TV, Karaman S, Detmar M, Wiig H, Alitalo K. 2015. A dural lymphatic vascular system that drains brain interstitial fluid and macromolecules. *J Exp Med* 212:991-9.
71. Louveau A, Smirnov I, Keyes TJ, Eccles JD, Rouhani SJ, Peske JD, Derecki NC, Castle D, Mandell JW, Lee KS, Harris TH, Kipnis J. 2015. Structural and functional features of central nervous system lymphatic vessels. *Nature* 523:337-41.
72. Da Mesquita S, Louveau A, Vaccari A, Smirnov I, Cornelison RC, Kingsmore KM, Contarino C, Onengut-Gumuscu S, Farber E, Raper D, Viar KE, Powell RD, Baker W, Dabhi N, Bai R, Cao R, Hu S, Rich SS, Munson JM, Lopes MB, Overall CC, Acton ST, Kipnis J. 2018. Functional aspects of meningeal lymphatics in ageing and Alzheimer's disease. *Nature* 560:185-191.
73. Samuel MA, Diamond MS. 2005. Alpha/Beta Interferon Protects against Lethal West Nile Virus Infection by Restricting Cellular Tropism and Enhancing Neuronal Survival. *Journal of Virology* 79:13350-13361.
74. Horvath CM. 2004. The Jak-STAT pathway stimulated by interferon alpha or interferon beta. *Sci STKE* 2004:tr10.
75. Scherbik SV, Paranjape JM, Stockman BM, Silverman RH, Brinton MA. 2006. RNase L Plays a Role in the Antiviral Response to West Nile Virus. *Journal of Virology* 80:2987.
76. Samuel MA, Whitby K, Keller BC, Marri A, Barchet W, Williams BRG, Silverman RH, Gale M, Diamond MS. 2006. PKR and RNase L Contribute to Protection against Lethal West Nile Virus Infection by Controlling Early Viral Spread in the Periphery and Replication in Neurons. *Journal of Virology* 80:7009.
77. Cho H, Shrestha B, Sen GC, Diamond MS. 2013. A role for Ifit2 in restricting West Nile virus infection in the brain. *J Virol* 87:8363-71.
78. Gorman MJ, Poddar S, Farzan M, Diamond MS. 2016. The Interferon-Stimulated Gene Ifitm3 Restricts West Nile Virus Infection and Pathogenesis. *J Virol* 90:8212-25.
79. Lucas TM, Richner JM, Diamond MS. 2015. The Interferon-Stimulated Gene Ifi2712a Restricts West Nile Virus Infection and Pathogenesis in a Cell-Type- and Region-Specific Manner. *J Virol* 90:2600-15.
80. Szretter KJ, Brien JD, Thackray LB, Virgin HW, Cresswell P, Diamond MS. 2011. The interferon-inducible gene viperin restricts West Nile virus pathogenesis. *J Virol* 85:11557-66.
81. Hershkovitz O, Rosental B, Rosenberg LA, Navarro-Sanchez ME, Jivov S, Zilka A, Gershoni-Yahalom O, Brient-Litzler E, Bedouelle H, Ho JW, Campbell KS, Rager-Zisman B, Despres P, Porgador A. 2009. NKp44 receptor mediates interaction of the envelope glycoproteins from the West Nile and dengue viruses with NK cells. *J Immunol* 183:2610-21.
82. Shrestha B, Samuel MA, Diamond MS. 2006. CD8+ T cells require perforin to clear West Nile virus from infected neurons. *J Virol* 80:119-29.
83. Suthar MS, Brassil MM, Blahnik G, McMillan A, Ramos HJ, Proll SC, Belisle SE, Katze MG, Gale M, Jr. 2013. A systems biology approach reveals that tissue tropism to West Nile virus is regulated by antiviral genes and innate immune cellular processes. *PLoS Pathog* 9:e1003168.
84. Suthar MS, Ma DY, Thomas S, Lund JM, Zhang N, Daffis S, Rudensky AY, Bevan MJ, Clark EA, Kaja MK, Diamond MS, Gale M, Jr. 2010. IPS-1 is essential for the control of West Nile virus infection and immunity. *PLoS Pathog* 6:e1000757.
85. Lazear HM, Lancaster A, Wilkins C, Suthar MS, Huang A, Vick SC, Clepper L, Thackray L, Brassil MM, Virgin HW, Nikolich-Zugich J, Moses AV, Gale M, Jr., Früh K, Diamond MS. 2013. IRF-3, IRF-5, and IRF-7 coordinately regulate the type I IFN response in myeloid dendritic cells downstream of MAVS signaling. *PLoS Pathog* 9:e1003118.

86. Pinto AK, Ramos HJ, Wu X, Aggarwal S, Shrestha B, Gorman M, Kim KY, Suthar MS, Atkinson JP, Gale M, Jr., Diamond MS. 2014. Deficient IFN signaling by myeloid cells leads to MAVS-dependent virus-induced sepsis. *PLoS Pathog* 10:e1004086.
87. Roe K, Giordano D, Young LB, Draves KE, Holder U, Suthar MS, Gale M, Jr., Clark EA. 2019. Dendritic cell-associated MAVS is required to control West Nile virus replication and ensuing humoral immune responses. *PLoS One* 14:e0218928.
88. Zhao J, Vijay R, Zhao J, Gale M, Jr., Diamond MS, Perlman S. 2016. MAVS Expressed by Hematopoietic Cells Is Critical for Control of West Nile Virus Infection and Pathogenesis. *J Virol* 90:7098-7108.
89. Bachem A, Hartung E, Güttler S, Mora A, Zhou X, Hegemann A, Plantinga M, Mazzini E, Stoitzner P, Gurka S, Henn V, Mages HW, Kroczeck RA. 2012. Expression of XCR1 Characterizes the Batf3-Dependent Lineage of Dendritic Cells Capable of Antigen Cross-Presentation. *Frontiers in immunology* 3:214-214.
90. Williams M, Dutertre C-A, Scott CL, McGovern N, Sichien D, Chakarov S, Van Gassen S, Chen J, Poidinger M, De Prijck S, Tavernier SJ, Low I, Irac SE, Mattar CN, Sumatoh HR, Low GHL, Chung TJK, Chan DKH, Tan KK, Hon TLK, Fossum E, Bogen B, Choolani M, Chan JKY, Larbi A, Luche H, Henri S, Saeys Y, Newell EW, Lambrecht BN, Malissen B, Ginhoux F. 2016. Unsupervised High-Dimensional Analysis Aligns Dendritic Cells across Tissues and Species. *Immunity* 45:669-684.
91. Hildner K, Edelson BT, Purtha WE, Diamond M, Matsushita H, Kohyama M, Calderon B, Schraml BU, Unanue ER, Diamond MS, Schreiber RD, Murphy TL, Murphy KM. 2008. Batf3 deficiency reveals a critical role for CD8alpha+ dendritic cells in cytotoxic T cell immunity. *Science* 322:1097-100.
92. Throsby M, Geuijen C, Goudsmit J, Bakker AQ, Korimbocus J, Kramer RA, Clijsters-van der Horst M, de Jong M, Jongeneelen M, Thijsse S, Smit R, Visser TJ, Bijl N, Marissen WE, Loeb M, Kelvin DJ, Preiser W, ter Meulen J, de Kruif J. 2006. Isolation and characterization of human monoclonal antibodies from individuals infected with West Nile Virus. *J Virol* 80:6982-92.
93. Vogt MR, Moesker B, Goudsmit J, Jongeneelen M, Austin SK, Oliphant T, Nelson S, Pierson TC, Wilschut J, Throsby M, Diamond MS. 2009. Human monoclonal antibodies against West Nile virus induced by natural infection neutralize at a postattachment step. *J Virol* 83:6494-507.
94. Engle MJ, Diamond MS. 2003. Antibody prophylaxis and therapy against West Nile virus infection in wild-type and immunodeficient mice. *J Virol* 77:12941-9.
95. Giordano D, Draves KE, Young LB, Roe K, Bryan MA, Dresch C, Richner JM, Diamond MS, Gale M, Jr., Clark EA. 2017. Protection of mice deficient in mature B cells from West Nile virus infection by passive and active immunization. *PLoS Pathog* 13:e1006743.
96. Koblishke M, Spitzer FS, Florian DM, Aberle SW, Malafa S, Fae I, Cassaniti I, Jungbauer C, Knapp B, Laferl H, Fischer G, Baldanti F, Stiasny K, Heinz FX, Aberle JH. 2020. CD4 T Cell Determinants in West Nile Virus Disease and Asymptomatic Infection. *Front Immunol* 11:16.
97. Sitati EM, Diamond MS. 2006. CD4+ T-cell responses are required for clearance of West Nile virus from the central nervous system. *J Virol* 80:12060-9.
98. Parsons R, Lelic A, Hayes L, Carter A, Marshall L, Eveleigh C, Drebot M, Andonova M, McMurtrey C, Hildebrand W, Loeb MB, Bramson JL. 2008. The memory T cell response to West Nile virus in symptomatic humans following natural infection is not influenced by age and is dominated by a restricted set of CD8+ T cell epitopes. *J Immunol* 181:1563-72.
99. Piazza P, McMurtrey CP, Lelic A, Cook RL, Hess R, Yablonsky E, Borowski L, Loeb MB, Bramson JL, Hildebrand WH, Rinaldo CR. 2010. Surface phenotype and functionality of WNV specific T cells differ with age and disease severity. *PLoS One* 5:e15343.
100. Shrestha B, Diamond MS. 2004. Role of CD8+ T cells in control of West Nile virus infection. *J Virol* 78:8312-21.
101. Kaech SM, Cui W. 2012. Transcriptional control of effector and memory CD8+ T cell differentiation. *Nat Rev Immunol* 12:749-61.

102. Kim S, Pinto AK, Myers NB, Hawkins O, Doll K, Kaabinejadian S, Netland J, Bevan MJ, Weidanz JA, Hildebrand WH, Diamond MS, Hansen TH. 2014. A novel T-cell receptor mimic defines dendritic cells that present an immunodominant West Nile virus epitope in mice. *European journal of immunology* 44:1936-1946.
103. Pinto AK, Daffis S, Brien JD, Gainey MD, Yokoyama WM, Sheehan KC, Murphy KM, Schreiber RD, Diamond MS. 2011. A temporal role of type I interferon signaling in CD8+ T cell maturation during acute West Nile virus infection. *PLoS Pathog* 7:e1002407.
104. Aguilar-Valenzuela R, Netland J, Seo YJ, Bevan MJ, Grakoui A, Suthar MS. 2018. Dynamics of Tissue-Specific CD8(+) T Cell Responses during West Nile Virus Infection. *J Virol* 92.
105. Graham JB, Da Costa A, Lund JM. 2014. Regulatory T cells shape the resident memory T cell response to virus infection in the tissues. *Journal of immunology (Baltimore, Md : 1950)* 192:683-690.
106. Purtha WE, Myers N, Mitaksov V, Sitati E, Connolly J, Fremont DH, Hansen TH, Diamond MS. 2007. Antigen-specific cytotoxic T lymphocytes protect against lethal West Nile virus encephalitis. *Eur J Immunol* 37:1845-54.
107. Durrant DM, Daniels BP, Pasieka T, Dorsey D, Klein RS. 2015. CCR5 limits cortical viral loads during West Nile virus infection of the central nervous system. *J Neuroinflammation* 12:233.
108. Zhang B, Chan YK, Lu B, Diamond MS, Klein RS. 2008. CXCR3 mediates region-specific antiviral T cell trafficking within the central nervous system during West Nile virus encephalitis. *J Immunol* 180:2641-9.
109. Zhang B, Patel J, Croyle M, Diamond MS, Klein RS. 2010. TNF-alpha-dependent regulation of CXCR3 expression modulates neuronal survival during West Nile virus encephalitis. *J Neuroimmunol* 224:28-38.
110. Bardina SV, Brown JA, Michlmayr D, Hoffman KW, Sum J, Pletnev AG, Lira SA, Lim JK. 2017. Chemokine Receptor Ccr7 Restricts Fatal West Nile Virus Encephalitis. *J Virol* 91.
111. Acharya D, Wang P, Paul AM, Dai J, Gate D, Lowery JE, Stokic DS, Leis AA, Flavell RA, Town T, Fikrig E, Bai F. 2017. Interleukin-17A Promotes CD8+ T Cell Cytotoxicity To Facilitate West Nile Virus Clearance. *J Virol* 91.
112. Ramos HJ, Lanteri MC, Blahnik G, Negash A, Suthar MS, Brassil MM, Sodhi K, Treuting PM, Busch MP, Norris PJ, Gale M, Jr. 2012. IL-1beta signaling promotes CNS-intrinsic immune control of West Nile virus infection. *PLoS Pathog* 8:e1003039.
113. Durrant DM, Daniels BP, Klein RS. 2014. IL-1R1 signaling regulates CXCL12-mediated T cell localization and fate within the central nervous system during West Nile Virus encephalitis. *J Immunol* 193:4095-106.
114. Sitati E, McCandless EE, Klein RS, Diamond MS. 2007. CD40-CD40 ligand interactions promote trafficking of CD8+ T cells into the brain and protection against West Nile virus encephalitis. *J Virol* 81:9801-11.
115. Seo YJ, Jothikumar P, Suthar MS, Zhu C, Grakoui A. 2016. Local Cellular and Cytokine Cues in the Spleen Regulate In Situ T Cell Receptor Affinity, Function, and Fate of CD8(+) T Cells. *Immunity* 45:988-998.
116. Cupovic J, Onder L, Gil-Cruz C, Weiler E, Caviezel-Firner S, Perez-Shibayama C, Rulicke T, Bechmann I, Ludewig B. 2016. Central Nervous System Stromal Cells Control Local CD8(+) T Cell Responses during Virus-Induced Neuroinflammation. *Immunity* 44:622-33.
117. Lopes Pinheiro MA, Kooij G, Mizee MR, Kamermans A, Enzmann G, Lyck R, Schwaninger M, Engelhardt B, de Vries HE. 2016. Immune cell trafficking across the barriers of the central nervous system in multiple sclerosis and stroke. *Biochim Biophys Acta* 1862:461-71.
118. Durrant DM, Robinette ML, Klein RS. 2013. IL-1R1 is required for dendritic cell-mediated T cell reactivation within the CNS during West Nile virus encephalitis. *J Exp Med* 210:503-16.
119. Burdeinick-Kerr R, Govindarajan D, Griffin DE. 2009. Noncytolytic clearance of sindbis virus infection from neurons by gamma interferon is dependent on Jak/STAT signaling. *J Virol* 83:3429-35.

120. Wang T, Scully E, Yin Z, Kim JH, Wang S, Yan J, Mamula M, Anderson JF, Craft J, Fikrig E. 2003. IFN-gamma-producing gamma delta T cells help control murine West Nile virus infection. *J Immunol* 171:2524-31.
121. Shrestha B, Pinto AK, Green S, Bosch I, Diamond MS. 2012. CD8+ T cells use TRAIL to restrict West Nile virus pathogenesis by controlling infection in neurons. *J Virol* 86:8937-48.
122. Shrestha B, Diamond MS. 2007. Fas ligand interactions contribute to CD8+ T-cell-mediated control of West Nile virus infection in the central nervous system. *J Virol* 81:11749-57.
123. Bell JK, Askins J, Hall PR, Davies DR, Segal DMJPotNAoS. 2006. The dsRNA binding site of human Toll-like receptor 3. *J Biol Chem* 281:8792-8797.
124. Choe J, Kelker MS, Wilson IAJS. 2005. Crystal structure of human toll-like receptor 3 (TLR3) ectodomain. *J Biol Chem* 280:581-585.
125. Kawai T, Akira S. 2010. The role of pattern-recognition receptors in innate immunity: update on Toll-like receptors. *Nature Immunology* 11:373-384.
126. Daffis S, Samuel MA, Suthar MS, Gale M, Jr., Diamond MS. 2008. Toll-like receptor 3 has a protective role against West Nile virus infection. *J Virol* 82:10349-58.
127. Town T, Bai F, Wang T, Kaplan AT, Qian F, Montgomery RR, Anderson JF, Flavell RA, Fikrig E. 2009. Toll-like receptor 7 mitigates lethal West Nile encephalitis via interleukin 23-dependent immune cell infiltration and homing. *Immunity* 30:242-53.
128. Szretter KJ, Daffis S, Patel J, Suthar MS, Klein RS, Gale M, Jr., Diamond MS. 2010. The innate immune adaptor molecule MyD88 restricts West Nile virus replication and spread in neurons of the central nervous system. *J Virol* 84:12125-38.
129. Muñoz-Planillo R, Kuffa P, Martínez-Colón G, Smith BL, Rajendiran TM, Núñez G. 2013. K⁺ efflux is the common trigger of NLRP3 inflammasome activation by bacterial toxins and particulate matter. *Immunity* 38:1142-53.
130. Miao EA, Alpujch-Aranda CM, Dors M, Clark AE, Bader MW, Miller SI, Aderem A. 2006. Cytoplasmic flagellin activates caspase-1 and secretion of interleukin 1beta via Ipaf. *Nat Immunol* 7:569-75.
131. Martinon F, Burns K, Tschopp J. 2002. The inflammasome: a molecular platform triggering activation of inflammatory caspases and processing of proIL-beta. *Mol Cell* 10:417-26.
132. Liu X, Zhang Z, Ruan J, Pan Y, Magupalli VG, Wu H, Lieberman J. 2016. Inflammasome-activated gasdermin D causes pyroptosis by forming membrane pores. *Nature* 535:153-8.
133. Kumar M, Roe K, Orillo B, Muruve DA, Nerurkar VR, Gale M, Jr., Verma S. 2013. Inflammasome adaptor protein Apoptosis-associated speck-like protein containing CARD (ASC) is critical for the immune response and survival in west Nile virus encephalitis. *J Virol* 87:3655-67.
134. Aarreberg LD, Wilkins C, Ramos HJ, Green R, Davis MA, Chow K, Gale M, Jr. 2018. Interleukin-1 β Signaling in Dendritic Cells Induces Antiviral Interferon Responses. *mBio* 9.
135. Shipley JG, Vandergaast R, Deng L, Mariuzza RA, Fredericksen BL. 2012. Identification of multiple RIG-I-specific pathogen associated molecular patterns within the West Nile virus genome and antigenome. *Virology* 432:232-238.
136. Gack MU, Shin YC, Joo CH, Urano T, Liang C, Sun L, Takeuchi O, Akira S, Chen Z, Inoue S, Jung JU. 2007. TRIM25 RING-finger E3 ubiquitin ligase is essential for RIG-I-mediated antiviral activity. *Nature* 446:916-920.
137. Gao D, Yang YK, Wang RP, Zhou X, Diao FC, Li MD, Zhai ZH, Jiang ZF, Chen DY. 2009. REUL is a novel E3 ubiquitin ligase and stimulator of retinoic-acid-inducible gene-I. *PLoS One* 4:e5760.
138. Chow KT, Gale M, Jr., Loo YM. 2018. RIG-I and Other RNA Sensors in Antiviral Immunity. *Annu Rev Immunol* 36:667-694.
139. Quicke KM, Kim KY, Horvath CM, Suthar MS. 2019. RNA Helicase LGP2 Negatively Regulates RIG-I Signaling by Preventing TRIM25-Mediated Caspase Activation and Recruitment Domain Ubiquitination. *J Interferon Cytokine Res* 39:669-683.

140. Saito T, Hirai R, Loo YM, Owen D, Johnson CL, Sinha SC, Akira S, Fujita T, Gale M, Jr. 2007. Regulation of innate antiviral defenses through a shared repressor domain in RIG-I and LGP2. *Proc Natl Acad Sci U S A* 104:582-7.
141. Hou F, Sun L, Zheng H, Skaug B, Jiang QX, Chen ZJ. 2011. MAVS forms functional prion-like aggregates to activate and propagate antiviral innate immune response. *Cell* 146:448-61.
142. You F, Wang P, Yang L, Yang G, Zhao YO, Qian F, Walker W, Sutton R, Montgomery R, Lin R, Iwasaki A, Fikrig E. 2013. ELF4 is critical for induction of type I interferon and the host antiviral response. *Nat Immunol* 14:1237-46.
143. Mitchell S, Vargas J, Hoffmann A. 2016. Signaling via the NFkappaB system. *Wiley Interdiscip Rev Syst Biol Med* 8:227-41.
144. Subramanian N, Natarajan K, Clatworthy MR, Wang Z, Germain RN. 2013. The adaptor MAVS promotes NLRP3 mitochondrial localization and inflammasome activation. *Cell* 153:348-61.
145. Yu CY, Chiang RL, Chang TH, Liao CL, Lin YL. 2010. The interferon stimulator mitochondrial antiviral signaling protein facilitates cell death by disrupting the mitochondrial membrane potential and by activating caspases. *J Virol* 84:2421-31.
146. Zhang W, Gong J, Yang H, Wan L, Peng Y, Wang X, Sun J, Li F, Geng Y, Li D, Liu N, Mei G, Cao Y, Yan Q, Li H, Zhang Y, He X, Zhang Q, Zhang R, Wu F, Zhong H, Wei C. 2020. The Mitochondrial Protein MAVS Stabilizes p53 to Suppress Tumorigenesis. *Cell Rep* 30:725-738.e4.
147. Castanier C, Garcin D, Vazquez A, Arnoult D. 2010. Mitochondrial dynamics regulate the RIG-I-like receptor antiviral pathway. *EMBO Rep* 11:133-8.
148. Tal MC, Sasai M, Lee HK, Yordy B, Shadel GS, Iwasaki A. 2009. Absence of autophagy results in reactive oxygen species-dependent amplification of RLR signaling. *Proc Natl Acad Sci U S A* 106:2770-5.
149. Allen IC, Moore CB, Schneider M, Lei Y, Davis BK, Scull MA, Gris D, Roney KE, Zimmermann AG, Bowzard JB, Ranjan P, Monroe KM, Pickles RJ, Sambhara S, Ting JP. 2011. NLRX1 protein attenuates inflammatory responses to infection by interfering with the RIG-I-MAVS and TRAF6-NF- κ B signaling pathways. *Immunity* 34:854-65.
150. Yasukawa K, Oshiumi H, Takeda M, Ishihara N, Yanagi Y, Seya T, Kawabata S, Koshiba T. 2009. Mitofusin 2 inhibits mitochondrial antiviral signaling. *Sci Signal* 2:ra47.
151. Liu XY, Wei B, Shi HX, Shan YF, Wang C. 2010. Tom70 mediates activation of interferon regulatory factor 3 on mitochondria. *Cell Res* 20:994-1011.
152. Onoguchi K, Onomoto K, Takamatsu S, Jogi M, Takemura A, Morimoto S, Julkunen I, Namiki H, Yoneyama M, Fujita T. 2010. Virus-infection or 5'ppp-RNA activates antiviral signal through redistribution of IPS-1 mediated by MFN1. *PLoS Pathog* 6:e1001012.
153. Fredericksen BL, Keller BC, Fornek J, Katze MG, Gale M, Jr. 2008. Establishment and maintenance of the innate antiviral response to West Nile Virus involves both RIG-I and MDA5 signaling through IPS-1. *J Virol* 82:609-16.
154. Lazear HM, Pinto AK, Ramos HJ, Vick SC, Shrestha B, Suthar MS, Gale M, Jr., Diamond MS. 2013. Pattern recognition receptor MDA5 modulates CD8+ T cell-dependent clearance of West Nile virus from the central nervous system. *J Virol* 87:11401-15.
155. Luo H, Winkelmann E, Xie G, Fang R, Peng BH, Li L, Lazear HM, Paessler S, Diamond MS, Gale M, Jr., Barrett AD, Wang T. 2017. MAVS Is Essential for Primary CD4(+) T Cell Immunity but Not for Recall T Cell Responses following an Attenuated West Nile Virus Infection. *J Virol* 91.
156. Da Costa A, Garza E, Graham JB, Swarts JL, Soerens AG, Gale M, Lund JM. 2017. Extrinsic MAVS signaling is critical for Treg maintenance of Foxp3 expression following acute flavivirus infection. *Sci Rep* 7:40720.
157. Suthar MS, Ramos HJ, Brassil MM, Netland J, Chappell CP, Blahnik G, McMillan A, Diamond MS, Clark EA, Bevan MJ, Gale M, Jr. 2012. The RIG-I-like receptor LGP2 controls CD8(+) T cell survival and fitness. *Immunity* 37:235-48.

158. Chancey C, Grinev A, Volkova E, Rios M. 2015. The global ecology and epidemiology of West Nile virus. *Biomed Res Int* 2015:376230.
159. Krow-Lucal E, Lindsey NP, Lehman J, Fischer M, Staples JE. 2017. West Nile Virus and Other Nationally Notifiable Arboviral Diseases - United States, 2015. *MMWR Morb Mortal Wkly Rep* 66:51-55.
160. Patel H, Sander B, Nelder MP. 2015. Long-term sequelae of West Nile virus-related illness: a systematic review. *Lancet Infect Dis* 15:951-9.
161. Lazear HM, Pinto AK, Vogt MR, Gale M, Jr., Diamond MS. 2011. Beta interferon controls West Nile virus infection and pathogenesis in mice. *J Virol* 85:7186-94.
162. Marin-Lopez A, Calvo-Pinilla E, Moreno S, Utrilla-Trigo S, Nogales A, Brun A, Fikrig E, Ortego J. 2019. Modeling Arboviral Infection in Mice Lacking the Interferon Alpha/Beta Receptor. *Viruses* 11.
163. Samuel MA, Diamond MS. 2005. Alpha/beta interferon protects against lethal West Nile virus infection by restricting cellular tropism and enhancing neuronal survival. *J Virol* 79:13350-61.
164. Samuel MA, Diamond MS. 2006. Pathogenesis of West Nile Virus infection: a balance between virulence, innate and adaptive immunity, and viral evasion. *J Virol* 80:9349-60.
165. Matullo CM, O'Regan KJ, Hensley H, Curtis M, Rall GF. 2010. Lymphocytic choriomeningitis virus-induced mortality in mice is triggered by edema and brain herniation. *J Virol* 84:312-20.
166. Rua R, Lee JY, Silva AB, Swafford IS, Maric D, Johnson KR, McGavern DB. 2019. Infection drives meningeal engraftment by inflammatory monocytes that impairs CNS immunity. *Nat Immunol* 20:407-419.
167. Herz J, Filiano AJ, Smith A, Yogev N, Kipnis J. 2017. Myeloid Cells in the Central Nervous System. *Immunity* 46:943-956.
168. Anandasabapathy N, Victora GD, Meredith M, Feder R, Dong B, Kluger C, Yao K, Dustin ML, Nussenzweig MC, Steinman RM, Liu K. 2011. Flt3L controls the development of radiosensitive dendritic cells in the meninges and choroid plexus of the steady-state mouse brain. *J Exp Med* 208:1695-705.
169. Serot JM, Foliguet B, Bene MC, Faure GC. 1997. Ultrastructural and immunohistological evidence for dendritic-like cells within human choroid plexus epithelium. *Neuroreport* 8:1995-8.
170. Ganguly D, Haak S, Sisirak V, Reizis B. 2013. The role of dendritic cells in autoimmunity. *Nat Rev Immunol* 13:566-77.
171. Gardner A, Ruffell B. 2016. Dendritic Cells and Cancer Immunity. *Trends Immunol* 37:855-865.
172. Williams M, Ginhoux F, Jakubzick C, Naik SH, Onai N, Schraml BU, Segura E, Tussiwand R, Yona S. 2014. Dendritic cells, monocytes and macrophages: a unified nomenclature based on ontogeny. *Nat Rev Immunol* 14:571-8.
173. Buskiewicz IA, Montgomery T, Yasewicz EC, Huber SA, Murphy MP, Hartley RC, Kelly R, Crow MK, Perl A, Budd RC, Koenig A. 2016. Reactive oxygen species induce virus-independent MAVS oligomerization in systemic lupus erythematosus. *Sci Signal* 9:ra115.
174. Kim S, Pinto AK, Myers NB, Hawkins O, Doll K, Kaabinejadian S, Netland J, Bevan MJ, Weidanz JA, Hildebrand WH, Diamond MS, Hansen TH. 2014. A novel T-cell receptor mimic defines dendritic cells that present an immunodominant West Nile virus epitope in mice. *Eur J Immunol* 44:1936-46.
175. Korn T, Kallies A. 2017. T cell responses in the central nervous system. *Nat Rev Immunol* 17:179-194.
176. Klein RS, Lin E, Zhang B, Luster AD, Tollett J, Samuel MA, Engle M, Diamond MS. 2005. Neuronal CXCL10 directs CD8+ T-cell recruitment and control of West Nile virus encephalitis. *J Virol* 79:11457-66.
177. Halle S, Halle O, Forster R. 2017. Mechanisms and Dynamics of T Cell-Mediated Cytotoxicity In Vivo. *Trends Immunol* 38:432-443.

178. Lanteri MC, Heitman JW, Owen RE, Busch T, Geftter N, Kiely N, Kamel HT, Tobler LH, Busch MP, Norris PJ. 2008. Comprehensive analysis of west nile virus-specific T cell responses in humans. *J Infect Dis* 197:1296-306.
179. Shrestha B, Zhang B, Purtha WE, Klein RS, Diamond MS. 2008. Tumor necrosis factor alpha protects against lethal West Nile virus infection by promoting trafficking of mononuclear leukocytes into the central nervous system. *J Virol* 82:8956-64.
180. Funk KE, Klein RS. 2019. CSF1R antagonism limits local restimulation of antiviral CD8(+) T cells during viral encephalitis. *J Neuroinflammation* 16:22.
181. Shwetank, Abdelsamed HA, Frost EL, Schmitz HM, Mockus TE, Youngblood BA, Lukacher AE. 2017. Maintenance of PD-1 on brain-resident memory CD8 T cells is antigen independent. *Immunol Cell Biol* 95:953-959.
182. Prasad S, Hu S, Sheng WS, Chauhan P, Singh A, Lokensgard JR. 2017. The PD-1: PD-L1 pathway promotes development of brain-resident memory T cells following acute viral encephalitis. *J Neuroinflammation* 14:82.
183. Wherry EJ, Kurachi M. 2015. Molecular and cellular insights into T cell exhaustion. *Nat Rev Immunol* 15:486-99.
184. Malek TR. 2008. The biology of interleukin-2. *Annu Rev Immunol* 26:453-79.
185. Sathaliyawala T, Kubota M, Yudanin N, Turner D, Camp P, Thome JJ, Bickham KL, Lerner H, Goldstein M, Sykes M, Kato T, Farber DL. 2013. Distribution and compartmentalization of human circulating and tissue-resident memory T cell subsets. *Immunity* 38:187-97.
186. Xin A, Masson F, Liao Y, Preston S, Guan T, Gloury R, Olshansky M, Lin JX, Li P, Speed TP, Smyth GK, Ernst M, Leonard WJ, Pellegrini M, Kaech SM, Nutt SL, Shi W, Belz GT, Kallies A. 2016. A molecular threshold for effector CD8(+) T cell differentiation controlled by transcription factors Blimp-1 and T-bet. *Nat Immunol* 17:422-32.
187. Burdeinick-Kerr R, Griffin DE. 2005. Gamma interferon-dependent, noncytolytic clearance of sindbis virus infection from neurons in vitro. *J Virol* 79:5374-85.
188. Garber C, Soung A, Vollmer LL, Kanmogne M, Last A, Brown J, Klein RS. 2019. T cells promote microglia-mediated synaptic elimination and cognitive dysfunction during recovery from neuropathogenic flaviviruses. *Nat Neurosci* 22:1276-1288.
189. Wherry EJ, Ha SJ, Kaech SM, Haining WN, Sarkar S, Kalia V, Subramaniam S, Blattman JN, Barber DL, Ahmed R. 2007. Molecular signature of CD8+ T cell exhaustion during chronic viral infection. *Immunity* 27:670-84.
190. Lanteri MC, O'Brien KM, Purtha WE, Cameron MJ, Lund JM, Owen RE, Heitman JW, Custer B, Hirschhorn DF, Tobler LH, Kiely N, Prince HE, Ndhlovu LC, Nixon DF, Kamel HT, Kelvin DJ, Busch MP, Rudensky AY, Diamond MS, Norris PJ. 2009. Tregs control the development of symptomatic West Nile virus infection in humans and mice. *J Clin Invest* 119:3266-77.
191. Lanciotti RS, Kerst AJ, Nasci RS, Godsey MS, Mitchell CJ, Savage HM, Komar N, Panella NA, Allen BC, Volpe KE, Davis BS, Roehrig JT. 2000. Rapid detection of west nile virus from human clinical specimens, field-collected mosquitoes, and avian samples by a TaqMan reverse transcriptase-PCR assay. *J Clin Microbiol* 38:4066-71.
192. O'Neal JT, Upadhyay AA, Wolabaugh A, Patel NB, Bosinger SE, Suthar MS. 2019. West Nile Virus-Inclusive Single-Cell RNA Sequencing Reveals Heterogeneity in the Type I Interferon Response within Single Cells. *J Virol* 93.
193. Lau KS, Cortez-Retamozo V, Philips SR, Pittet MJ, Lauffenburger DA, Haigis KM. 2012. Multi-scale in vivo systems analysis reveals the influence of immune cells on TNF-alpha-induced apoptosis in the intestinal epithelium. *PLoS Biol* 10:e1001393.
194. Love MI, Huber W, Anders S. 2014. Moderated estimation of fold change and dispersion for RNA-seq data with DESeq2. *Genome Biol* 15:550.
195. Loo YM, Gale M, Jr. 2011. Immune signaling by RIG-I-like receptors. *Immunity* 34:680-92.

196. Sena LA, Li S, Jairaman A, Prakriya M, Ezponda T, Hildeman DA, Wang CR, Schumacker PT, Licht JD, Perlman H, Bryce PJ, Chandel NS. 2013. Mitochondria are required for antigen-specific T cell activation through reactive oxygen species signaling. *Immunity* 38:225-36.
197. Chang CH, Curtis JD, Maggi LB, Jr., Faubert B, Villarino AV, O'Sullivan D, Huang SC, van der Windt GJ, Blagih J, Qiu J, Weber JD, Pearce EJ, Jones RG, Pearce EL. 2013. Posttranscriptional control of T cell effector function by aerobic glycolysis. *Cell* 153:1239-51.
198. Klein Geltink RI, O'Sullivan D, Corrado M, Bremser A, Buck MD, Buescher JM, Firat E, Zhu X, Niedermann G, Caputa G, Kelly B, Warthorst U, Rensing-Ehl A, Kyle RL, Vandersarren L, Curtis JD, Patterson AE, Lawless S, Grzes K, Qiu J, Sanin DE, Kretz O, Huber TB, Janssens S, Lambrecht BN, Rambold AS, Pearce EJ, Pearce EL. 2017. Mitochondrial Priming by CD28. *Cell* 171:385-397.e11.
199. Phan AT, Doedens AL, Palazon A, Tyrakis PA, Cheung KP, Johnson RS, Goldrath AW. 2016. Constitutive Glycolytic Metabolism Supports CD8(+) T Cell Effector Memory Differentiation during Viral Infection. *Immunity* 45:1024-1037.
200. Geltink RIK, Kyle RL, Pearce EL. 2018. Unraveling the Complex Interplay Between T Cell Metabolism and Function. *Annu Rev Immunol* 36:461-488.
201. Buck MD, O'Sullivan D, Klein Geltink RI, Curtis JD, Chang CH, Sanin DE, Qiu J, Kretz O, Braas D, van der Windt GJ, Chen Q, Huang SC, O'Neill CM, Edelson BT, Pearce EJ, Sesaki H, Huber TB, Rambold AS, Pearce EL. 2016. Mitochondrial Dynamics Controls T Cell Fate through Metabolic Programming. *Cell* 166:63-76.
202. Suthar MS, Diamond MS, Gale M, Jr. 2013. West Nile virus infection and immunity. *Nat Rev Microbiol* 11:115-28.
203. Koshihara T, Yasukawa K, Yanagi Y, Kawabata S. 2011. Mitochondrial membrane potential is required for MAVS-mediated antiviral signaling. *Sci Signal* 4:ra7.
204. Horner SM, Liu HM, Park HS, Briley J, Gale M, Jr. 2011. Mitochondrial-associated endoplasmic reticulum membranes (MAM) form innate immune synapses and are targeted by hepatitis C virus. *Proc Natl Acad Sci U S A* 108:14590-5.
205. Horner SM, Wilkins C, Badil S, Iskarpatyoti J, Gale M, Jr. 2015. Proteomic analysis of mitochondrial-associated ER membranes (MAM) during RNA virus infection reveals dynamic changes in protein and organelle trafficking. *PLoS One* 10:e0117963.
206. Sun W, Wang H, Qi CF, Wu J, Scott B, Bolland S. 2019. Antiviral Adaptor MAVS Promotes Murine Lupus With a B Cell Autonomous Role. *Front Immunol* 10:2452.
207. Rahman AH, Cui W, Larosa DF, Taylor DK, Zhang J, Goldstein DR, Wherry EJ, Kaech SM, Turka LA. 2008. MyD88 plays a critical T cell-intrinsic role in supporting CD8 T cell expansion during acute lymphocytic choriomeningitis virus infection. *J Immunol* 181:3804-10.
208. Rahman AH, Zhang R, Blosser CD, Hou B, Defranco AL, Maltzman JS, Wherry EJ, Turka LA. 2011. Antiviral memory CD8 T-cell differentiation, maintenance, and secondary expansion occur independently of MyD88. *Blood* 117:3123-30.
209. Zhao Y, De Trez C, Flynn R, Ware CF, Croft M, Salek-Ardakani S. 2009. The adaptor molecule MyD88 directly promotes CD8 T cell responses to vaccinia virus. *J Immunol* 182:6278-86.
210. Ling GS, Crawford G, Buang N, Bartok I, Tian K, Thielens NM, Bally I, Harker JA, Ashton-Rickardt PG, Rutschmann S, Strid J, Botto M. 2018. C1q restrains autoimmunity and viral infection by regulating CD8(+) T cell metabolism. *Science* 360:558-563.
211. Wu J, Chen YJ, Dobbs N, Sakai T, Liou J, Miner JJ, Yan N. 2019. STING-mediated disruption of calcium homeostasis chronically activates ER stress and primes T cell death. *J Exp Med* 216:867-883.
212. Steinbach K, Vincenti I, Kreutzfeldt M, Page N, Muschwackh A, Wagner I, Drexler I, Pinschewer D, Korn T, Merkler D. 2016. Brain-resident memory T cells represent an autonomous cytotoxic barrier to viral infection. *J Exp Med* 213:1571-87.

213. Mundt S, Mrdjjen D, Utz SG, Greter M, Schreiner B, Becher B. 2019. Conventional DCs sample and present myelin antigens in the healthy CNS and allow parenchymal T cell entry to initiate neuroinflammation. *Sci Immunol* 4.
214. Urban SL, Jensen IJ, Shan Q, Pewe LL, Xue HH, Badovinac VP, Harty JT. 2020. Peripherally induced brain tissue-resident memory CD8(+) T cells mediate protection against CNS infection. *Nat Immunol* 21:938-949.
215. Esterházy D, Canesso MCC, Mesin L, Muller PA, de Castro TBR, Lockhart A, ElJalby M, Faria AMC, Mucida D. 2019. Compartmentalized gut lymph node drainage dictates adaptive immune responses. *Nature* 569:126-130.
216. Moseman EA, Blanchard AC, Nayak D, McGavern DB. 2020. T cell engagement of cross-presenting microglia protects the brain from a nasal virus infection. *Sci Immunol* 5.
217. Quick ED, Leser JS, Clarke P, Tyler KL. 2014. Activation of intrinsic immune responses and microglial phagocytosis in an ex vivo spinal cord slice culture model of West Nile virus infection. *J Virol* 88:13005-14.
218. Lomelino CL, Andring JT, McKenna R, Kilberg MS. 2017. Asparagine synthetase: Function, structure, and role in disease. *J Biol Chem* 292:19952-19958.
219. Seki SM, Stevenson M, Rosen AM, Arandjelovic S, Gemta L, Bullock TNJ, Gaultier A. 2017. Lineage-Specific Metabolic Properties and Vulnerabilities of T Cells in the Demyelinating Central Nervous System. *J Immunol* 198:4607-4617.
220. Page N, Klimek B, De Roo M, Steinbach K, Soldati H, Lemeille S, Wagner I, Kreutzfeldt M, Di Liberto G, Vincenti I, Lingner T, Salinas G, Brück W, Simons M, Murr R, Kaye J, Zehn D, Pinschewer DD, Merkler D. 2018. Expression of the DNA-Binding Factor TOX Promotes the Encephalitogenic Potential of Microbe-Induced Autoreactive CD8(+) T Cells. *Immunity* 48:937-950.e8.
221. Milner JJ, Toma C, Yu B, Zhang K, Omilusik K, Phan AT, Wang D, Getzler AJ, Nguyen T, Crotty S, Wang W, Pipkin ME, Goldrath AW. 2017. Runx3 programs CD8(+) T cell residency in non-lymphoid tissues and tumours. *Nature* 552:253-257.
222. Pan Y, Tian T, Park CO, Lofftus SY, Mei S, Liu X, Luo C, O'Malley JT, Gehad A, Teague JE, Divito SJ, Fuhlbrigge R, Puigserver P, Krueger JG, Hotamisligil GS, Clark RA, Kupper TS. 2017. Survival of tissue-resident memory T cells requires exogenous lipid uptake and metabolism. *Nature* 543:252-256.
223. Bengsch B, Johnson AL, Kurachi M, Odorizzi PM, Pauken KE, Attanasio J, Stelekati E, McLane LM, Paley MA, Delgoffe GM, Wherry EJ. 2016. Bioenergetic Insufficiencies Due to Metabolic Alterations Regulated by the Inhibitory Receptor PD-1 Are an Early Driver of CD8(+) T Cell Exhaustion. *Immunity* 45:358-73.
224. Scharping NE, Menk AV, Moreci RS, Whetstone RD, Dadey RE, Watkins SC, Ferris RL, Delgoffe GM. 2016. The Tumor Microenvironment Represses T Cell Mitochondrial Biogenesis to Drive Intratumoral T Cell Metabolic Insufficiency and Dysfunction. *Immunity* 45:701-703.
225. Song M, Sandoval TA, Chae C-S, Chopra S, Tan C, Rutkowski MR, Raundhal M, Chaurio RA, Payne KK, Konrad C, Bettigole SE, Shin HR, Crowley MJP, Cerliani JP, Kossenkov AV, Motorykin I, Zhang S, Manfredi G, Zamarin D, Holcomb K, Rodriguez PC, Rabinovich GA, Conejo-Garcia JR, Glimcher LH, Cubillos-Ruiz JR. 2018. IRE1 α -XBP1 controls T cell function in ovarian cancer by regulating mitochondrial activity. *Nature* 562:423-428.
226. Yu YR, Imrichova H, Wang H, Chao T, Xiao Z, Gao M, Rincon-Restrepo M, Franco F, Genolet R, Cheng WC, Jandus C, Coukos G, Jiang YF, Locasale JW, Zippelius A, Liu PS, Tang L, Bock C, Vannini N, Ho PC. 2020. Disturbed mitochondrial dynamics in CD8(+) TILs reinforce T cell exhaustion. *Nat Immunol* 21:1540-1551.
227. Li C, Zhu B, Son YM, Wang Z, Jiang L, Xiang M, Ye Z, Beckermann KE, Wu Y, Jenkins JW, Siska PJ, Vincent BG, Prakash YS, Peikert T, Edelson BT, Taneja R, Kaplan MH, Rathmell JC, Dong H, Hitosugi T, Sun J. 2019. The Transcription Factor Bhlhe40 Programs Mitochondrial Regulation of Resident CD8(+) T Cell Fitness and Functionality. *Immunity* 51:491-507.e7.

228. O'Donnell LA, Henkins KM, Kulkarni A, Matullo CM, Balachandran S, Pattisapu AK, Rall GF. 2015. Interferon gamma induces protective non-canonical signaling pathways in primary neurons. *J Neurochem* 135:309-22.
229. Herz J, Johnson KR, McGavern DB. 2015. Therapeutic antiviral T cells noncytopathically clear persistently infected microglia after conversion into antigen-presenting cells. *J Exp Med* 212:1153-69.
230. Di Liberto G, Pantelyushin S, Kreutzfeldt M, Page N, Musardo S, Coras R, Steinbach K, Vincenti I, Klimek B, Lingner T, Salinas G, Lin-Marq N, Staszewski O, Costa Jordão MJ, Wagner I, Egervari K, Mack M, Bellone C, Blümcke I, Prinz M, Pinschewer DD, Merkler D. 2018. Neurons under T Cell Attack Coordinate Phagocyte-Mediated Synaptic Stripping. *Cell* 175:458-471.e19.
231. Hikita N, Seto T, Yamashita K, Iritani N, Aata M, Ogura H, Shintaku H. 2015. Relationship between Severity of Aseptic Meningitis and Cerebrospinal Fluid Cytokine Levels. *Osaka City Med J* 61:63-71.
232. Jarvis JN, Meintjes G, Bicanic T, Buffa V, Hogan L, Mo S, Tomlinson G, Kropf P, Noursadeghi M, Harrison TS. 2015. Cerebrospinal fluid cytokine profiles predict risk of early mortality and immune reconstitution inflammatory syndrome in HIV-associated cryptococcal meningitis. *PLoS Pathog* 11:e1004754.
233. Wippel C, Maurer J, Förtsch C, Hupp S, Bohl A, Ma J, Mitchell TJ, Bunkowski S, Brück W, Nau R, Iliev AI. 2013. Bacterial cytolysin during meningitis disrupts the regulation of glutamate in the brain, leading to synaptic damage. *PLoS Pathog* 9:e1003380.
234. Schmidt AK, Reich A, Falkenburger B, Schulz JB, Brandenburg LO, Ribes S, Tauber SC. 2015. Adjuvant granulocyte colony-stimulating factor therapy results in improved spatial learning and stimulates hippocampal neurogenesis in a mouse model of pneumococcal meningitis. *J Neuropathol Exp Neurol* 74:85-94.
235. Kreutzfeldt M, Bergthaler A, Fernandez M, Brück W, Steinbach K, Vorm M, Coras R, Blümcke I, Bonilla WV, Fleige A, Forman R, Müller W, Becher B, Misgeld T, Kerschensteiner M, Pinschewer DD, Merkler D. 2013. Neuroprotective intervention by interferon- γ blockade prevents CD8⁺ T cell-mediated dendrite and synapse loss. *The Journal of experimental medicine* 210:2087-2103.
236. Kipnis J, Cohen H, Cardon M, Ziv Y, Schwartz M. 2004. T cell deficiency leads to cognitive dysfunction: implications for therapeutic vaccination for schizophrenia and other psychiatric conditions. *Proc Natl Acad Sci U S A* 101:8180-5.
237. Alves de Lima K, Rustenhoven J, Da Mesquita S, Wall M, Salvador AF, Smirnov I, Martellosi Cebinelli G, Mamuladze T, Baker W, Papadopoulos Z, Lopes MB, Cao WS, Xie XS, Herz J, Kipnis J. 2020. Meningeal $\gamma\delta$ T cells regulate anxiety-like behavior via IL-17a signaling in neurons. *Nat Immunol* 21:1421-1429.
238. Park KH, Lee MS, Lee SO, Choi SH, Kim YS, Woo JH, Kang JK, Lee SA, Kim SH. 2014. Kinetics of T-cell-based assays on cerebrospinal fluid and peripheral blood mononuclear cells in patients with tuberculous meningitis. *Korean J Intern Med* 29:793-9.
239. Jarvis JN, Casazza JP, Stone HH, Meintjes G, Lawn SD, Levitz SM, Harrison TS, Koup RA. 2013. The phenotype of the *Cryptococcus*-specific CD4⁺ memory T-cell response is associated with disease severity and outcome in HIV-associated cryptococcal meningitis. *J Infect Dis* 207:1817-28.
240. Stewart BS, Demarest VL, Wong SJ, Green S, Bernard KA. 2011. Persistence of virus-specific immune responses in the central nervous system of mice after West Nile virus infection. *BMC Immunol* 12:6.
241. Garber C, Soung A, Vollmer LL, Kanmogne M, Last A, Brown J, Klein RS. T cells promote microglia-mediated synaptic elimination and cognitive dysfunction during recovery from neuropathogenic flaviviruses.